

Spring 1972

Methods for acoustic holography and acoustic measurements

Wolfgang Fischer

New Jersey Institute of Technology

Follow this and additional works at: <https://digitalcommons.njit.edu/dissertations>



Part of the [Electrical and Electronics Commons](#)

Recommended Citation

Fischer, Wolfgang, "Methods for acoustic holography and acoustic measurements" (1972). *Dissertations*. 1282.
<https://digitalcommons.njit.edu/dissertations/1282>

This Dissertation is brought to you for free and open access by the Theses and Dissertations at Digital Commons @ NJIT. It has been accepted for inclusion in Dissertations by an authorized administrator of Digital Commons @ NJIT. For more information, please contact digitalcommons@njit.edu.

Copyright Warning & Restrictions

The copyright law of the United States (Title 17, United States Code) governs the making of photocopies or other reproductions of copyrighted material.

Under certain conditions specified in the law, libraries and archives are authorized to furnish a photocopy or other reproduction. One of these specified conditions is that the photocopy or reproduction is not to be “used for any purpose other than private study, scholarship, or research.” If a user makes a request for, or later uses, a photocopy or reproduction for purposes in excess of “fair use” that user may be liable for copyright infringement,

This institution reserves the right to refuse to accept a copying order if, in its judgment, fulfillment of the order would involve violation of copyright law.

Please Note: The author retains the copyright while the New Jersey Institute of Technology reserves the right to distribute this thesis or dissertation

Printing note: If you do not wish to print this page, then select “Pages from: first page # to: last page #” on the print dialog screen

The Van Houten library has removed some of the personal information and all signatures from the approval page and biographical sketches of theses and dissertations in order to protect the identity of NJIT graduates and faculty.

INFORMATION TO USERS

This dissertation was produced from a microfilm copy of the original document. While the most advanced technological means to photograph and reproduce this document have been used, the quality is heavily dependent upon the quality of the original submitted.

The following explanation of techniques is provided to help you understand markings or patterns which may appear on this reproduction.

1. The sign or "target" for pages apparently lacking from the document photographed is "Missing Page(s)". If it was possible to obtain the missing page(s) or section, they are spliced into the film along with adjacent pages. This may have necessitated cutting thru an image and duplicating adjacent pages to insure you complete continuity.
2. When an image on the film is obliterated with a large round black mark, it is an indication that the photographer suspected that the copy may have moved during exposure and thus cause a blurred image. You will find a good image of the page in the adjacent frame.
3. When a map, drawing or chart, etc., was part of the material being photographed the photographer followed a definite method in "sectioning" the material. It is customary to begin photoing at the upper left hand corner of a large sheet and to continue photoing from left to right in equal sections with a small overlap. If necessary, sectioning is continued again — beginning below the first row and continuing on until complete.
4. The majority of users indicate that the textual content is of greatest value, however, a somewhat higher quality reproduction could be made from "photographs" if essential to the understanding of the dissertation. Silver prints of "photographs" may be ordered at additional charge by writing the Order Department, giving the catalog number, title, author and specific pages you wish reproduced.

University Microfilms

300 North Zeeb Road
Ann Arbor, Michigan 48106

A Xerox Education Company

72-26,333

FISCHER, Wolfgang Klaus, 1941-
METHODS FOR ACOUSTIC HOLOGRAPHY AND ACOUSTIC
MEASUREMENTS.

Newark College of Engineering, D.Eng.Sc., 1972
Engineering, electrical

University Microfilms, A XEROX Company, Ann Arbor, Michigan

PLEASE NOTE:

Some pages may have
indistinct print.

Filmed as received.

University Microfilms, A Xerox Education Company

METHODS FOR ACOUSTIC HOLOGRAPHY AND
ACOUSTIC MEASUREMENTS

BY

WOLFGANG KLAUS FISCHER

A DISSERTATION

PRESENTED IN PARTIAL FULFILLMENT OF

THE REQUIREMENTS FOR THE DEGREE

OF

DOCTOR OF ENGINEERING SCIENCE IN ELECTRICAL ENGINEERING

AT

NEWARK COLLEGE OF ENGINEERING

This dissertation is to be used only with due regard to the rights of the author. Bibliographical references may be noted, but passages must not be copied without permission of the College and without credit being given in subsequent written or published work.

Newark, New Jersey

1972

ABSTRACT

In this dissertation, a novel "four-step acoustical holographic imaging system" is described and several means for its implementation are analyzed both theoretically and experimentally. This system is compared with other methods of acoustical holography, (ie. permitting to obtain a visible, 3-D image of an object insonified with supersonic waves) and some of its advantages are indicated.

The use of optical holographic techniques to convert an arbitrary acoustic image to a visible image is investigated and a new method - the "holographic sound image converter" - is introduced and analyzed. This converter consists of the "holographic interferometer" and an appropriate "coupler". Unlike present acoustic detectors, it exhibits the ability to simultaneously detect a quantity related to the vibration amplitude at each point of the acoustical diffraction pattern. Other advantages of this technique are frequency selectivity and the possibility of amplification and "reference wave simulation." This converter is a non-scanned device; yet it features all of the desirable characteristics normally associated only with scanned, linear detectors.

The new technique of "shifted reference holographic interferometry" is presented. This technique, as shown

in the analysis, permits increasing the sensitivity of conventional time-averaged holographic interferometry by approximately one order of magnitude. Experimental results confirm this prediction.

Holographic techniques are also applied to the measurement of acoustic parameters and several ways of implementing this application are proposed and investigated. In a number of experiments, the advantages of the holographic method in the field of sonics and ultrasonics are demonstrated, and a theoretical relation comparing this method to the Schlieren method is developed and experimentally confirmed.

A theoretical and experimental study of some possible "couplers", each capable of augmenting the displacement amplitude of an acoustical diffraction pattern as it is transferred from a surface bounded by water to one bounded by air, is also conducted. The "couplers" investigated range from a simple, acoustic impedance transformer to a mosaic of velocity amplifiers.

A detailed study is conducted on the development and testing of a mechanical velocity transformer consisting of two lossy, nearly quarter-wave plates. The theoretical relations describing the behavior of such plates are developed and experimentally verified. An advantage

of 9.5 (19.6 dB) at 916 KHz has been obtained across the water/air interface - primarily due to the construction of tuned aluminum-epoxy plates.

A useful method for "tuning" quarter-wave metal-epoxy plates is introduced and demonstrated. Other methods suitable for the measurement of the speed of sound and the attenuation coefficient of epoxy are also discussed.

"Shifted reference holographic interferometry" and the partial impedance matching of water to air, afforded by the tuned velocity transformer, result in a high sensitivity of this optical detector of acoustic vibrations. It is shown that, by these methods, a "holographic sound image converter" having a threshold intensity of 2.8 mw/cm² at 1 MHz appears feasible. Higher sensitivities (1.6×10^{-11} w/cm²) and full realization of all of the advantages of the "holographic converter" are expected with the use of an "active coupler", ie. one which makes use of electronic amplification.

APPROVAL OF DISSERTATION
METHODS FOR ACOUSTIC HOLOGRAPHY AND
ACOUSTIC MEASUREMENTS

BY

WOLFGANG KLAUS FISCHER

FOR

DEPARTMENT OF ELECTRICAL ENGINEERING
NEWARK COLLEGE OF ENGINEERING

BY

FACULTY COMMITTEE

APPROVED: _____ CHAIRMAN

NEWARK, NEW JERSEY

JUNE, 1972

PREFACE

The recent success of holographic imaging with visible radiation (optical holography) has generated a new interest in acoustical holography. The realization of the full advantages of this acoustic imaging process is impeded, however, by both theoretical and technological limitations. The theoretical limitations are largely dictated by the necessity of using visible radiation to reconstruct a converted acoustical hologram which has been originally recorded with acoustic radiation. On the other hand, the technological limitations arise primarily from the lack of a suitable detector - a device which can convert the acoustical interference pattern to a visible pattern.

This latter consideration has motivated a study on the use of optical holographic techniques to achieve a more satisfactory acoustic image conversion. The application of such techniques appears particularly desirable since, among other advantages, it inherently obviates the need for scanning the receiving aperture.

The first chapter briefly discusses the various problems and limitations that presently confront the acoustical holographic imaging process. The need for a suitable sound detector is also introduced.

This need becomes more evident as some of the present, existing detectors are reviewed in Chapter II. Extensive references are cited in this discussion so that the interested reader may familiarize himself more fully with any particular device.

Unlike the converters described in Chapter II, the holographic and Schlieren methods discussed in Chapter III permit the "side-view" visualization of sound waves propagating in an optically transparent medium. These two methods are examined in some detail, both theoretically and experimentally, and their usefulness as measuring devices for determining acoustic parameters is demonstrated. Although these visualization schemes may appear irrelevant to the acoustical holographic imaging process, the theoretical techniques introduced in this chapter as well as the experimental results obtained with "frequency shifted" holograms are essential for later work. Furthermore, both methods are used extensively for the calibration of piezoelectric crystals.

Chapter IV discusses a number of optical interferometers which permit the detection and measurement of small vibration amplitudes. Included in this discussion is a technique for increasing the sensitivity of conventional, time-averaged holographic interferometry by

approximately one order of magnitude. The resultant system, denoted as the "shifted reference holographic interferometer" forms the basis of the "holographic sound image converter" which is described in Chapter V.

This chapter proposes a novel, four-step acoustical holographic imaging system of which the (optical) "holographic converter" is the central sub-system. This converter is composed of the "holographic interferometer" and an appropriate "coupler" which transfers the acoustic image (to be recorded) from one medium to another. The characteristics of the "holographic converter" are noted and compared to those of existing acoustic detectors. Also described are a number of possible, practical couplers.

One of these couplers, namely a simple velocity transformer consisting of two quarter-wave resonant plates, is analyzed in Chapter VI. The theoretical relations describing the behavior of such plates are developed and the means for realizing a practical, working system are presented. In particular, the experimental techniques used to construct, test and tune metal-epoxy plates are described in detail. In addition, their performance as determined from the frequency dependence of the displacement amplitude transmission coefficient of the resultant system, is compared to theoretical predictions.

Conclusions and further recommendations are discussed in Chapter VII.

The author wishes to thank the members of the thesis committee, Dr. Mauro Zambuto, Dr. Raj Misra, Dr. Warren Ball and Dr. Werner Wenisch for their valuable suggestions, criticisms, guidance, and encouragement throughout this study.

Special gratitude is also extended to Dr. Robert McMillan and Mr. Walter Schmiedskamp for their assistance in the solution of the countless problems encountered during the experimental phase of this work.

Of course, this research would never have been possible without the facilities provided by the Electrical Engineering Department of Newark College of Engineering and without the financial assistance provided by the New London Laboratory of the Naval Underwater Systems Center (formerly the U. S. Navy Underwater Sound Laboratory).

TABLE OF CONTENTS

	Page
ABSTRACT	ii
PREFACE	vi
LIST OF FIGURES	xii
LIST OF TABLES	xvii
Chapter	
I EXTENSION OF OPTICAL HOLOGRAPHY TO ACOUSTICAL HOLOGRAPHY	1
Historical Considerations	
Theoretical Limitations	
Technological Problem	
II REVIEW OF SONIC AND ULTRASONIC DETECTORS . . .	12
Non-Scanned Detectors	
Scanned Detectors	
III HOLOGRAPHIC AND SCHLIEREN SOUND VISUALIZATION SYSTEMS	50
The Holographic System for Visualizing Sound Waves	
The Schlieren System for Visualizing Sound Waves	
Special Case of Plane Progressive Sound Waves	
Experimental Results and Comparisons	
IV DETECTING AND MEASURING THE DISPLACEMENT AMPLITUDE OF VIBRATING OBJECTS	97

	Modified Michelson Interferometer	
	Laser Feedback Interferometer	
	"Holographic Interferometer"	
V	FOUR-STEP ACOUSTICAL HOLOGRAPHY WITH THE OPTICAL "HOLOGRAPHIC INTERFEROMETER"	121
	Generation and Transference of the Acoustical Hologram	
	Recording the Acoustical Hologram	
	Reconstructing the Converted Acoustical Hologram	
	The Optical "Holographic Acoustic Image Converter".	
VI	TWO QUARTER-WAVE VELOCITY TRANSFORMER (ACOUSTIC MATCHING PLATES)	146
	General Remarks	
	Design of Two, Lossy, Nearly Quarter-Wave Plates	
	Construction of Two Quarter-Wave Plates	
	Experimental Results	
VII	CONCLUSIONS AND RECOMMENDATIONS.	193
Appendix		
I	THEORY OF MULTILAYER FILMS FOR LONGITUDINAL ACOUSTIC WAVES	204
II	A LIQUID IMMERSION, PULSED SOUND TECHNIQUE FOR MEASURING THE SPEED OF SOUND IN THIN PLATES	214
	REFERENCES	223

LIST OF FIGURES

Figure		Page
1-1	Typical geometry for the holographic recording and reconstruction process	7
2-1	The Pohlman Cell	19
2-2	Töpler "dark-field" method for imaging the analog relief pattern	21
2-3	Method after Sokolov for imaging the analog relief pattern	23
2-4	Method for minimizing unwanted disturbances of the surface deformation	25
2-5	Real-time holographic imaging with the liquid surface deformation method	27
2-6	Arrangement of an ultrasonic grating in the liquid surface relief conversion system	28
2-7	A mechanically scanned image converter using a microphone point detector and a CRT for visual display	30
2-8	A mechanically scanned image converter using a plane, electronically simulated reference wave	32
2-9	An ultrasonic image converter which scans the voltage on the face of a mosaic of piezoelectric crystals	34
2-10	The basic ultrasonic camera	36
2-11	Arrangement for performing acoustical holography via the ultrasonic camera	38
2-12	Use of an image orthicon for ultrasonic image visualization	40
2-13	System for optically scanning a matrix of photodiodes to achieve image conversion	41

Figure	Page
2-14 An optically scanned ultrasonic image converter which responds to the velocity of the vibrating plane P_2	43
2-15 A converter which responds to the slope of the surface displacement	45
3-1a A typical Schlieren image showing the reflection and transmission of a sound wave by an aluminum plate	52
3-1b A reconstructed holographic image showing a similar phenomenon as above	52
3-2 Schematic of the basic geometry of the holographic method for visualizing sound waves	54
3-3 Diagram for calculating the mutual coherence at point P	56
3-4 Various methods of reconstructing images from holograms which have been recorded without the use of a diffusion screen	62
3-5 Schematic of the basic Schlieren system	65
3-6 Diagram for calculating the irradiance in the Schlieren image at x'	66
3-7 Theoretical distribution of irradiance due to a plane, progressive sound wave	72
3-8 Experimental arrangement used to record "zero order" holograms as well as Schlieren images	74
3-9 Two views of the above experimental arrangement	77
3-10 A Schlieren image showing the diffraction of a (1 MHz) sound wave by a $1/8''$ x $1''$ slot	80
3-11 A Schlieren image showing the focusing effect of a $1''$ I.D. plastic cylinder on a (1.64 MHz) sound wave	80

Figure		Page
3-12	Reconstructed image showing the "near-field" and "far-field" radiation patterns of a small crystal vibrating at 328 KHz	85
3-13	Reconstructed image of the standing wave pattern generated by a large crystal vibrating at 164 KHz	85
3-14	Reconstructed image of a diffusion screen showing the outline of a (3.23 MHz) sound wave	87
3-15	Image of the same sound wave as above, but reconstructed from a hologram which was recorded without the use of a diffusion screen	87
3-16	Comparison of the radiance distribution in the images formed by a Schlieren system and two holographic methods	89
3-17	Arrangement used to record holograms with a "frequency shifted" reference wave	91
3-18	Comparison of holographic reconstructed and Schlieren images	92
4-1	Arrangement of the modified Michelson interferometer	98
4-2	The laser feedback interferometer and a simple method of analyzing its principle of operation	104
4-3	Investigating the vibrations of a piezoelectric crystal with the laser feedback interferometer	110
4-4	Investigating the vibration of a piezoelectric crystal with the holographic interferometer	113
4-5	Arrangement of the "shifted reference holographic interferometer" and geometry for calculating ϵ_{mR}	115
5-1	Step 1 - Forming the acoustical hologram on surface S_2	123

Figure		Page
5-2a	Step 2 - Recording an optical hologram of the surface S_2 with a shifted reference frequency	126
5-2b	Step 3 - Photographing the reconstructed image of the optical hologram to obtain the converted acoustical hologram	126
5-3	Step 4 - Reconstructing the converted acoustical hologram with visible radiation	128
5-4	Performance of an infinitely thin membrane used as a coupler	131
5-5a	The "stepped horn" velocity transformer	135
5-5b	The two quarter-wave mechanical velocity transformer	135
5-6	A mechanical-electrical-mechanical velocity amplifier suitable for use with the holographic sound image converter	139
6-1	A resonant mechanical transformer used for velocity augmentation across the air/water interface	148
6-2	Typical frequency response of the displacement amplitude transmission coefficient	153
6-3	A completed steel-epoxy casting shown in its curing stage	167
6-4	An arrangement which may be used to test the performance of metal-epoxy resonant plates	171
6-5	Illustration of the actual reflection method used to measure the relative vibration amplitude of the epoxy surface	172
6-6	Oscillogram obtained as per Figure II-1 for a low-frequency, steel-epoxy system	179
6-7	Transducer used in Figure 6-4 to determine the frequency dependence of $ t_d $	179

Figure		Page
6-8	Frequency response of the relative gain of a steel-epoxy system for the epoxy thicknesses indicated in Table 6-4	181
6-9	Frequency response of a "tuned" aluminum-epoxy system	185
I-1	The propagation of a sound wave through three different media (normal incidence)	205
I-2	Sound transmission from medium "w" to medium "a" through two intervening layers	211
II-1	The pulsed sound, immersion technique for determining the half-wave resonant frequency of thin plates	215
II-2	Oscillograms obtained per Figure II-1 for steel (a, b and c) and polystyrene (a', b' and c') plates	217

LIST OF TABLES

Table		Page
2-1	Sensitivities of the various detectors discussed in Chapter II	47 48
6-1	Tuned resonant plates (water-steel-epoxy-air)	156
6-2	Tuned resonant plates (water-aluminum-epoxy-air)	158
6-3	"Untuned" aluminum-epoxy plates	161
6-4	Tuning data for a steel-epoxy system	177
6-5	Performance comparison between high and low-frequency plates	188

Chapter I

EXTENSION OF OPTICAL HOLOGRAPHY TO ACOUSTICAL HOLOGRAPHYHistorical Considerations

The word "holography" is used to denote the two-step process of wavefront recording and reconstruction. This process is by now well understood and has been thoroughly analyzed.⁵⁴ Since its conception by Gabor,²⁸ holography lay relatively dormant until the development of the laser which provided the necessary tool - namely an intense, nearly monochromatic and highly coherent source of light.

As is well known, in reconstruction, the holographic imaging process produces, besides others, a wavefront which is identical to that which originated from the object during the recording process. Hence, the corresponding holographic image cannot be distinguished from the original object and is, necessarily, three-dimensional in nature. While this three-dimensional character of the reconstructed image is probably the most sensational feature of holography, equally important are its interferometric properties. Some of these properties will be discussed more fully in chapters III and IV.

In Gabor's original work, the three wavefronts originating from the hologram during the reconstruction process were coaxial; thereby making it difficult to obtain a clear,

undisturbed image of the object. However, complete spatial separation of these wavefronts is possible with the introduction of an off-axis reference beam⁵⁴ (as opposed to the on-axis reference beam used by Gabor). Due to the success of this technique, nearly all holograms are now recorded by an appropriate split-beam technique.

The extension of optical holography to acoustical holography stems from the consideration that the energy used for the holographic recording process must be

1. of a wave nature
2. sufficiently coherent

Acoustic fields generally meet these two requirements. Since most acoustic imaging is performed in a gaseous or liquid medium (which cannot support acoustical transverse waves) the radiation normally consists of longitudinal sound waves which, of course, obey the laws of wave propagation. The condition that these waves be sufficiently coherent is met by the fact that the electronic oscillators which excite the sound transducers can achieve stabilities of one part in a million. In water at 1 MHz, this would result in a coherence length of 1.5 Km. - a quantity which is enormous compared to the coherence length of a laser.

Although the fulfillment of the above two requirements by acoustic waves predicts the possibility of successfully constructing an acoustical diffraction pattern, and therefore

an acoustic holographic pattern, some difficulties arise in the recording of this diffraction pattern and in the reconstruction of the acoustical hologram. A brief resume of the major problems which beset acoustical holography at its present state follows.

Theoretical Limitations

It should be noted that the complete acoustical holographic process requires

1. The construction of an acoustical interference pattern (acoustical hologram) with (usually longitudinal) acoustic waves of relatively large wavelengths (generally 0.15 to 1.5 mm in water)
2. The recording of this interference pattern to obtain the converted acoustical hologram
3. The reconstruction of the converted acoustical hologram with a completely different form of radiation (light) - This radiation is transverse in nature and of extremely short wavelength (6.328×10^{-4} mm for a HeNe laser)

The different nature of the recording and reconstructing waves causes primarily technological problems in recording. The fact that their wavelengths are vastly different imposes severe theoretical limitations on the entire acoustical imaging process.

Most of the difficulties listed below are common to all holographic imaging systems, but are accentuated in acoustical holography by the necessity to use relatively long wavelengths in recording and very short wavelengths

for the reconstructing wave.

Specular Reflections. Relative to ultrasonic wavelengths (0.15 to 1.5 mm) most objects appear essentially smooth and act as reflectors with varying degrees of reflecting power rather than as diffusers. Therefore, imaging such objects with acoustic waves presents problems analogous to those encountered in optical holography when imaging a number of mirrors which are situated in a dark room.

Speckling.¹⁶ This phenomenon occurs whenever a "rough" surface is "illuminated" with coherent radiation. In optics, the light which is reflected from neighboring points on the object produces a stationary interference pattern in space. To the eye, this diffraction pattern appears as a speckled pattern superimposed on the scattering surface.

The apparent size of these "speckles" depends on the resolution of the imaging system. Hence, since the resolution of acoustical imaging systems can be as low as several centimeters, the size of these "speckles" can be quite large relative to the object; and parts of the object in the reconstructed image can be completely obstructed by these "speckles".

Speckling can be minimized by increasing the resolution of the imaging system. Other techniques which attempt

to decrease the grain size make use of the randomness of the speckled pattern.

Resolution Loss. Assuming that the acoustical holographic imaging system is capable of resolving the individual acoustical interference fringes, the highest resolution is obtained by the aperture that intercepts the largest number of these fringes (Rayleigh criterion). It follows that the size of the aperture, for a given resolution, increases with the wavelength.

Because of the large wavelength of acoustical radiation, the resolution, to which one is accustomed in optical holography, cannot be attained in acoustical holography in a practical manner. As a comparison, the resolution that is obtained from a 1 cm.² optical hologram ($\lambda = 6328 \text{ \AA}$) can be achieved in acoustical holography only if the detector aperture is at least 560 square meters (@ 1 MHz. in water).

Image Distortion. Besides obvious sources of distortion such as turbid media, interaction of the sound wave with the object, non-linearity of the medium, etc. a major source of image distortion results from the small ratio μ of reconstructing to recording wavelength. Meier⁶³ has determined the effect of such scaling as well as of the scaling of the hologram dimensions, on the magnification of the reconstructed image. With reference to Figure 1-1, if the dimensions of the hologram and object are small

compared to z_o , z_r and z_c , then

$$M_{lat} = \frac{m}{1 + \frac{m^2}{\mu} \frac{z_o}{z_c} - \frac{z_o}{z_r}} \quad (1)$$

upper sign - virtual image
lower sign - real image

$$M_{long} = \pm \frac{1}{\mu} M_{lat}^2 \quad (2)$$

where

M_{lat} = lateral magnification of the reconstructed image

M_{long} = longitudinal magnification of the reconstructed image

m = the ratio of the dimensions of the hologram during the reconstruction process to the dimensions of the hologram during the recording process (hologram dimension scaling)

μ = the ratio of the wavelength of the radiation during the reconstruction process to the wavelength of the radiation during the recording process

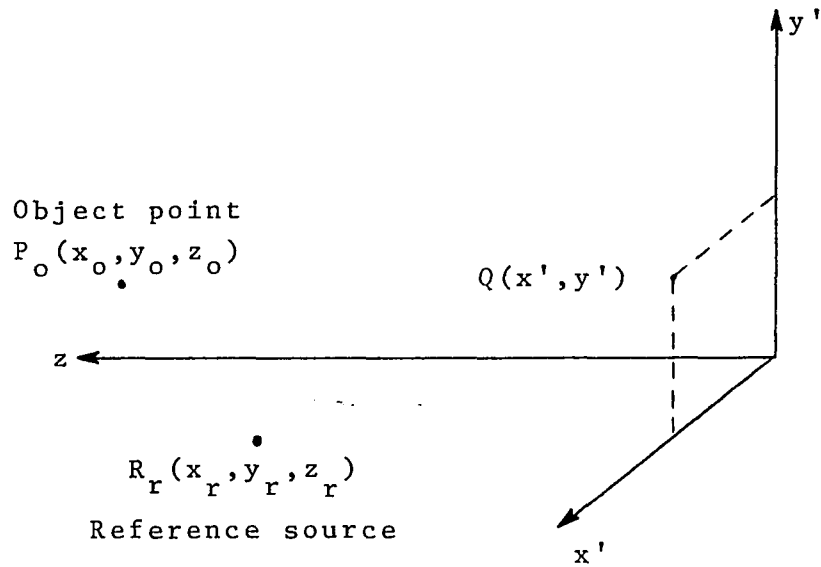
z_o = radius of curvature of the object beam

z_r = radius of curvature of the reference beam

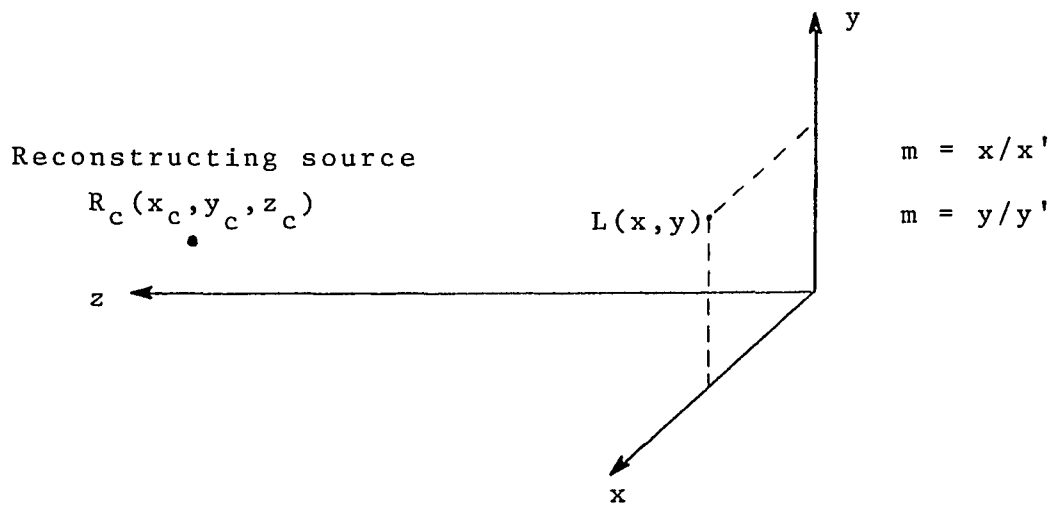
z_c = radius of curvature of the reconstructing wave

In optical holography neither hologram nor wavelength scaling is usually necessary. With $m = \mu = 1$, an undistorted image ($|M_{lat}| = |M_{long}|$) of unit magnification is readily obtained by choosing $z_c = z_r$.

The situation is quite different in acoustical holography since μ is commonly 10^{-4} . Without any scaling of the hologram dimensions ($m=1$), the longitudinal magnification of the reconstructed image usually exceeds the lateral



Geometry for the recording process



Geometry for the reconstruction process

Figure 1-1 Typical geometry for the holographic recording and reconstruction process

magnification by several orders of magnitude.

It is possible, however, to obtain an undistorted image, that is, $|M_{lat}| = |M_{long}|$ when

$$m(1 - mz_0/z_c) = \mu(1 - z_0/z_r) \quad (3)$$

In particular, if the reference and reconstructing waves are both plane ($z_r = z_c = \infty$), an undistorted image results when $m = \mu$. Hence, for this case, the hologram dimensions must be reduced by 10^4 . Another special condition arises when $z_r = z_0$ (Fourier hologram), in which case $|M_{lat}| = |M_{long}| = \mu$ when $m = z_c/z_r$.

Unfortunately, this simple concept of scaling in order to achieve an undistorted reconstructed image cannot be fully realized in practice since the scaled hologram is too small to successfully reconstruct the image and the resultant image, which is also demagnified by 10^4 , requires the use of a microscope to view it properly.

Thurstone^{92,93} has investigated other types of scaling with some encouraging results, but the fact remains that the necessary wavelength scaling imposes serious limitations on the three dimensional aspect of acoustic holography.

Technological Problems

The second major type of problems that confront acoustical holography results from the lack of a suitable device that can record the acoustical diffraction pattern in a completely satisfactory manner.

It may be appropriate to list some of the desirable features that a suitable detector should display

1. Low system complexity
2. High sensitivity
3. High selectivity to the frequency of vibration
4. High resolution capability
5. Insensitivity to the angle of incidence

In addition, although the introduction of non linearity is mandatory in the recording of a hologram, the detector itself may be either a linear or a square-law device - a fact which is important in acoustical holography since a linear detector allows the "simulation" of a reference wave (see Chapter II).

Of course, the detector should also respond to some characteristic of the acoustical interference pattern. The characteristics that are often used can be grouped as follows

1. Basic parameters
 - a. instantaneous pressure
 - b. velocity
 - c. vibration amplitude
 - d. density
2. Quadratic effect
 - a. radiation pressure
3. Secondary effects
 - a. heating
 - b. cavitation
 - c. action on a photographic emulsion

Evidently, such a large number of characteristics of the acoustical diffraction pattern leads to a variety of ultrasonic detectors. A number of these are described in Chapter II, and from that discussion, it will become apparent

that those systems which respond to the instantaneous pressure, velocity or vibration amplitude (linear detectors) can be quite sensitive, but usually require some means of scanning. This scanning, which may be mechanical, optical, or electronic, usually makes the system rather complex.

The so-called non-scanned detectors are usually non-selective devices which make use of secondary effects, and normally their sensitivity is several orders of magnitude lower than that of the scanned detectors (essentially because electronic amplification is not possible).

Furthermore, most ultrasonic detectors require that the sound wave impinge at near normal incidence. However, this requirement may be of relatively minor importance if the reference wave can be simulated artificially.

Remembering the above desirable features, it will become evident that, despite the existence of a great variety of ultrasonic detectors, none of these at present, fulfill their function in such an admirable manner as does their counterpart, the photographic emulsion, in optical holography.

The research which is described in this dissertation is concerned with this problem of recording the acoustical diffraction pattern. In particular, the concept of using

the interferometric properties of optical holographic techniques to record the acoustical diffraction pattern, is explored. The work encompasses a somewhat detailed study of using acoustical resonant "matching" plates to augment the vibration amplitude of points within the acoustical interference pattern. Other methods of amplification (not studied in detail) are also proposed (see Chapters V and VI).

Chapter II

REVIEW OF SONIC AND ULTRASONIC DETECTORS

In this chapter, some of the numerous acoustic image detectors are briefly described. The various image converters are presented in two major groups, namely non-scanned and scanned detectors. Non-scanned detectors are further classified in accordance with the dominant mechanism responsible for detection, while scanned detectors are classified on the basis of the type of scanning used.

As these detectors are discussed, their application to acoustical holographic systems is noted. Finally, a comparison of non-scanned and scanned detectors is made with reference to the desirable characteristics listed on page 9.

Further surveys and listings of acoustic image detectors can be found in references 7, 35, 51, 75, 86 and 96. Of these, the surveys by Rozenberg⁷⁵ and more recently by Berger⁷ are probably the most complete.

Non-Scanned Detectors

The non-scanned detectors which are described here generally have one common feature - they do not make use of mechanical resonance. Since the detection is usually based on quadratic or secondary effects, these detectors are square-law devices and therefore, they exhibit no frequency selectivity.

Photographic and chemical. The fact that acoustic radiation influences a photographic emulsion was first reported by Marinenco⁵⁶ in 1933. He apparently made use of the fluorescence which is associated with cavitation of the medium.⁴⁴ It was this weak emission of light which caused the latent image. His results were confirmed by Ernst²³ and Bennet⁵ who irradiated photographic emulsions with relatively high acoustic intensities (greater than 1 watt/cm²).

Later Bennet⁶ demonstrated that luminescence is not a necessary feature to produce an image, i.e. a direct action of the acoustic radiation on the emulsion exists. Using both water and a developer solution as the transmitting medium, Bennet also found that the degree of softening of the emulsion affected the speed of the image formation.

This effect was confirmed by Berger⁸, noting that by pre-soaking the emulsion for 3 to 4 hours, the ultrasonic exposure time can be reduced from 4 hours to one hour. He also confirmed that emulsion speed, i.e. the light sensitivity of the emulsion, has no effect on the ultrasonic exposure time.

The above methods required that the emulsion be exposed to the sound radiation in a darkroom. But in the same article⁸, Berger also reported exposures without darkroom

techniques. With an iodine-water solution as the transmitting medium, a light-exposed photographic emulsion yellowed in irradiated areas; furthermore, these areas became more resistant to fixing. Thus, upon fixing, the film is clear in unirradiated regions and yellow in irradiated areas.

As a variation of this technique, Torkikai⁹⁴ and Arkhangel'skii² ultrasonically exposed ordinary light-exposed photographic paper suspended in a developer solution. It was reported that the ultrasonic field is able to accelerate processes which are associated with the diffusion of the developer into the gelatin layer of the photographic paper. By an exhaustive set of experiments, Arkhangel'skii determined the relative blackening of the paper as a function of the ultrasonic exposure time and the acoustic intensity. A threshold intensity of 0.05 watt/cm^2 for a 40 second exposure time was reported. He further noted that the resolution of the detector could be equal to the thickness of the photolayer (0.01 mm.) if streaming effects are eliminated.

The method of ultrasonically exposing a photographic emulsion has been used to record acoustical holograms. In a manner completely analogous to split-beam optical holography, Greguss³⁴ used two sound waves, one acted as a reference wave while the other insonified the object. A hologram

was produced by subjecting a photographic emulsion to the intense radiation of the two interfering sound waves.

When water, which normally contains air bubbles, is subjected to intense acoustic radiation, cavitation of the water medium results. This process which releases oxygen and subsequently hydrogen peroxide (H_2O_2), can be used to oxidize various organic compounds.

37,77

Rust, Haul, and Studt^{37,77} reportedly made use of this method by oxidizing a potassium-iodide-starch solution. They constructed a mosaic of 8x8 cells and filled each with the potassium-iodide-starch solution. Upon oxidation, this solution releases iodine; hence the color of the solution becomes blue in areas of high ultrasonic intensity. The authors performed several experiments which indicated that the amount of iodine separated from the solution is linearly proportional to the ultrasonic intensity and exposure time. It was also demonstrated that the individual cell thickness must be larger than one wavelength in order to obtain any chemical reaction. The threshold intensity of this method was reported to be 0.4 watt/cm^2 (presumably cavitation did not occur below this value), however, by adding small amounts of carbon tetrachloride (CCl_4) or chloroform to the medium the threshold intensity was lowered to 0.07 watt/cm^2 .

Other compounds which have been oxidized ultrasonically are leucobases.²⁴ These substances are obtained from dyes and, upon oxidation, they regain their original color.

In a somewhat different manner, Bennet⁴ used sound waves to accelerate the reaction between starch and iodine. He constructed a starch plate and placed it in water to which a dilute solution of iodine had been added. Those areas which were irradiated by ultrasound assumed a bluish tint, and the resultant image was semi-permanent. A sensitivity of 1 watt/cm² for a one minute exposure time was reported.

Thermal. Any material which is irradiated by super-sonic waves will absorb a certain amount of energy and will usually convert most of this into heat. This heating effect can be utilized either directly or indirectly in both scanned and non-scanned detectors.

²⁴ Ernst and ⁷⁷ Rust made use of this effect by irradiating thermochromatic materials (the color of these materials depends on their temperature) and recording their changes in color in areas of high acoustic intensity.

This method was further advanced by Woodmansee⁹⁷ who suggested the use of liquid crystals, a good introduction to which is given by Ferguson.²⁵ Woodmansee noted that certain mixtures of cholesteric liquid crystals change

their color from red to blue within one second for a temperature change of 1°C. Holograms using a liquid crystal display have recently been reported by Augustine.³

The heating effect may also be used to affect the luminescence of thermo-sensitive phosphors which have previously been saturated (excited) - usually by ultraviolet radiation.

53

Leistner and Herforth investigated the effect of ultrasound on the luminescence of continuously excited phosphors and found that the luminescence may be increased or decreased when irradiated ultrasonically.

78

Schreiber and Degner also saturated a phosphor (ZnS-Cds) with ultraviolet radiation, and then removed the ultraviolet source and ultrasonically exposed the phosphor from 5 to 30 seconds. They demonstrated that the phosphor experienced an extinction of phosphorescence in areas of high acoustic intensity.

69

Petermann, using a Ca-SrS phosphorescent plate, obtained similar results. He reported a threshold intensity of 0.05 watt/cm² with a resolution of 0.2 mm at 3 MHz and with a one minute exposure time. Chomse, Hoffmann, and Seidel¹⁴ observed this quenching also with organic phosphors.

Mechanical and Optical. A very simple and quite sensitive mechanical detector is the Pohlman cell which^{71,72}

makes use of the "radiation pressure" of acoustic waves. As described by Borgnis,¹⁰ "radiation pressure" is not a pressure in the usual sense of the word, but rather, it is a tensor. This tensorial characteristic is utilized in the Pohlman cell in the following manner.

Referring to Figure 2-1, the aluminum disks in the upper and lower region of the cell where no sound is present, are randomly oriented due to normal thermal motion, and light reflected from these flakes uniformly illuminates the screen. However, under the influence of ultrasound, the "radiation pressure" exerts shearing forces on the disks and tends to align them normally to the ultrasonic beam. The resultant light distribution on the screen will then consist of bright areas due to light reflected from aligned disks, superimposed on a grey background due to light reflected from randomly oriented disks. A threshold intensity of 3×10^{-7} watt/cm² with a reaction time of several minutes was reported.

It is apparent that if a sound wave is to be detected, it must be able to orient a large number of aluminum disks in the same direction. Hence, only sound waves which are nearly plane can be detected successfully. A consequence of this is that the Pohlman technique is limited to the through-transmission method of material inspection,⁹⁵ i.e. Gabor holography.

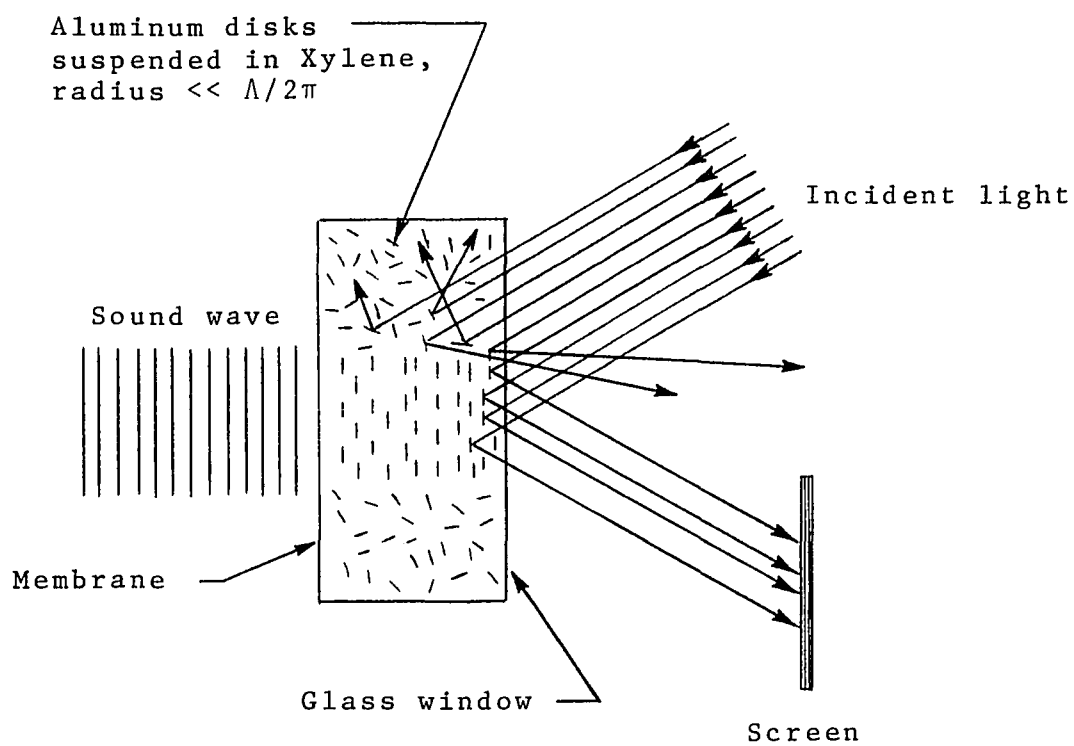


Figure 2-1 The Pohlman Cell

The "radiation pressure" may also be used to deform a surface. If the surface is a liquid-air interface, it has been shown⁶⁷ that the surface deformation due to two interfering acoustic waves consists of the superposition of the following three components:

1. a large, static and spatially uniform displacement
2. a spatially varying deformation independent of time
3. a small spatial and time varying deformation

The time independent, spatially varying deformation is the dominant information-carrying process and it is a function of the resultant acoustic intensity distribution at the interface. The recording of this deformation constitutes the converted acoustical hologram.

The deformed surface (analog relief pattern) may be observed by reflecting light from (or refracting light through)⁷⁹ the surface. (Schuster shows that the reflection method is more sensitive than the refraction method.)

Using reflected light, there are basically two methods available for forming an image of the analog relief pattern.

1. The Töpler "dark-field" method is illustrated in Figure 2-2. The lens is positioned so that it images the water surface onto the screen, and the spatial filter (which is situated in the focal plane of the lens) is adjusted, in the absence of ultrasound at the interface, so that none of the light is allowed to pass. When the surface is deformed by a sound wave, some of the light is deflected past the "stop"

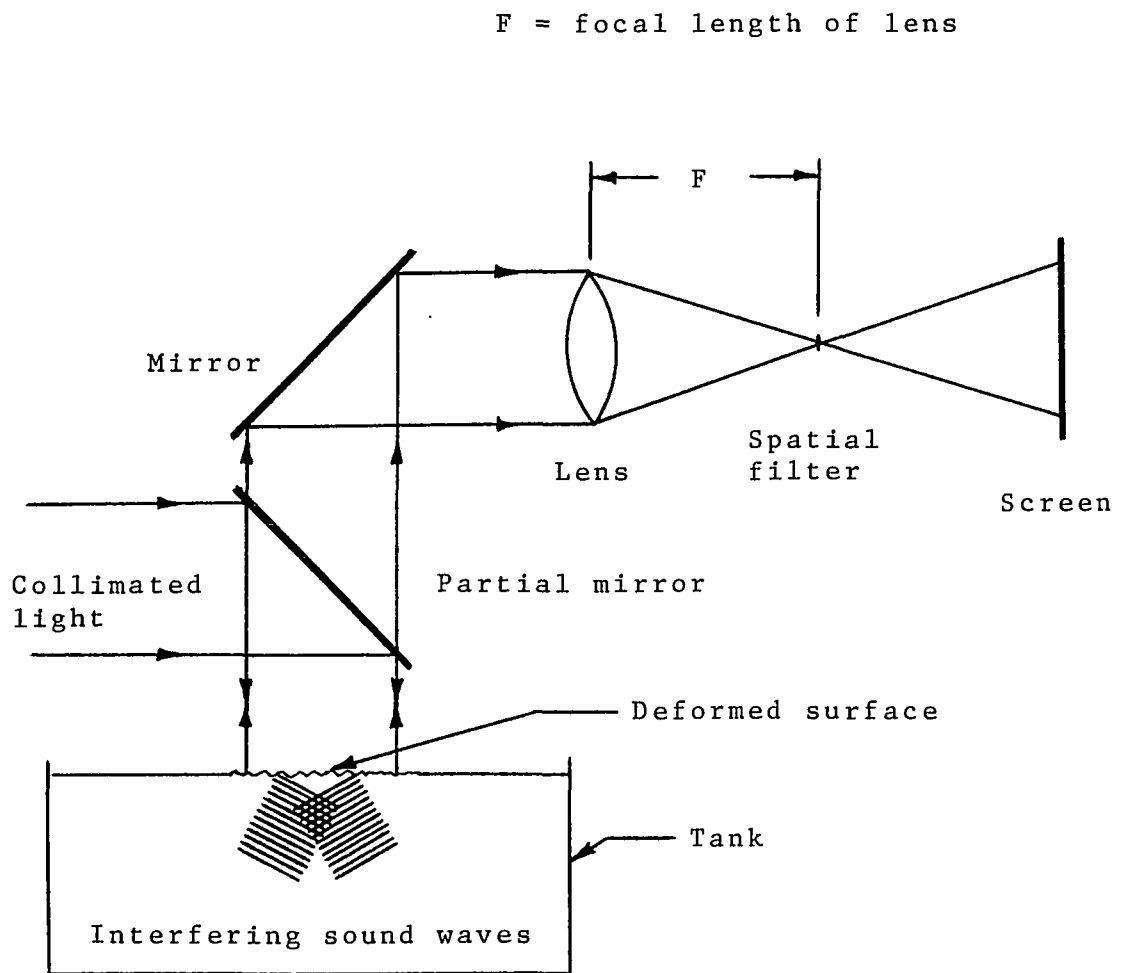


Figure 2-2 Töpler "dark-field" method for imaging the analog relief pattern

and illuminates the screen. Hence, regions of the surface which are insonified are imaged brightly on a dark background. Of course, the "negative" of this image can be obtained if the "stop" is replaced with a circular aperture which passes only undeflected light.

88

2. A method suggested by Sokolov (see Figure 2-3) and further analyzed by Pigulevskii (70) also relies on the curvature of the different surface elements of the relief pattern. An image of the relief pattern is formed on the screen by virtue of the fact that the cross-sectional area and hence the radiance of the light pencils reflected from differential elements of the relief pattern varies with the curvature of that element. Consequently, in the image, insonified regions of the surface appear darker than those regions which are not insonified.

Although the liquid surface "levitation" technique is a simple and convenient conversion method, analyses show that the surface deformation is not directly proportional to the acoustic intensity at the interface; but rather, the conversion process suppresses high spatial frequencies. This decreases the resolution and introduces image distortions. Further distortions result from the large, static displacement which is spatially uniform only for the interference of two unbounded plane waves.

The optical system which is used to image the analog relief pattern produces a "high-pass" filtering effect on the image since the irradiance in the image is related to the spatial derivative of the height of each differential surface element. Hence, the overall conversion process from the acoustic intensity at the liquid-air interface to the irradiance in the optical image exhibits "band-pass"

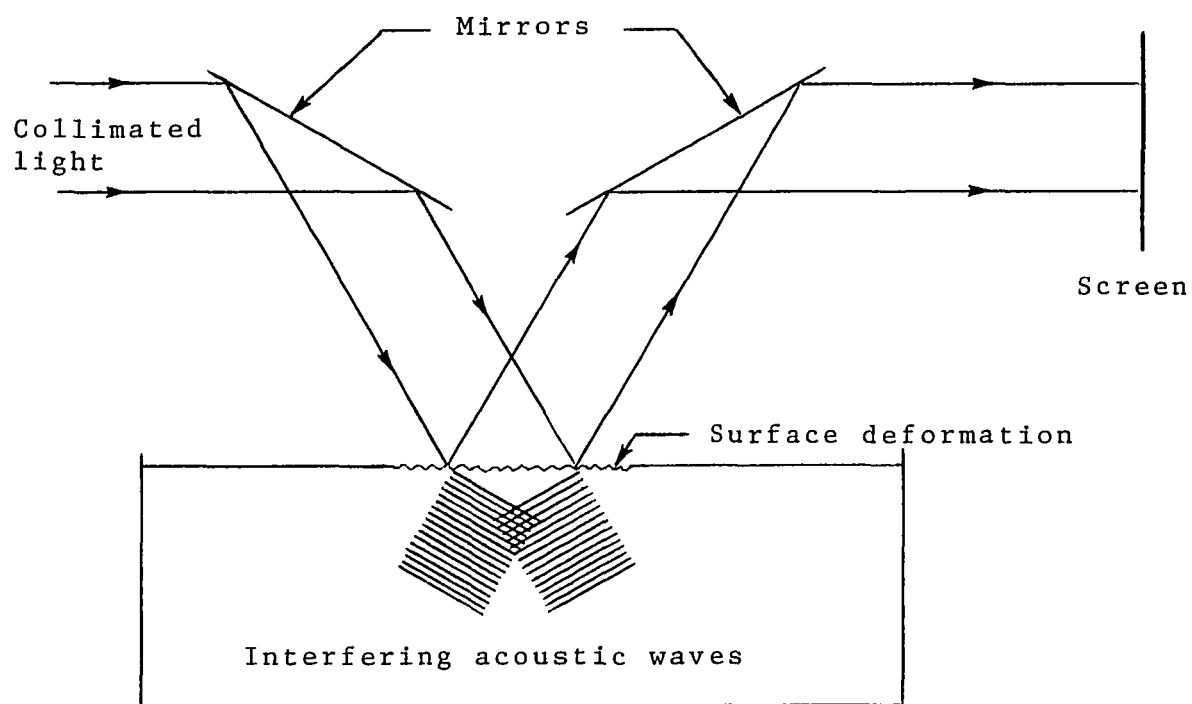


Figure 2-3 Method after Sokolov for imaging the analog relief pattern

characteristics.

68

Mueller and Sheridan used the Sokolov method of recording acoustical holograms. However, the quality of the reconstructed images was poor because of aberrations due mainly to streaming and oscillatory disturbances of the water surface.

29

These disturbances can be minimized by using a separate container for the deforming liquid. This also permits the use of a liquid having a low surface tension to increase the spatial frequency response of the surface (see Figure 2-4).

The Töpler and Sokolov recording techniques could be performed with "white" light. It is recognized, however, that the analog relief pattern is itself a hologram. Hence, if collimated, coherent light is reflected from (or refracted through) the deformed surface, the deformation will phase modulate the light to form an image of the original object. The arrangement for this one-step imaging process is illustrated in Figure 2-5. The spatial filter "stops" the zero diffraction order which is noise and allows the first diffraction orders to form the two images. The viewing optics merely magnify the lateral dimensions of the image.

11,12,84

Several authors have used this real-time imaging technique and obtained some of the best hologram reconstructions to date. Threshold intensities have been reported to be

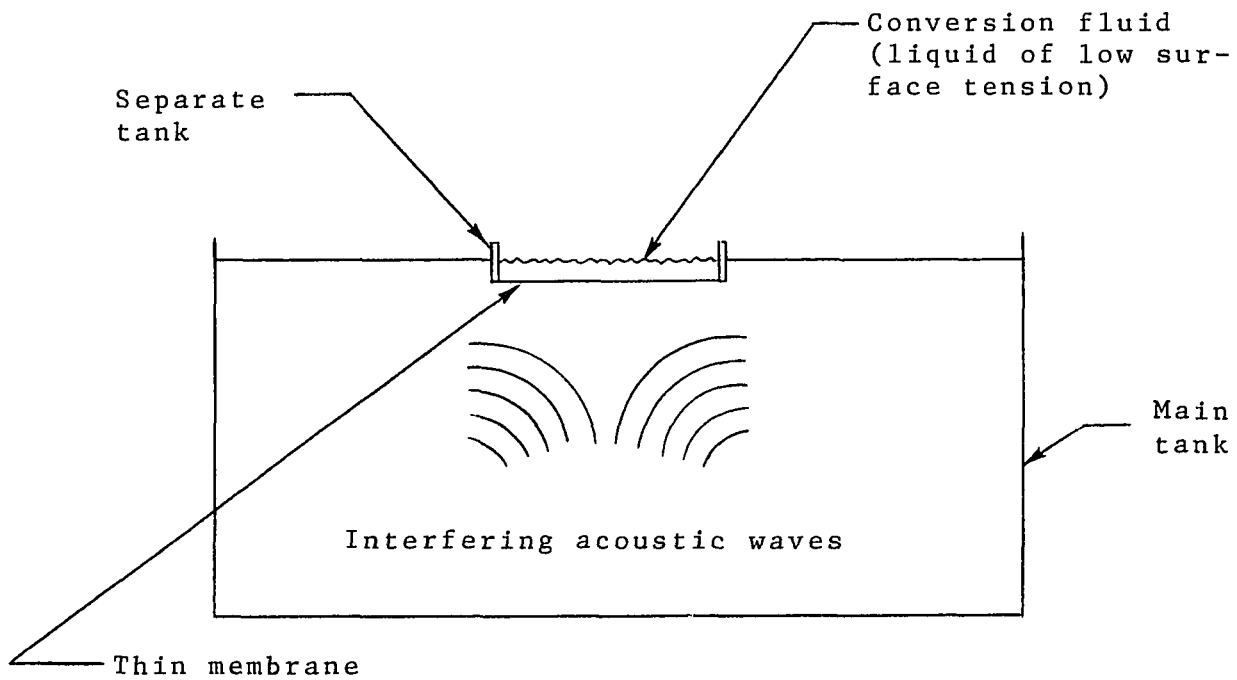


Figure 2-4 Method for minimizing unwanted disturbances of the surface deformation

between 1.5 and 10 milliwatt/cm².

As a variation of this technique, Young and Wolf⁹⁸ deformed a thermoplastic material which was heated during the ultrasonic exposure. Upon cooling the plastic, a permanent record of the deformation was obtained ("phase" hologram).

30

Recently, Green refined the liquid-surface-relief method by eliminating the acoustic reference wave and using instead an ultrasonic diffraction grating to modulate the acoustic image onto a high frequency, spatial carrier (see Figure 2-6). The technique appears limited, however, to "focused image holograms".

Scanned Detectors

It is apparent that detectors which make use of mechanical resonance can increase both their selectivity and sensitivity. Further, if the acoustical signal is converted to an electrical signal, even greater increases in sensitivity can be realized by utilizing electronic amplification.

Because of the relatively low ultrasonic frequencies (1 - 10 MHz.) such linear detectors are readily available; however, with the exception of the detectors suggested by this author (see Chapter V), all resonant detectors proposed to date must be scanned in order to explore the various

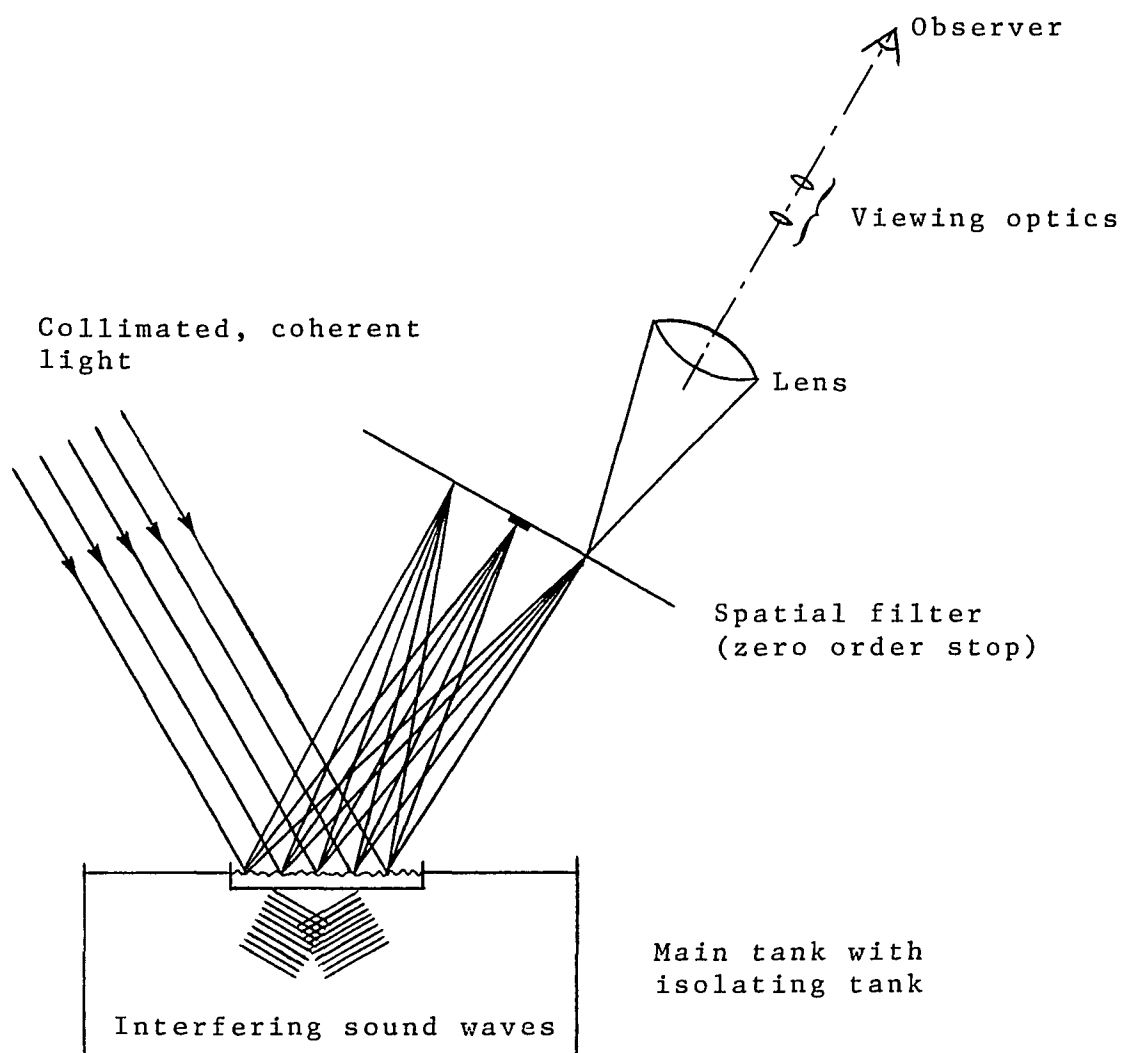


Figure 2-5 Real-time holographic imaging with the liquid surface deformation method

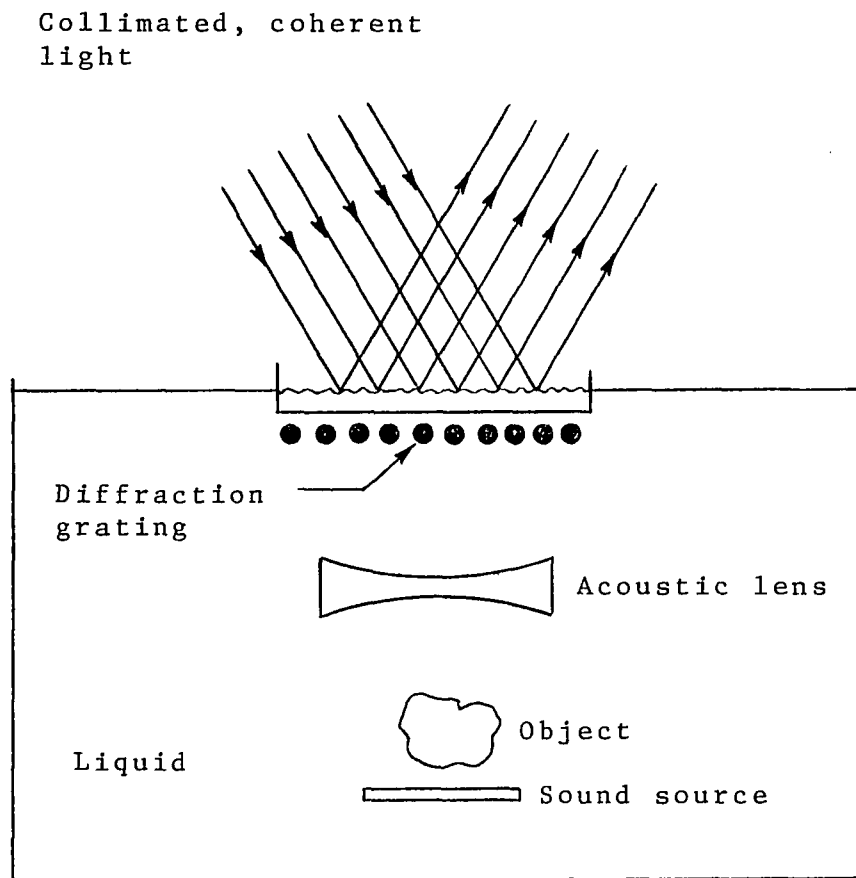


Figure 2-6 Arrangement of an ultrasonic grating in the liquid surface relief conversion system

points on the hologram plane.

Another disadvantage of all resonant detectors is their extreme angular sensitivity. In order to minimize lateral "spreading" of the acoustical disturbance, the incident sound waves must impinge nearly normally to the detector surface. In practice, this would preclude their use in split-beam acoustical holographic imaging systems since the angular separation between the object and reference waves is limited to a few degrees.

This problem, however, is effectively solved by "simulating" (usually electronically) the reference wave. Since the detector itself is linear, the correlation between the reference and object signals at each point of the aperture can be performed electronically and the non-linearity, which is mandatory for the recording of any hologram, can be introduced at a later stage of the detection process (see Figure 2-7). By appropriate programming, any reference wave can be simulated.¹⁹ Hence, with this technique, if the object wave can be selected to be nearly normal to the detector aperture, no acoustical interference pattern is actually formed; thus greatly reducing image distortion.

Obviously the detector aperture can also be scanned with a square-law device such as a thermocouple probe,²¹ but the more interesting acoustical image converters which will

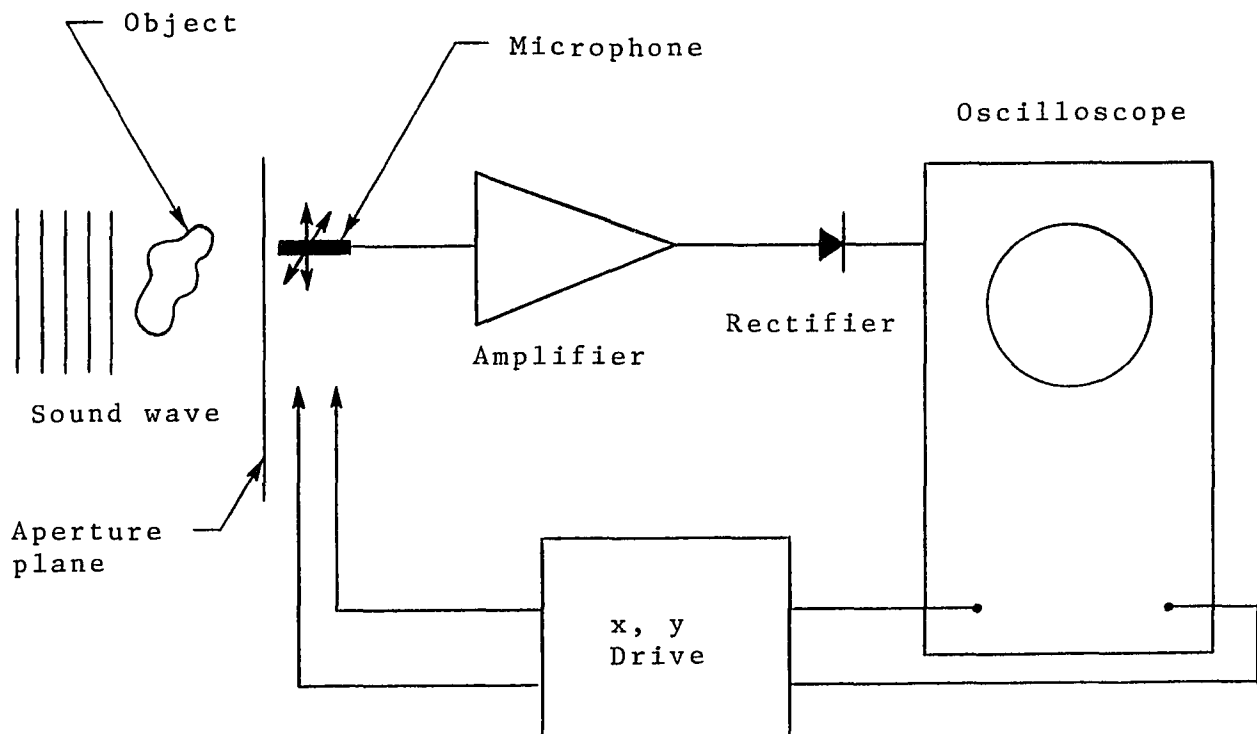


Figure 2-7 A mechanically scanned image converter using a microphone point detector and a cathode ray tube for visual display

be described presently make use of scanning with linear detectors.

Mechanical. A simple, scanned image converter is illustrated in Figure 2-7. A microphone (21 KHz) mechanically scans the aperture plane by means of the X, Y driving signal. The amplified and rectified signal then intensity modulates (z-modulates) a CRT whose electron beam is deflected by the same X, Y drive; so that the radiance of a point on the CRT is proportional to the acoustic pressure of the corresponding point in the aperture plane. The resulting radiance distribution may be photographed to obtain a permanent record of the diffraction pattern of the object.

Since the microphone is a linear device, it is possible to electronically simulate an acoustical reference wave. This was demonstrated by Massey⁵⁹ and Metherell⁶⁴ (see Figure 2-8). In this arrangement the phase of the electrical "reference" signal is independent of the instantaneous sensor position; hence, a plane wave, normally incident to the hologram plane is simulated. The light bulb introduces the necessary non-linearity discussed on page 29.

Similar arrangements, using a piezoelectric crystal as the "point" transducer, have also been used in mechanically scanned detection systems.^{11,12,20,73,83} The piezoelectric crystal is chosen to resonate in its fundamental thickness mode, i.e. thickness = $\Lambda/2$.

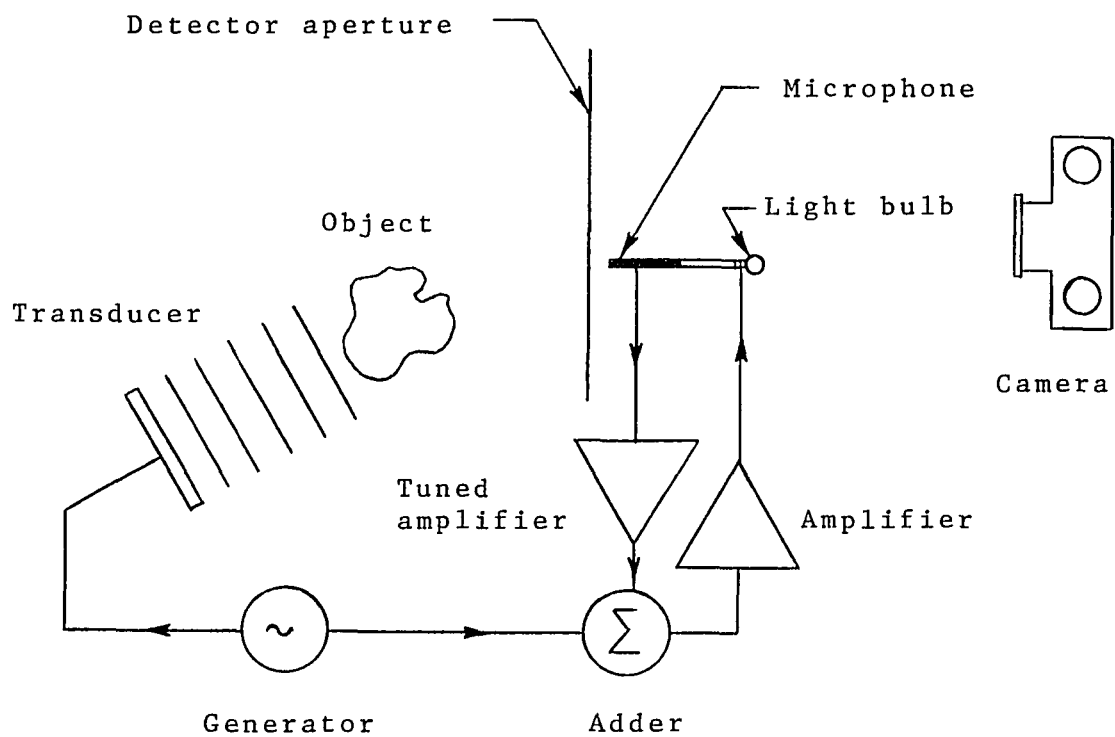


Figure 2-8 A mechanically scanned image converter using a plane, electronically simulated reference wave

The image converters described thus far have used a "point" transducer to scan the aperture plane. Sokolov⁸⁷ discovered that a large piezoelectric crystal essentially behaves as a mosaic of many "point" crystals in that the voltage induced across the crystal at a certain point is directly proportional to the instantaneous pressure at that point. Although there is not an exact one to one correspondence between voltage and pressure at each point due to transverse mode coupling, the lateral spread is usually confined to less than a millimeter (at 4 MHz.) and is least when the crystal resonates in its fundamental thickness mode. Sokolov proposed a mechanical scanning system using the Nipkow disk as well as an electronically scanned system to record the charge distribution across the face of the piezoelectric crystal.

Based on Sokolov's discovery, Suckling⁹⁰ devised an image visualization system in which a capacity probe mechanically scans the surface of a mosaic of nine, one square inch, X-cut piezoelectric quartz crystals (see Figure 2-9).

Electronic. As was mentioned on page 33, the voltage or charge distribution across a piezoelectric crystal due to a corresponding pressure distribution can be evaluated at each point by electronic means - usually a scanning electron beam. Sokolov⁸⁷ was the first to propose such a

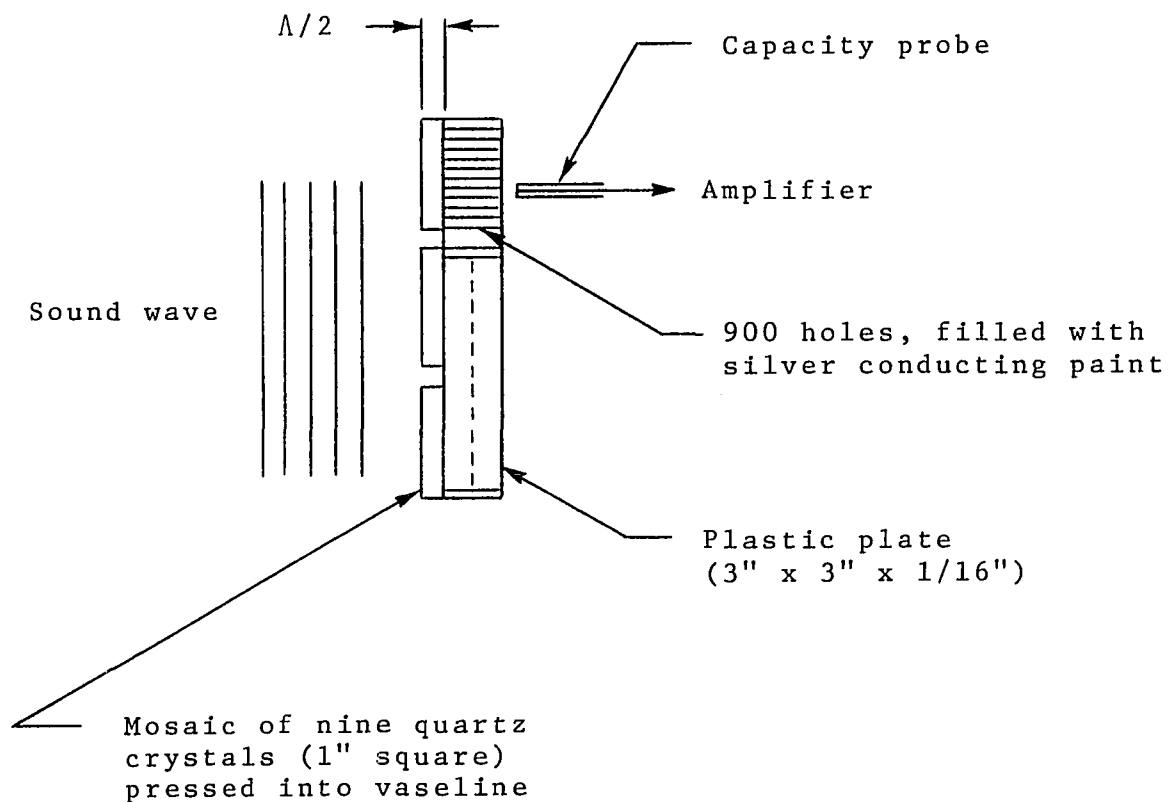


Figure 2-9 An ultrasonic image converter which scans the voltage distribution on the face of a mosaic of piezoelectric crystals

system; with some modifications, it is known as the ultrasonic camera. A description of the basic Sokolov tube follows (see Figure 2-10).

The Sokolov tube resembles the cathode ray tube in that both contain an electro gun in vacuum. The faceplate of this particular device is a piezoelectric crystal which is chosen to resonate in its fundamental thickness mode. Incident ultrasound creates resonant vibrations of this crystal and leads to the formation of charges of alternate sign on the inside surface of this crystal. As the high energy electron beam strikes a point on this surface, the crystal charge at that point influences secondary emission. Hence, the secondary emission current amplitude modulates the anode current as the beam scans the crystal surface.

Modifications of this basic detector have included:

1. Low-voltage scanning (no secondary emission)⁸⁶
2. Addition of stabilizing electrodes and an electron multiplier (42)
3. Partially matched crystal faces⁸⁶
4. Charlotte windows¹³

The performance of the ultrasonic camera has been investigated by several authors,^{40-43,45,86} and an excellent description of the history and the present state-of-the-art of the ultrasonic camera is given by Smyth.⁸⁵ The consensus indicates that, due to mode coupling, the resolution

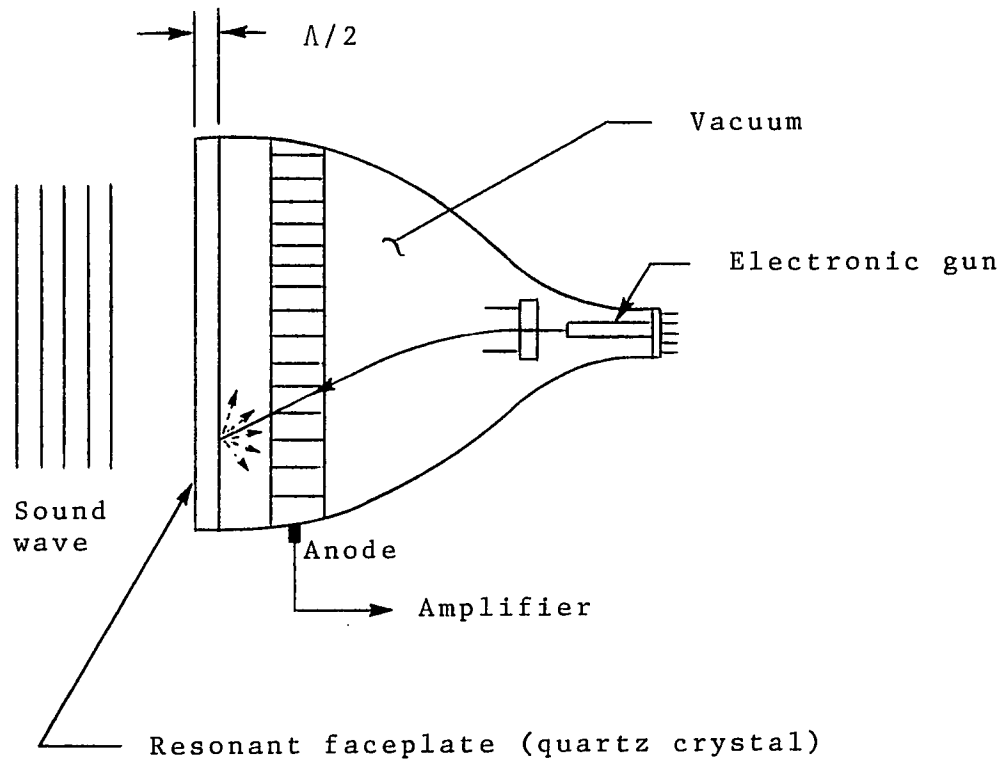


Figure 2-10 The basic ultrasonic camera

capability of the faceplate is of the order of the crystal thickness (for example, 0.2 mm @ 15 MHz for a quartz crystal). The crystal thickness cannot be made arbitrarily small, however, since the faceplate must support a vacuum. For the same reason, the size of the aperture cannot be made arbitrarily large. Practical sensitivities of 10^{-7} to 10^{-9} watt/cm² have been reported, while sensitivities of 10^{-11} watt/cm² are expected in the future.^{41,85}

The usefulness of the ultrasonic camera in the area of non-destructive testing has been well established. With the introduction of an acoustical reference wave, Marom, Fritzler, and Mueller⁵⁷ also demonstrated its use in an acoustical holographic system (Figure 2-11). In the arrangement shown, the angular separation between the object and reference waves was maintained at 10° in order to minimize broadening of the image detail as discussed on page 33. A resolution capability of 1 mm at 7 MHz was reported.

The sensitivity of the system, its resolution, and the angular separation of the reconstructed images was subsequently improved by the same authors²⁷ by using an electronically generated reference wave instead of the acoustic wave shown in Figure 2-11. In this manner they were able to allow the object wave to impinge normally to the piezoelectric faceplate.

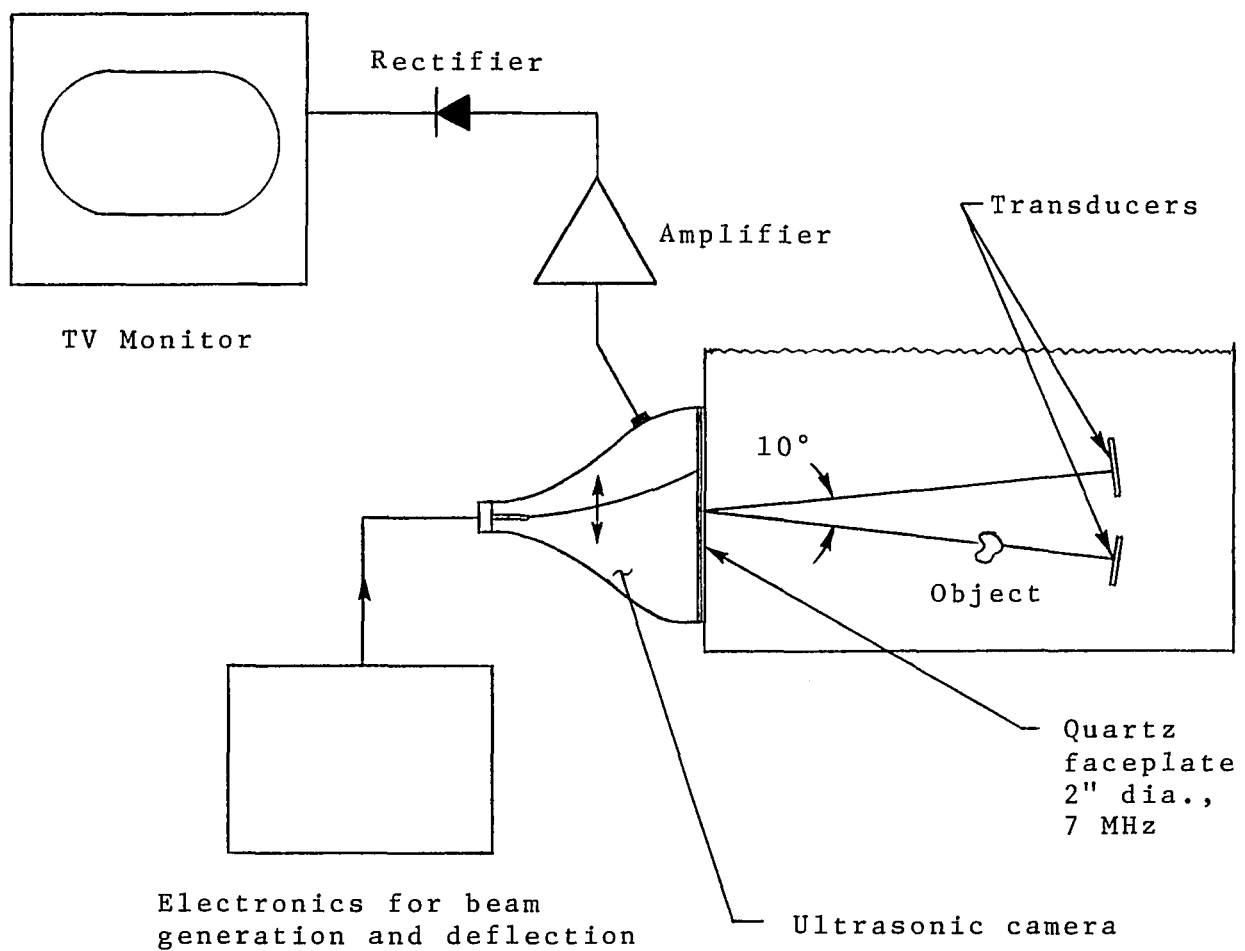


Figure 2-11 Arrangement for performing acoustical holography via the ultrasonic camera

A somewhat different electron beam scanning type of detector was reported by Davidson and Hull.¹⁷ An acoustic image is focused onto a matrix of individual piezoelectric crystals (see Figure 2-12), each of which is connected to an individual integrating network, rectifier, and amplifier. An image orthicon scans, by means of an electron beam, the voltage distribution on the faceplate; thereby generating a TV signal which is monitored on a TV screen. The authors claimed higher sensitivity, a more sharply defined range gating capability, and potentially higher resolution than the ultrasonic camera.

Optical. Instead of scanning the piezoelectric crystal surface of the ultrasonic camera with an electron beam, Smyth⁸⁵ proposed scanning it with a small light beam. Several advantages over the usual ultrasound camera were cited.

A somewhat different approach was described by Green^{32,33} (see Figure 2-13). A piezoelectric crystal is segmented and each segment is connected to a photodiode which is illuminated by a revolving pencil of light. As each photodiode turns "on", its nonlinear characteristics generate sum and difference frequency signals in that diode. Upon proper filtering, amplification, and rectification, the image of the ultrasound can be displayed on a cathode ray tube. Electronic simulation of an acoustical reference

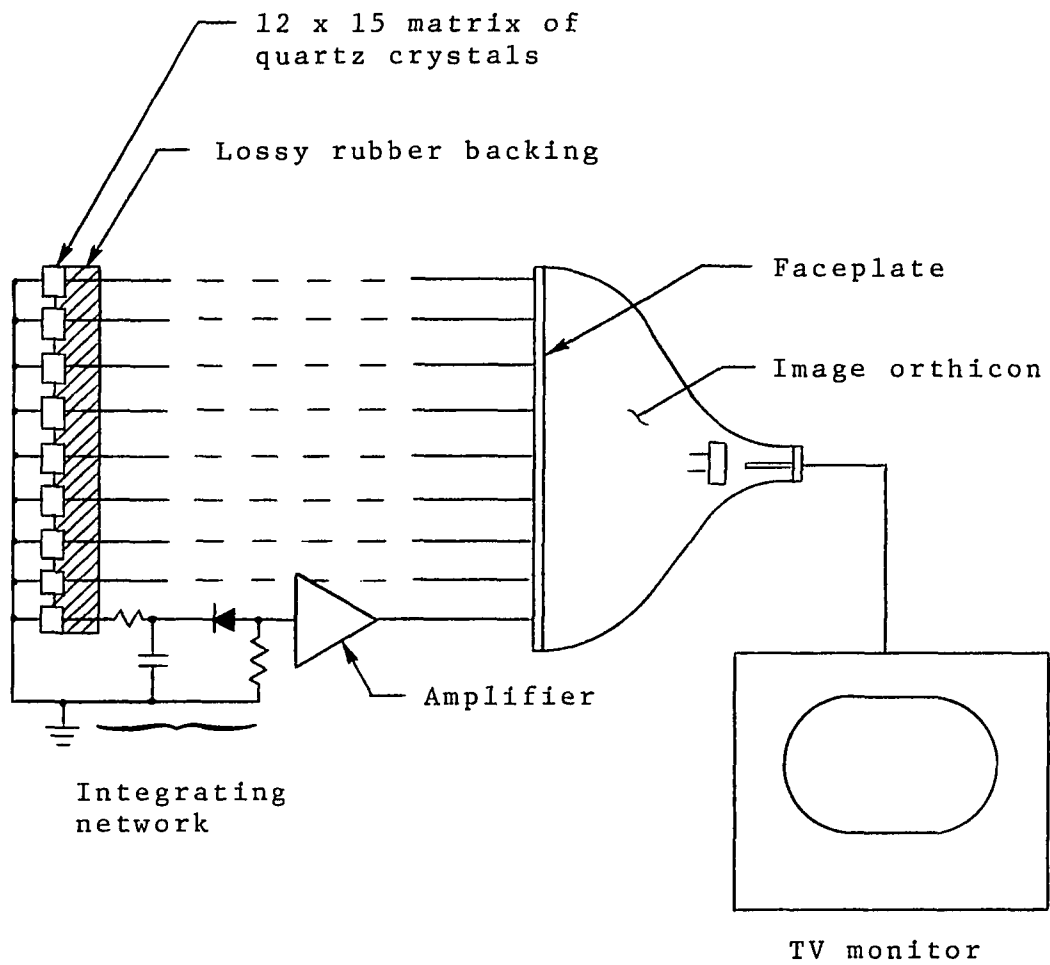


Figure 2-12 Use of an image orthicon for ultrasonic image visualization

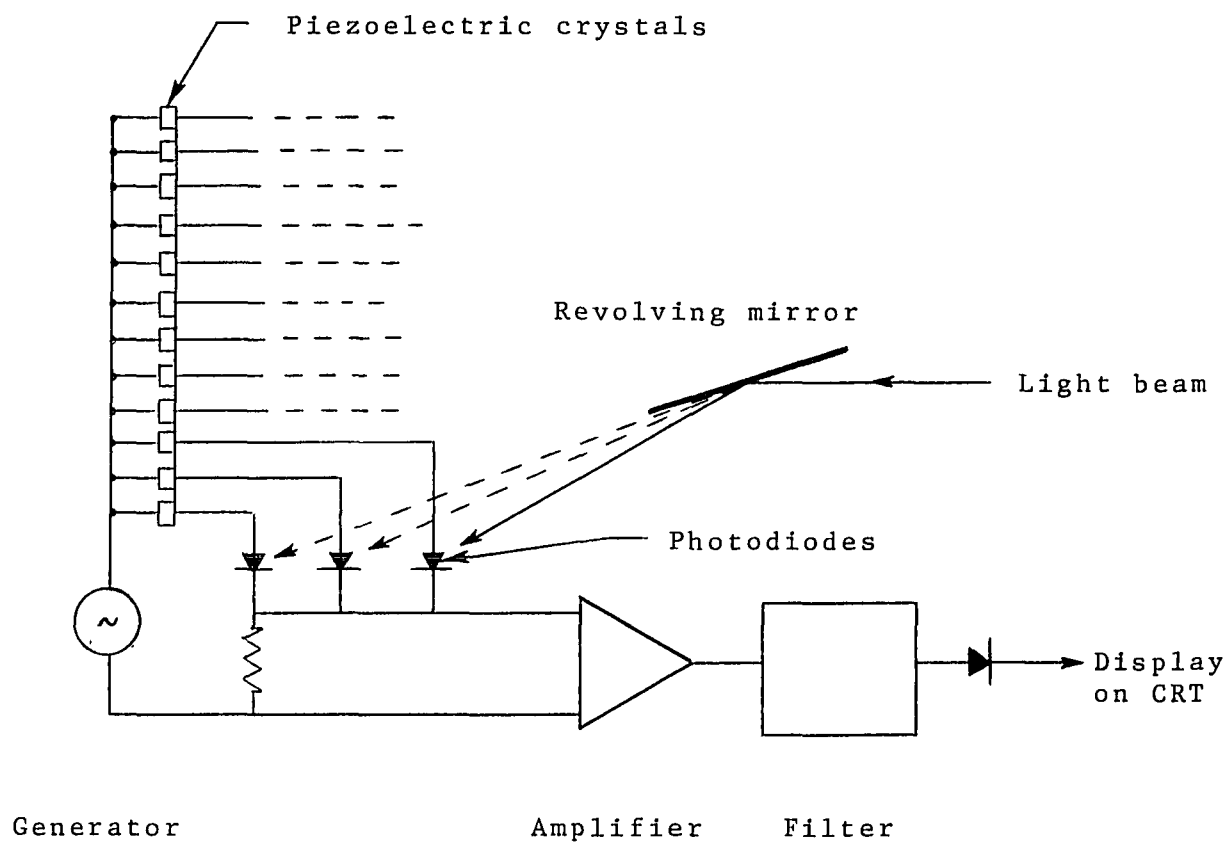


Figure 2-13 System for optically scanning a matrix of photodiodes to obtain an image of the ultrasound at the piezoelectric faceplate

wave can, of course also be included. Green has quoted a sensitivity of 5×10^{-12} watt/cm² for this system.

The scanned image converters discussed thus far have used sensors which respond to the pressure distribution at the aperture plane. However, as mentioned previously (page 9), other characteristics of the acoustic diffraction pattern can be detected.

58

Massey demonstrated an optical heterodyne converter which responds to the velocity of an acoustic wave. Referring to Figure 2-14, a monochromatic beam of light of frequency ω is split into two parts by beam splitter (1). One beam is incident on plane P_2 at the point \underline{m} which is vibrating at the frequency Ω . The other beam is slightly shifted in frequency from ω to ω_1 by means of the frequency translator.

Due to the vibratory motion of point \underline{m} , the instantaneous frequency ω_2 of the reflected light varies sinusoidally in time about the optical carrier frequency ω . (The velocity of point \underline{m} frequency modulates the incident light.) By means of the beam splitter (2), this light is mixed with the light emerging from the frequency translator; and sum and difference frequency components are generated by the nonlinearity of the photocell. Finally, proper filtering and FM demodulation yields a signal of frequency Ω

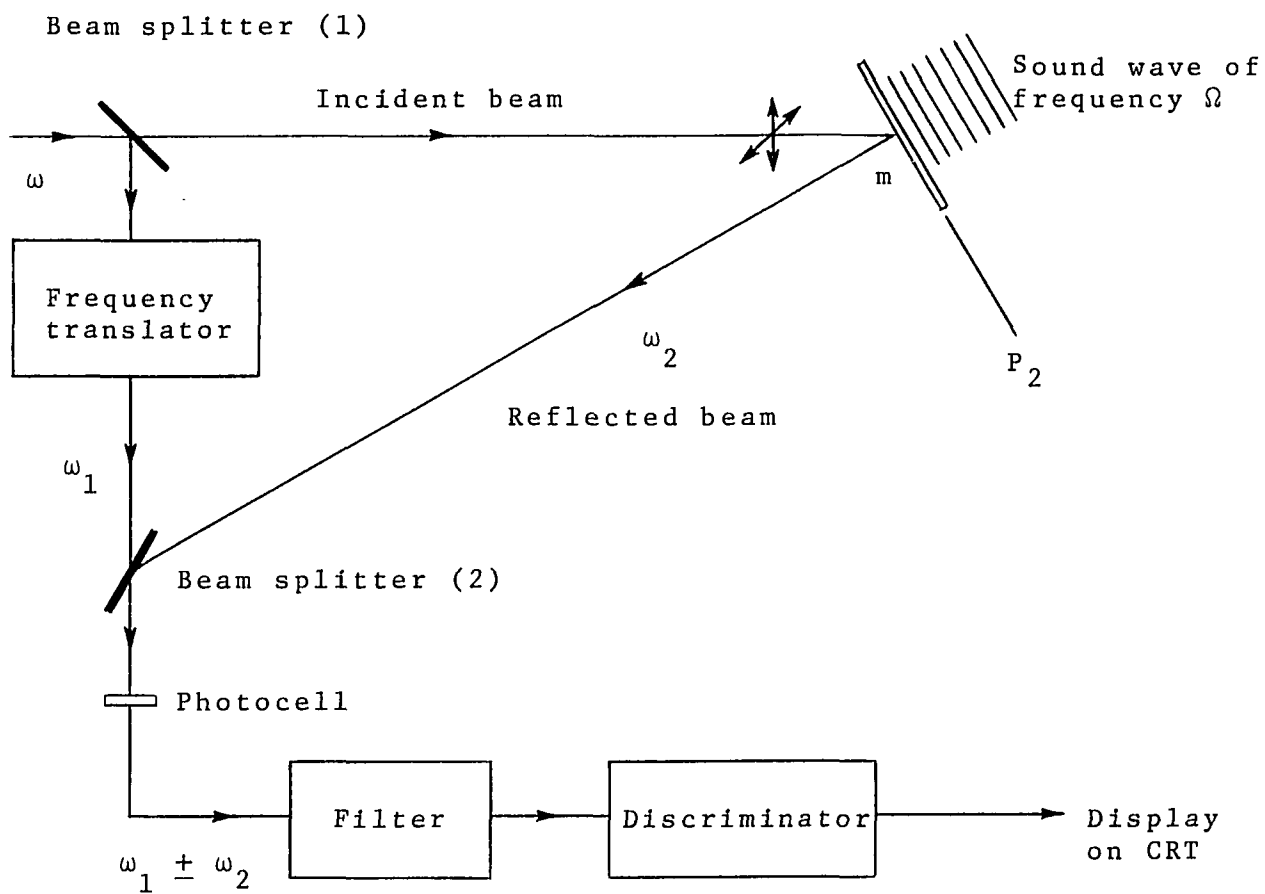


Figure 2-14 An optically scanned ultrasonic image converter which responds to the velocity of the vibrating plane P_2

whose instantaneous value is directly proportional to the speed of the vibrating point \underline{m} . As the incident light scans the plane P_2 in synchronism with a suitable display network, an image of the velocity distribution of the vibrating plane can be obtained.

Using a half-wave resonant plate (1 MHz) and a 1 mw, He-Ne laser, Massey reported a threshold intensity of 1.46×10^{-8} watt/cm².

A considerably simpler image converter due to Korpel^{1,52} is illustrated in Figure 2-15. A laser beam is focused to a diffraction limited spot at a point \underline{m} on the vibrating surface P_2 . The reflected light which is periodically deflected due to the motion of point \underline{m} , is partially intercepted by a knife edge. This action converts the periodic deflection into a variation of irradiance at the photocell whose output may be mixed with a "reference" signal. After filtering, amplification and rectification, the signal z-modulates a CRT so that, by proper scanning, an image of the time varying deformation of plane P_2 can be obtained. Note, however, that the system responds to the slope of the surface displacement, rather than the displacement itself.

Korpel visualized surface waves in this manner, and reported a threshold intensity of 10^{-7} watt/cm² at 1 MHz.

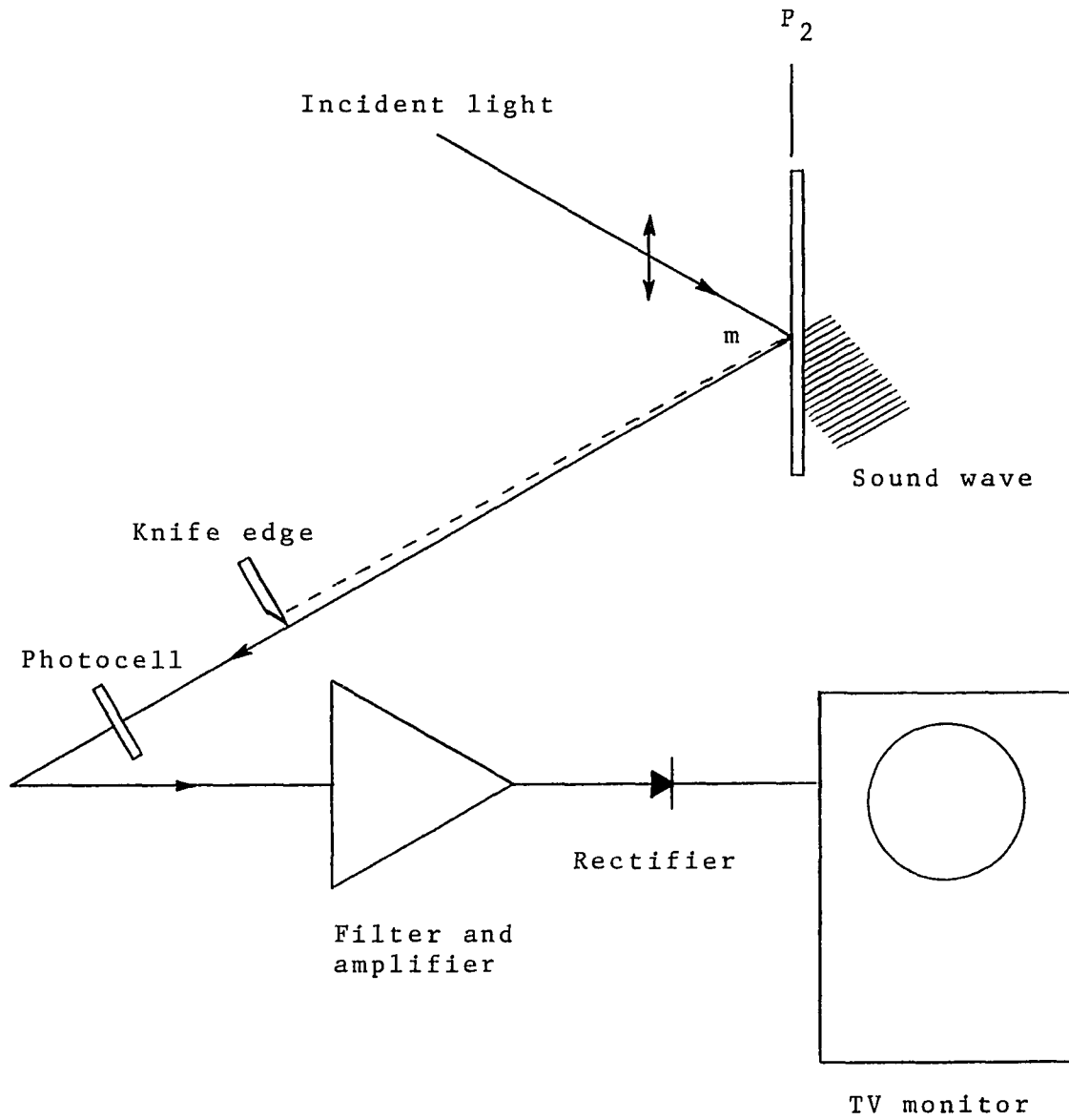


Figure 2-15 A converter which responds to the slope of the surface displacement

Conclusion

With regard to the pertinent features that any detector should display (see page 9), the following general conclusions can be listed.

System Complexity. The extreme simplicity and economy of the non-scanned detectors make these very attractive. The simultaneous recording of all points in the acoustical hologram plane can reduce processing times substantially. Indeed, the liquid surface levitation method allows instantaneous (real-time) reconstruction of the acoustical hologram (one-step imaging).

Scanned detectors, on the other hand, are more flexible, and the possibility of simulating a reference wave should reduce the amount of image distortion. The concept of "fast" scanning allows virtually instantaneous visualization of the acoustical hologram (but not its reconstruction).

Sensitivity. In general, scanned detectors exhibit a sensitivity which is several orders of magnitude higher than that of non-scanned detectors (with the exception of the Pohlman Cell). This is, of course, due to the use of electrical amplification. Table 2-1 conveniently lists, in order of decreasing sensitivity, the detectors which have been discussed in this chapter.

Selectivity. Usually the non-scanned detectors do not

TABLE 2-1

SENSITIVITIES OF THE VARIOUS DETECTORS DISCUSSED IN CHAP. II

Detector	Threshold intensity watt/cm ²	Page	Resolution capability	References
Optical scanning of photodiodes	5×10^{-12}	39		Green (32)
Mechanical scanning of a piezoelectric crystal with a capacity probe	5×10^{-12}	31		Smyth (85)
Electronic scanning of a piezoelectric crystal and an image orthicon	1×10^{-11}	39		Davidson (17)
Ultrasonic camera (modified Sokolov tube)	2×10^{-11}	35		Smyth (86)
	1×10^{-7}	35	.5mm @ 4 MHz	Smyth (86)
	5.7×10^{-7}	35		Kennedy (45)
		35	.2mm @ 15MHz	Jacobs (40)
		35	1 mm @ 7 MHz	Marom (57)
Mechanical scanning with a "point" piezoelectric crystal		31	.5mm @ 5 MHz	Preston (73)
Optical scanning with heterodyning	1.5×10^{-8}	42		Massey (58)
Optical scanning with a Schlieren arrangement	1×10^{-7}	44		Korpel (1,52)
Mechanical alignment of particles (Pohlman Cell)	3×10^{-7}	18		Pohlman (71,72)

TABLE 2-1 Continued

Detector	Threshold intensity watt/cm ²	Page	Resolution	References
Liquid surface levitation	5.5x10 ⁻⁴	20	0.2 mm	Schuster (79)
	1.5x10 ⁻³	20		Pigulevskii(70)
	3x10 ⁻³	20		Sette (80)
	1x10 ⁻²	24		Smith (84)
Mechanical scan- ning with a therocouple	0.01	29	.025mm @ 12MHz	Dunn (21)
Phosphor persist- ence changes	0.05	17	.2 mm @ 3 MHz	Petermann (69)
Light exposed photographic paper	0.05	14	.01mm @ 2 MHz	Arkhangelskii(2)
Oxidation of a potassium iodide starch solution	0.07	15		Haul (37)
Deformation of thermoplastics	0.1-1.0	26		Young (98)
Starch plate in an iodine starch solution	1.0	16		Bennet (4)
Light exposed photographic film (pre-soaked)	1.0	13		Berger (8)
	1.0-5.0	13		Bennet (5)

make use of mechanical resonance, consequently their selectivity is rather poor. Often the acoustical diffraction pattern must be isolated from unwanted acoustical disturbances. These precautions are minimized with resonant detectors.

Resolution. The resolution varies considerably for the various image converters described and no generalizations can be made. It is obvious, however, that besides the limiting influence of a small detector aperture, the resolution of resonant detectors is also decreased by image spreading due to mode coupling.

Chapter III

26

HOLOGRAPHIC AND SCHLIEREN SOUND VISUALIZATION SYSTEMS

The systems discussed thus far have dealt with the detection or measurement of some characteristic of a sound wave in a plane which is nearly normal to the direction of propagation of that sound wave.

Equally important are those systems which allow the visualization of sound waves in a plane containing the propagation vector, i.e. those systems which show an outline of a sound wave as it propagates through a medium. Among such visualization techniques are the familiar Schlieren system and the holographic system - both of which will be discussed in this chapter.

In both of these methods a plane, coherent light wave is made to traverse a region of an optically transparent medium in which a sound wave is propagating. The geometry is arranged so that the propagation vectors are normal to each other. As a result, the compressions and rarefractations generated in the medium by the sound wave yield a distribution of refractive indices which phase modulates the light wave in both space and time.

This phase modulation is periodic and diffracts the light into a theoretically infinite number of spectral orders. As will be seen, the Schlieren optical system

makes use of this phenomenon, and upon proper spatial filtering of the diffraction orders, an outline of the sound wave can be obtained. Figure 3-1a (to be explained more fully later) is a typical Schlieren image which shows the reflection and transmission of sound by a 1/8" thick aluminum plate.

The holographic method represents a new application of holography in ultrasonics. The holograms obtained by this system are a record of the spatial distribution of the mutual coherence between the light that has traversed the sound wave and a highly coherent reference wave. Figure 3-1b (also to be explained more fully later) shows a similar reflection and transmission phenomenon imaged with the holographic technique.

A more detailed analysis of these two methods and the experimental results obtained with them shall now be presented. It will also be demonstrated that under certain conditions, the irradiance in the Schlieren image and the reconstructed holographic image are identically distributed.

The Holographic System for Visualizing Sound Waves

Figure 3-2 schematically shows the basic geometry of this method. It is the familiar arrangement of plane reference, split-beam holography. As in the usual holographic system, an "object" wave interferes with a "reference" wave

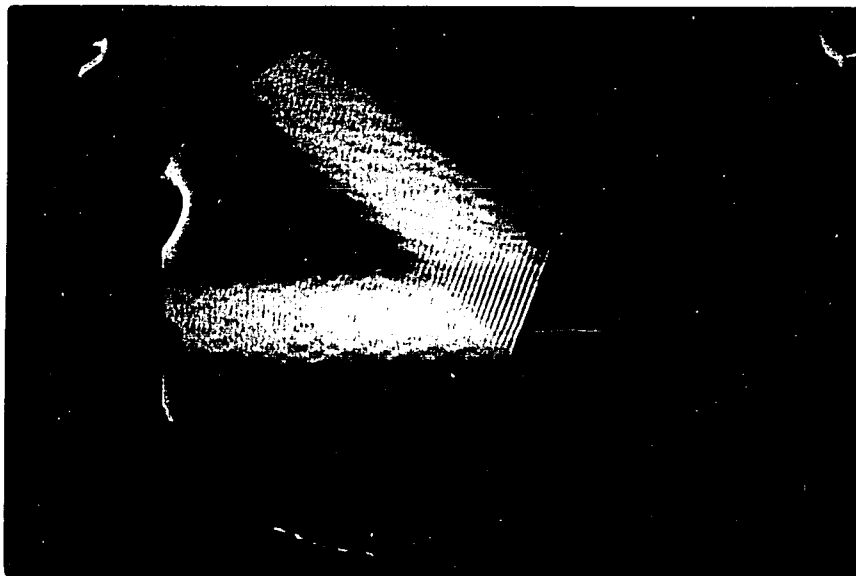


Figure 3-1a A typical Schlieren image showing the reflection and transmission of a sound wave by a 1/8" thick aluminum plate (1 MHz)

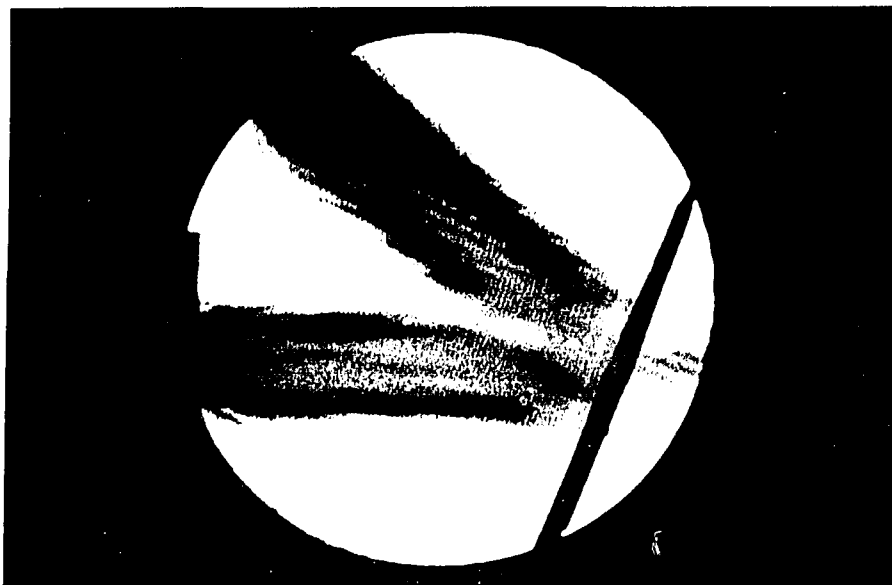


Figure 3-1b A reconstructed holographic image showing a similar phenomenon as above ($f = 988 \text{ KHz}$)

at the film plate, and the emulsion records the resultant interference pattern. However, in this case, the "object" wave is phase modulated by the sound wave. The resultant variation of mutual coherence between these two waves is detected by the holographic process and modifies the "brightness" of the reconstructed image in such a manner that the image of the diffusion screen will show an outline of the sound wave. As shown in the figure, it is also possible to translate the frequency of the "reference" wave by an integer multiple of the sound frequency Ω . This produces several advantages which will be discussed later.

The radiance distribution within the reconstructed image can be predicted from an extension of well known theory.⁵⁵ Under conditions of plane, quasimonochromatic radiation during recording, and for a plane, monochromatic reconstructing wave, the radiance \mathcal{R}_m' of a point m' in the reconstructed image corresponding to the object point m , is related to the modified complex degree of coherence g_{mR} in the following way

$$\mathcal{R}_m' \propto |g_{mR}|^2 \quad (3-1)$$

Hence, the problem reduces to one of calculating the modified complex degree of coherence between the radiation coming from the object point m and the reference source R (see Figure 3-2). For the conditions specified above,

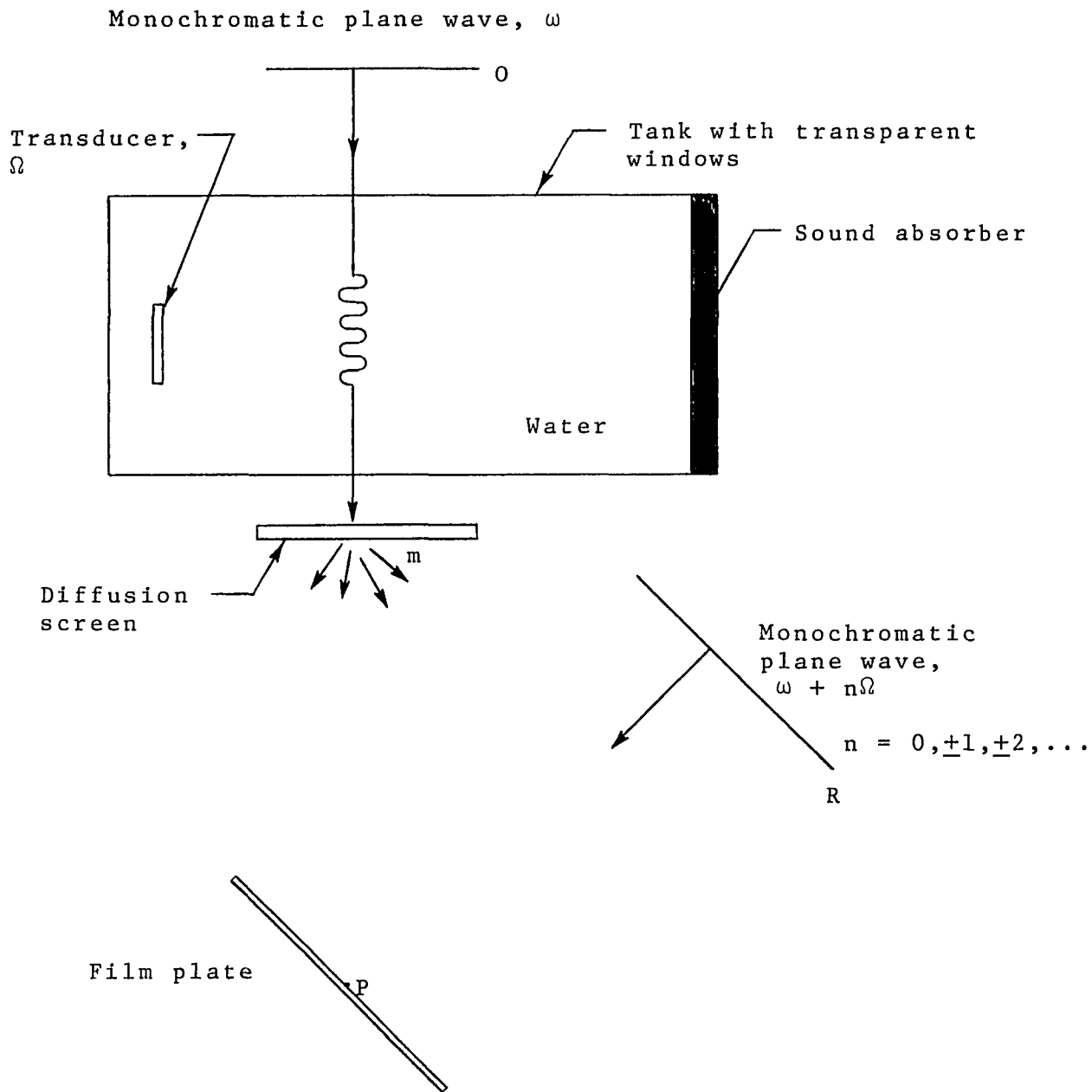


Figure 3-2 Schematic of the basic geometry of the holographic method for visualizing sound waves

this degree of coherence can be expressed as

$$g_{mR} = \frac{1}{T} \int_0^T \exp \left[i(\phi_R - \phi_m) \right] dt \quad (3-2)$$

where

T = exposure time of the photographic emulsion

ϕ_R = phase of the radiation coming from the reference source R

ϕ_m = phase of the radiation coming from the object point m

t = time

Referring to Figure 3-3, let m be the object point and P the point on the film plate at which the coherence is to be determined. The phases of the radiation at point P can be described as

$$\phi_R = (\omega + n\Omega)t - s_{RP} (\omega + n\Omega)/c \quad (3-3)$$

$$n=0, \underline{+1}, \underline{+2}, \dots$$

$$\phi_m = \omega t - s_{m0}(t)\omega/c - s_{mP}\omega/c - C_1 \quad (3-4)$$

where

ω = frequency of the illuminating radiation

Ω = frequency of the sound wave

$\omega+n\Omega$ = frequency of the reference radiation

s_{RP} = optical path length between the reference source and point P

$s_{m0}(t)$ = optical path length between the illuminating source and the object point m

s_{mP} = optical path length between points m and P

Plane wave illuminating
source of frequency ω

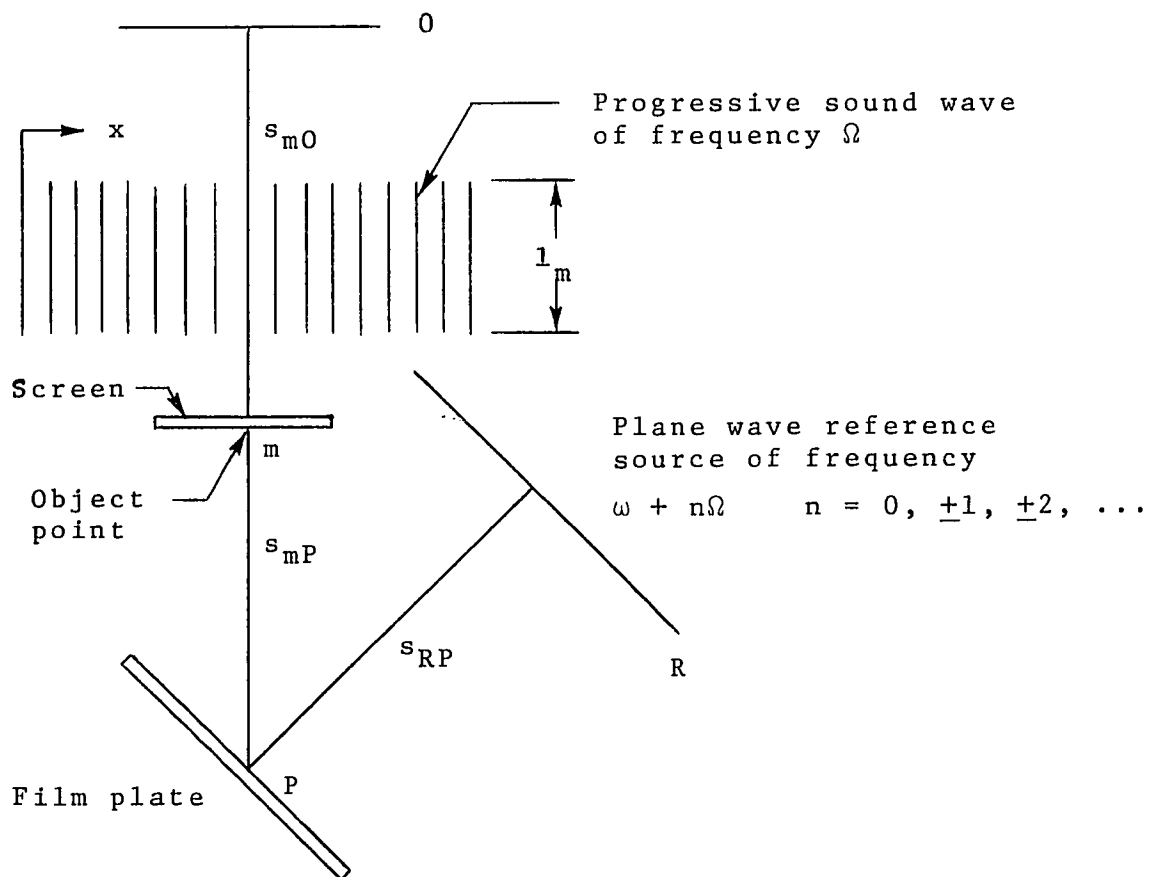


Figure 3-3 Diagram for calculating the mutual coherence
at point P

x = coordinate in the direction of sound propagation

c = speed of light in vacuum

C_1 = the constant phase shift between the reference and illuminating radiation

Strictly speaking, equation (3-4) should also account for scattering of the light (due to a gradient of refractive index) within the water medium and for scattering within the diffusion screen. The former is usually negligible for low intensity or low frequency sound waves (this is known as the Raman-Nath approximation⁷⁴) while the latter will be neglected for reasons which will become apparent shortly.

Therefore, neglecting both scattering effects, the phase of the illuminating radiation at point P becomes

$$\phi_m = \omega t - (s_{mP} + G_{m0})\omega/c - C_1 + l_m\mu(\alpha)\omega/c \quad (3-5)$$

where

G_{m0} = geometrical path length between the illuminating source 0 and the object point m

l_m = effective width of the sound beam traversed by the light wave in order to reach point m

$\mu(\alpha)$ = change of the refractive index in the water

and for progressive waves

$$\alpha = \Omega t - Kx \quad (\text{see note 1})$$

$$K = 2\pi/\Lambda$$

Λ = wavelength of sound in the water medium

Substituting equations (3-3) and (3-5) into (3-2)

$$g_{mR} = \exp(i\phi_0) \frac{1}{T} \int_0^T \exp \left\{ i \left[n\Omega t - k l_m \mu(\alpha) \right] \right\} dt \quad (3-6)$$

where

$$k = \omega/c = 2\pi/\lambda$$

λ = wavelength of the illuminating source

$$\phi_0 = k(G_{m0} + s_{mP} - s_{RP}) + C_1 - (n\Omega/c)s_{RP}$$

If the pressure variation within the medium is periodic, then $\mu(\alpha)$ and $\exp[ik l_m \mu(\alpha)]$ is also periodic and

$$\exp[ik l_m \mu(\alpha)] = \sum_{r=-\infty}^{\infty} \psi_r \exp(ir\alpha) \quad (3-7)$$

where the complex Fourier coefficients ψ_r are

$$\psi_r = \frac{1}{2\pi} \int_0^{2\pi} \exp \left\{ i[k l_m \mu(\alpha) - r\alpha] \right\} d\alpha \quad (3-8)$$

Remembering equations (3-6) and (3-7) and the definition of α , the modified complex degree of coherence g_{mR} becomes

Note 1. Since the spatial position of the object point m has been fixed, α is only a function of time in this analysis.

$$g_{mR} = \exp(i\phi_0) \sum_{r=-\infty}^{\infty} \psi_r \exp(irKx) \frac{1}{T} \int_0^T \exp[i(n-r)\Omega t] dt \quad (3-9)$$

which, for $T \gg 1/\Omega$, reduces to

$$g_{mR} = -\exp[i(\phi_0 + nKx)] \psi_n \quad (3-10)$$

Hence, the radiance in the reconstructed image at point m' corresponding to the object point m is

$$\mathcal{R}_{m'} \propto |g_{mR}|^2 = |\psi_n|^2$$

where

$$\psi_n = \frac{1}{2\pi} \int_0^{2\pi} \exp \left\{ i[kl_m \mu(\alpha) - n\alpha] \right\} d\alpha \quad (3-11)$$

The significance of shifting the frequency of the reference wave is now apparent. By shifting the optical frequency an n^{th} harmonic of the sound frequency, only the n^{th} Fourier coefficient of the phase of the "object" wave is used to modify the radiance of the reconstructed image.

A qualitative explanation of this process can be made if one remembers that a stationary interference pattern is obtained only if the two interfering light waves have the same frequency. Since the "object" wave consists of components having a frequency ω plus all harmonics of Ω , the frequency of the reference wave essentially determines which frequency component of the "object" wave is used to form a stationary interference pattern at the film plate. Hence, only the information contained within the n^{th} harmonic component is recorded holographically.

The diffusion screen in Figures 3-2 and 3-3 is used primarily for analytical convenience. It is apparent that the diffuser is neither necessary to the operation of this system nor desirable when accurate radiance distributions are to be obtained. In practice however, there are distinct advantages as well as disadvantages to using a diffusion screen.

When the diffusion screen is used during the recording process, the illumination at the film plate is diffuse. Hence, each point on the film plate receives information from every point on the object. This fact allows one to reconstruct the entire image of the object with any portion of the hologram. For the same reason, the reconstructed image is relatively insensitive to dust and scratches which may be present on any optical components. The disadvantage of this technique is that scattering within the diffusion screen tends to reduce the definition of the image of the sound wave.

The situation is reversed when the diffuser in Figure 3-2 is removed. In this case, the hologram itself, is a direct record of the spatial distribution of the mutual coherence between the light that has traversed the sound wave and the reference wave. No reduction of image definition occurs; on the other hand, the desirable characteristics of diffuse illumination cannot be realized.

The technique of reconstructing the image from a hologram which is recorded in accordance with Figure 3-2 but without the use of a diffusion screen, deserves some comments. Assume that the hologram is illuminated with coherent radiation of the same form as the original reference wave and that the reconstructed wavefront which normally corresponds to the object wave is observed. Since the eye is unable to focus on any one particular plane, the observer sees the original illuminating source whose radiance is modified by $|g_{mR}|^2$. An image of the sound wave can be obtained by replacing the observer's eye with a photographic emulsion. If a permanent record of the sound image is not required, the emulsion can be replaced by a diffusion screen which now serves as a plane of focalization for the observer's eye. Both of these techniques and the resultant images are illustrated in Figures 3-4a and 3-4b, respectively.

A hologram which has been recorded without a diffuser can also be illuminated with "white light" in order to form an outline of the sound wave. This is possible because the hologram is a direct record of the spatial distribution of the mutual coherence between the object and reference waves. Consider the case when the frequency of the reference wave is not shifted, i.e. when $n = 0$. Then, the coherence between the reference wave and the light that has not traversed the sound wave is high; hence, the fringe visibility

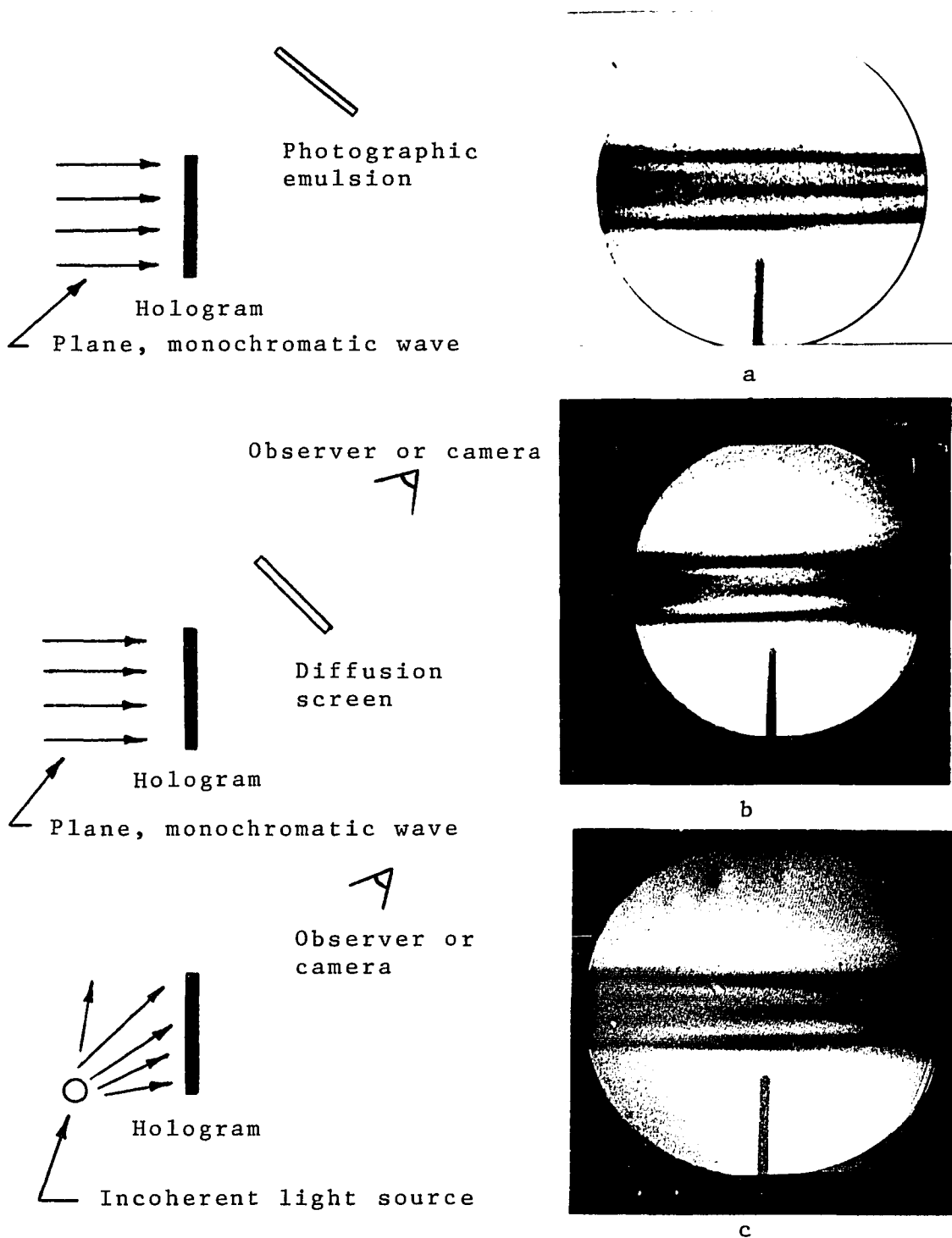


Figure 3-4 Various methods of reconstructing images from holograms which have been recorded without the use of a diffusion screen (see text)

in these regions of the film plate is also high. Conversely, the fringe visibility is low in those regions where the reference wave interferes with light that has traversed the sound beam. As the hologram is illuminated with "white light", strong diffraction occurs in those regions where the fringe visibility is high and little diffraction occurs in low visibility regions of the film plate. The resultant "image" of the sound wave is illustrated in Figure 3-4c.

The pictures shown in Figure 3-4 were all obtained from the same hologram and show a side-view of a sound wave propagating in water from left to right (the "pointer" in the lower half of each illustration is the image of a copper wire). The radiance distribution over the cross-section of the sound beam is, of course, a consequence of equation (3-11) and will be examined more fully later. Finally, the apparent discrepancy of the radiance distribution between the three illustrations is a consequence of the radiation and the geometry used during the "reconstruction" process and the control of photographic parameters. Illustration "a" shows, for example, the result when using high contrast photographic emulsions.

The Schlieren System for Visualizing Sound Waves

A simple Schlieren system is illustrated in Figure 3-5. As in the preceding section, the propagation vectors

of the light and sound waves are normal to each other so that, under the Raman-Nath approximation,⁷⁴ the sound waves act as a periodic phase grating of negligible thickness. Hence, the problem is one of imaging a time-varying, periodic phase object with plane, monochromatic light.

Due to the phase grating, an infinite number of spectral orders are expected in the "far-field". This Fraunhofer region is approximated in the focal plane of the lens in Figure 3-5. The lens is also situated in such a manner that it normally images the sound axis on the screen. As will be seen, if these diffraction orders are properly filtered, an outline of the sound wave can be obtained on the screen.

Referring to Figure 3-6, consider the one-dimensional problem of imaging a sound wave of uniform width l_m propagating along the x-axis. As in the previous discussion, the refractive index is assumed to be an arbitrary periodic function. A plane, monochromatic light wave of uniform width D and of frequency ω propagates in the z direction. Using the Fraunhofer diffraction integral, the complex amplitude of the light in the focal plane of the lens is³⁶

$$A(\zeta, t) = C_2 \sum_{r=-\infty}^{\infty} \psi_r W_r(\zeta) \exp [i(\omega - r\Omega)t] \quad (3-12)$$

where

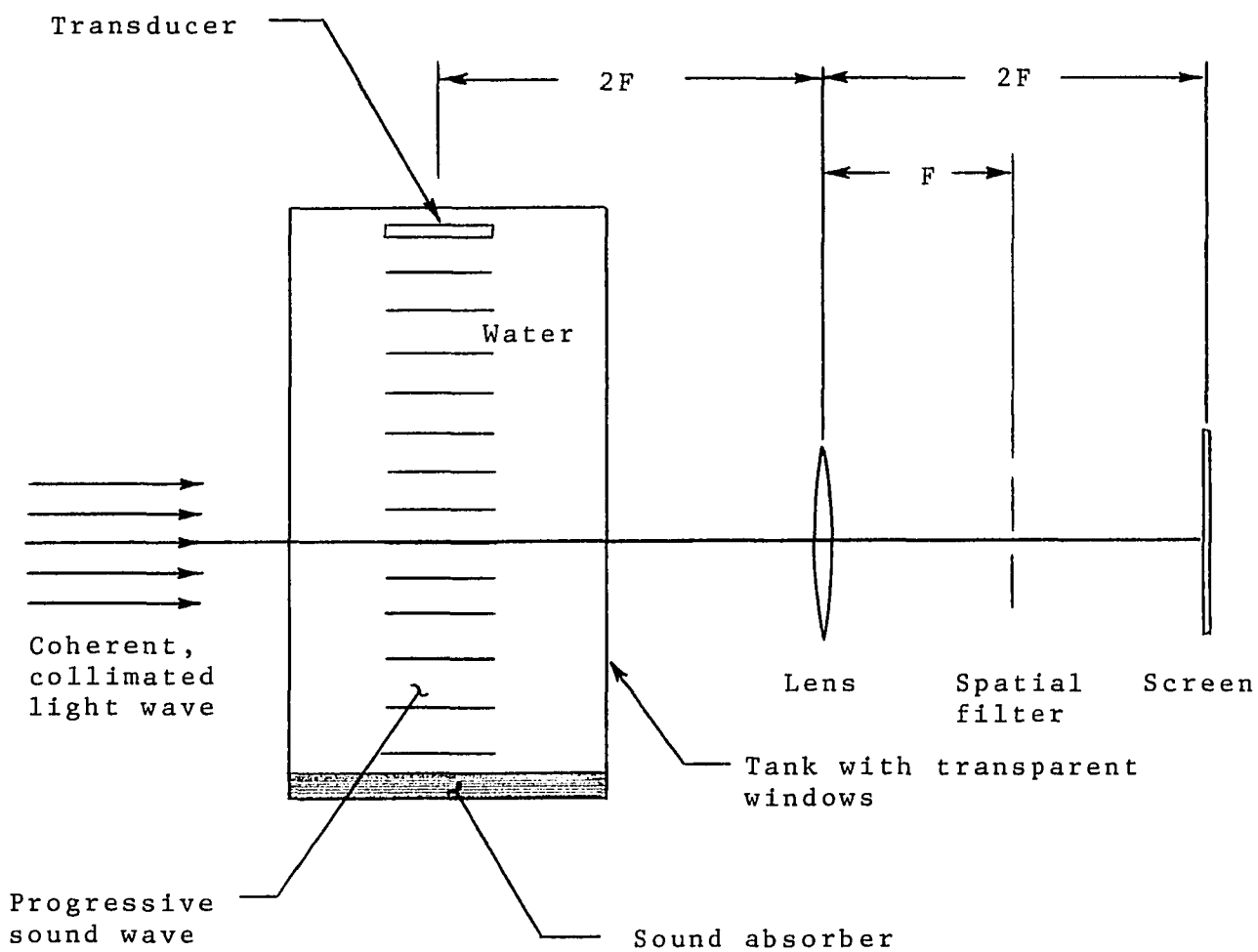


Figure 3-5 Schematic of the basic Schlieren system

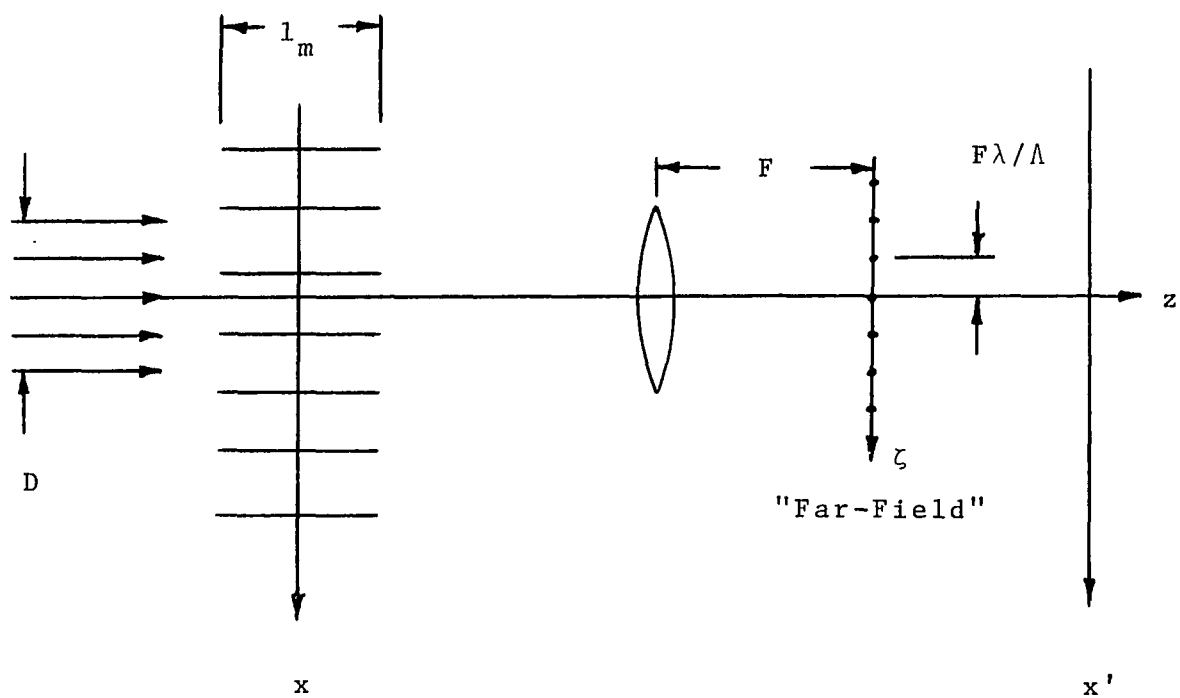


Figure 3-6 Diagram for calculating the irradiance in the Schlieren image at x'

$$W_r(\zeta) = D \operatorname{Sinc} \left[(rK - k\zeta/(F)D/2) \right] \quad (3-13)$$

$$\psi_r = \frac{1}{2\pi} \int_0^{2\pi} \exp \left\{ i[kl_m \mu(\alpha) - r\alpha] \right\} d\alpha \quad (3-14)$$

ζ = coordinate in the focal plane of the lens

F = focal length of the lens

C_2 = constant

D = uniform width of the light beam

l_m = uniform width of the sound beam

r = an integer, $0, \pm 1, \pm 2, \dots$

and where the other parameters have been defined on pages 55-58.

Examination of equations (3-12) and (3-13) shows that the diffraction orders are discrete in frequency and are located in space at

$$\zeta = rF\lambda/\Lambda \quad r=0, \pm 1, \pm 2, \dots \quad (3-15)$$

Furthermore, when $D \gg \Lambda$, the spectral orders can also be considered discrete in space (non-overlapping) so that the irradiance of each diffraction order is proportional to $|\psi_r|^2$.

The irradiance in the image plane x' can be obtained by again using the Fraunhofer diffraction integral. Hence, the complex amplitude in the image plane becomes

$$U(x',t) = C_3 \int_{-\infty}^{\infty} A(\zeta,t) \exp(-ikx'\zeta/F) d\zeta \quad (3-16)$$

where

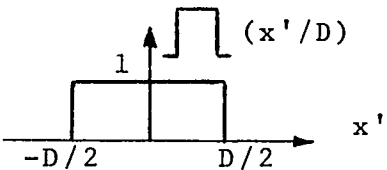
$U(x',t)$ = complex amplitude of the light in the image plane

C_3 = a constant

x' = coordinate in the image plane

Substituting equation (3-12) for $A(\zeta,t)$ and evaluating the integral yields

$$U(x',t) = C_2 C_3 F/k \int \text{rect}(x'/D) \exp(i\omega t) \cdot \sum_{r=-\infty}^{\infty} \psi_r \exp[-ir(\Omega t + Kx')] \quad (3-17)$$

where $\text{rect}(x'/d) \equiv \begin{cases} 0 & |x'| > D/2 \\ 1 & |x'| < D/2 \end{cases}$ 

Assuming that $D \gg \lambda$ so that the spectral orders are discrete in space, the radiance within the Schlieren image is

$$\mathcal{R}_{x'} \propto \sum_r |\psi_r|^2 \quad (3-18)$$

Any spatial filtering of the spectral orders will be reflected in the summation over r . In particular, if only the r^{th} order is allowed to pass, then

$$\mathcal{R}_{x'} \propto |\psi_r|^2 \quad (3-19)$$

Comparing equations (3-11) and (3-19), it is noted that the distributions of irradiance within the Schlieren and the reconstructed image are equivalent within a constant multiplier if $n = r$. Hence, for the conditions specified (plane wave, monochromatic radiation and validity of the Raman-Nath approximation), the above distributions of irradiance due to any arbitrary periodic variation of refractive index, are equivalent within a constant if the order of the reference frequency that is used to record the hologram and the spectral order that is used to form the Schlieren image are the same. This equivalence of the radiance distributions is not completely unexpected since in both of these systems the phase shift of the light that has traversed the sound wave (see Figures 3-2 and 3-5) is the same. The manner in which this wave is processed by the holographic and Schlieren system is, of course, entirely different.

Special Case of Plane Progressive Sound Waves

When the sound wave is plane and progressive, the radiance distribution in the reconstructed or Schlieren image assumes a particularly familiar form. For such a wave, the change of the refractive index can be expressed as

$$\mu(\alpha) = N \sin (\alpha + \alpha') \quad (3-20)$$

where N is the maximum change of the refractive index and α' is a constant phase. For this function, the Fourier

coefficient ψ_n becomes (see equation (3-11) or (3-14))

$$\psi_n = J_n(kl_m N) \quad (3-21)$$

where $J_n(kl_m N)$ is the n^{th} order Bessel function of the Raman-Nath parameter $(kl_m N)$. Hence, the radiance in the holographic reconstructed image or the Schlieren image has the following form:

$$\mathcal{R} \propto J_n^2(kl_m N) \quad (3-22)$$

It will be noted from this relation or equation (3-11) that, when $n \neq 0$, those regions where no sound is present (the background) appears dark in the reconstructed or Schlieren image. Because of the dark background, a low intensity sound wave may be made visible whereas, when $n = 0$, it may not be detected. Hence, the effect of using diffracted light to form the Schlieren image or of using a shifted reference wave to record the hologram is an enhancement of the sensitivity of the respective visualization system. (This effect is demonstrated later.) It should also be apparent that the final sensitivity is limited only by fog in the photographic process.

Once the Raman-Nath parameter has been determined, the absolute acoustic pressure may be calculated if the relationship between pressure and refractive index (piezo-optic coefficient) for the particular medium is known.

As an example, consider a plane, progressive sound wave having a circular cross-section. Such a wave is approximately generated by a large piezoelectric disk. Further assume that the hologram is recorded with an "unshifted" reference wave, or that in the Schlieren system, only the zeroth diffraction order is allowed to pass the spatial filter ($n = r = 0$). Under these conditions, the radiance distribution that is expected in either image of the sound wave is proportional to $J_0^2(kl_m N)$. This function is illustrated in Figure 3-7.

Since the sound beam is circular, the effective width l_m and therefore, the Raman-Nath parameter ($kl_m N$) will vary from zero at the edges of the sound beam to a maximum at its center. Referring to Figure 3-7, the radiance distribution will be symmetrical about the sound axis and will fluctuate through a series of maxima (at $kl_m N = 0, 3.832, 7.016, \text{etc.}$) and minima (at $kl_m N = 2.405, 5.520, 8.654, \text{etc.}$). The radiance at the center of the sound beam axis is $J_0^2(kLN)$ where L is the effective beam diameter. From the positions of these maxima and minima, it is possible to calculate both L and (kLN) . In this manner, a piezoelectric crystal may be calibrated. Thus, for a water medium and He-Ne laser light illumination ($\lambda = 6328 \text{ \AA}$), the total power radiated by the transducer is

$$P = 0.195 (kLN)^2 \text{ watts} \quad (3-23)$$

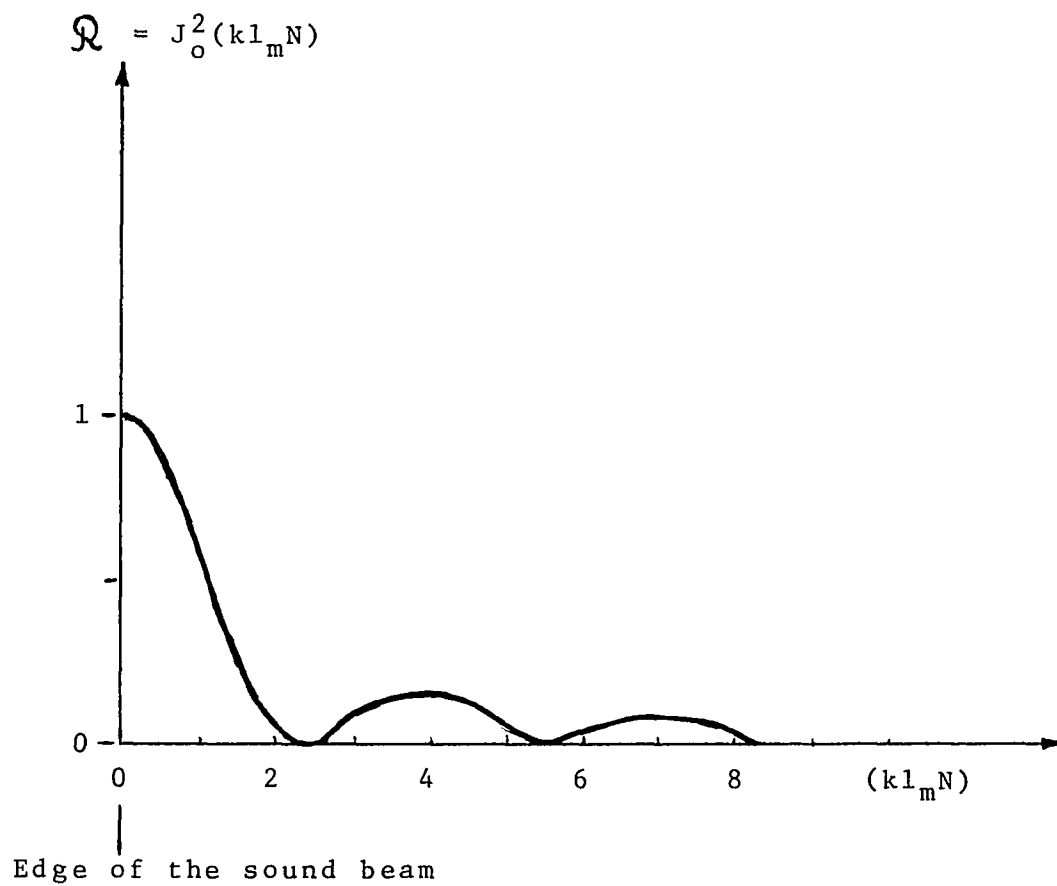


Figure 3-7 Theoretical distribution of irradiance due to a plane, progressive sound wave

In practice the calibration of piezoelectric crystals is facilitated by using a Schlieren system in which only the zeroth diffraction order is allowed to pass. For low sound intensities, the crystal voltage is directly proportional to the Raman-Nath parameter. Therefore, it is only necessary to record the crystal voltage at which the radiance of the sound beam axis approaches its first minimum. At this point, (kLN) is equal to 2.405.

The calibration of piezoelectric crystals based on the assumption of plane acoustic waves is, of course, not strictly accurate. However, most mechanical methods for calibrating transducers are based on this assumption;³⁸ and compared to these, the optical method is inherently more accurate since the acoustic field is not disturbed during the measurement.

Experimental Results and Comparisons

Sound waves were made visible by holographic techniques (using both "shifted" and "unshifted" reference frequencies) and a Schlieren system. A diagram of the actual arrangement used to record holograms with "unshifted" reference frequencies as well as Schlieren images is shown in Figure 3-8. As can be seen, both outputs of the laser are utilized. The front beam (more intense) is spatially filtered and collimated and is then made to traverse a water medium in which a sound wave is propagating. If a

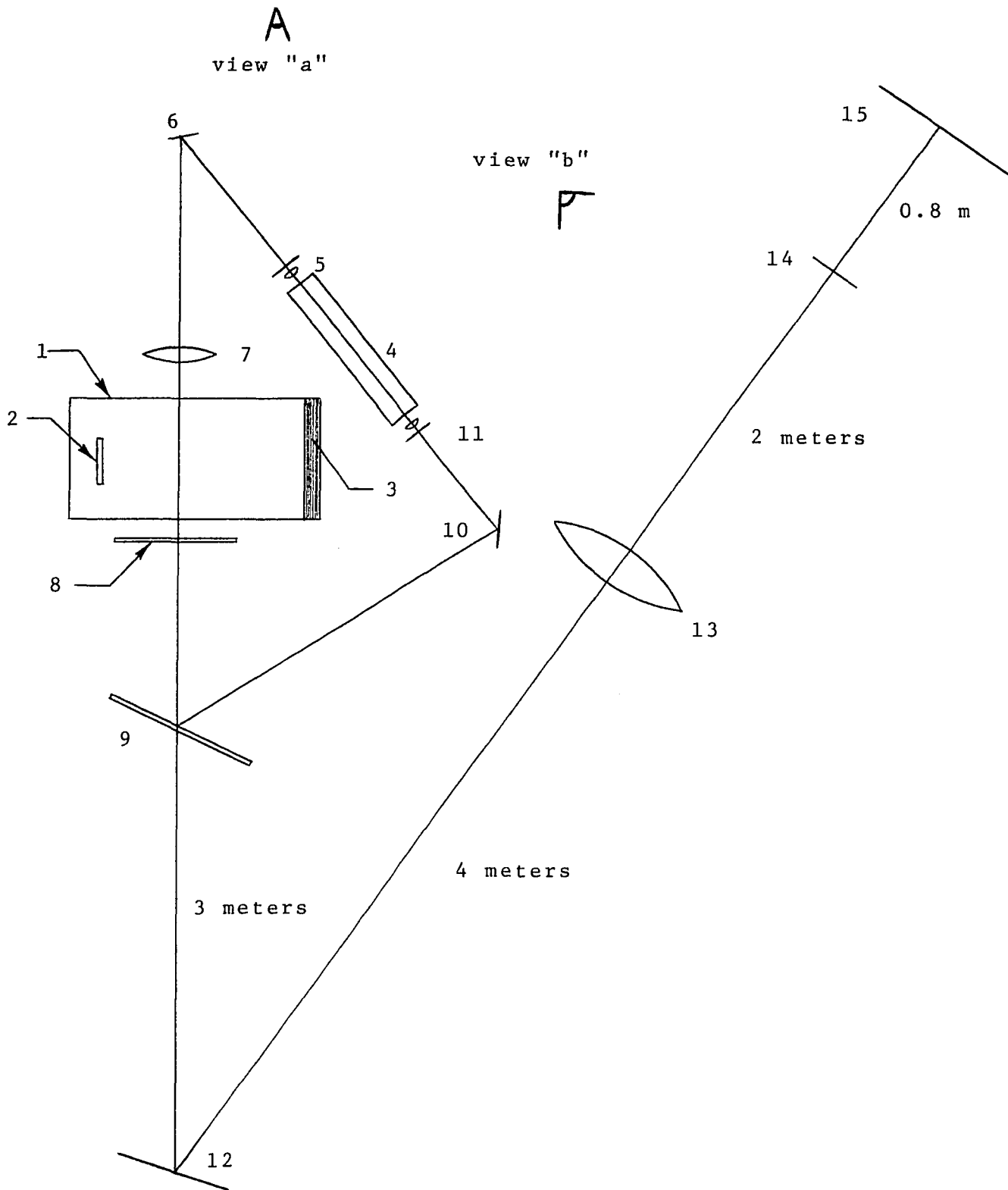


Figure 3-8
Experimental arrangement used to record "zero-order" holograms as well as Schlieren images.

hologram is to be recorded (with or without a diffusion screen), the rear output of the laser serves as a highly coherent reference source (see note 2). On the other hand, if a Schlieren image is to be obtained, the rear output of the laser is not used and the diffusion screen (8) and the film plate (9) are removed. In this manner, both a hologram and a Schlieren image may be recorded under the same acoustical conditions and with a minimum amount of disturbance between recordings. The specific components used in this arrangement are

1. Tank - commercial, 10 gal. aquarium tank
2. Transducer - see text
3. Sound absorber - various layers of butyl rubber and nylon carpeting
4. Laser - Spectra Physics, model 131, 1 mw, 6328 Å
5. Spatial filter - x20 objective with a pinhole
6. Mirror - first surface, magnetic base, 1-1/2" dia.
7. Collimating lens - 8.9 cm dia., 63.5 cm F.L.
8. Diffusion screen - 1/6" thick glass, ground on one side
9. Film holder and film plate
10. Mirror - first surface, magnetic base, 1-1/2" dia.
11. Spatial filter - x20 objective with a pinhole

Note 2. Although the previously discussed theory strictly applies only for a plane reference wave, the spherical reference wave (with a large radius of curvature) used in Figure 3-8 is a reasonably accurate approximation to a plane wave.

12. Mirror - first surface, 4"x5"
13. Lens - 8" diameter, approximately 2 meter F.L.
14. Spatial filter - see text
15. Camera or screen

The figure also shows the approximate dimensions between the components which comprise the Schlieren system.

In order to appreciate the large, physical size of the experimental arrangement, Figure 3-9 shows two views as observed from the points indicated in Figure 3-8. In Figure 3-9a, the diffusion screen (8), the film holder (9) and part of the spatial filter (11) have been removed so that this form of the layout is suitable for obtaining Schlieren images. Barely visible on the far wall in this picture is the mirror (12) which reflects the modulated light beam back across the table and to the remaining components which comprise the Schlieren system (see Figure 3-9b). Figure 3-9b shows the lens (13), the spatial filter (14) and the camera (15 - lens removed) which was used to record the Schlieren images.

The Schlieren images shown in Figures 3-1a (which was introduced earlier), 3-10 and 3-11 were obtained with the optical arrangement shown in Figure 3-9 and with the spatial filter (14) adjusted so that all but the central, undiffracted spectral order were allowed to pass. Under this condition, those regions of the image corresponding to areas where no

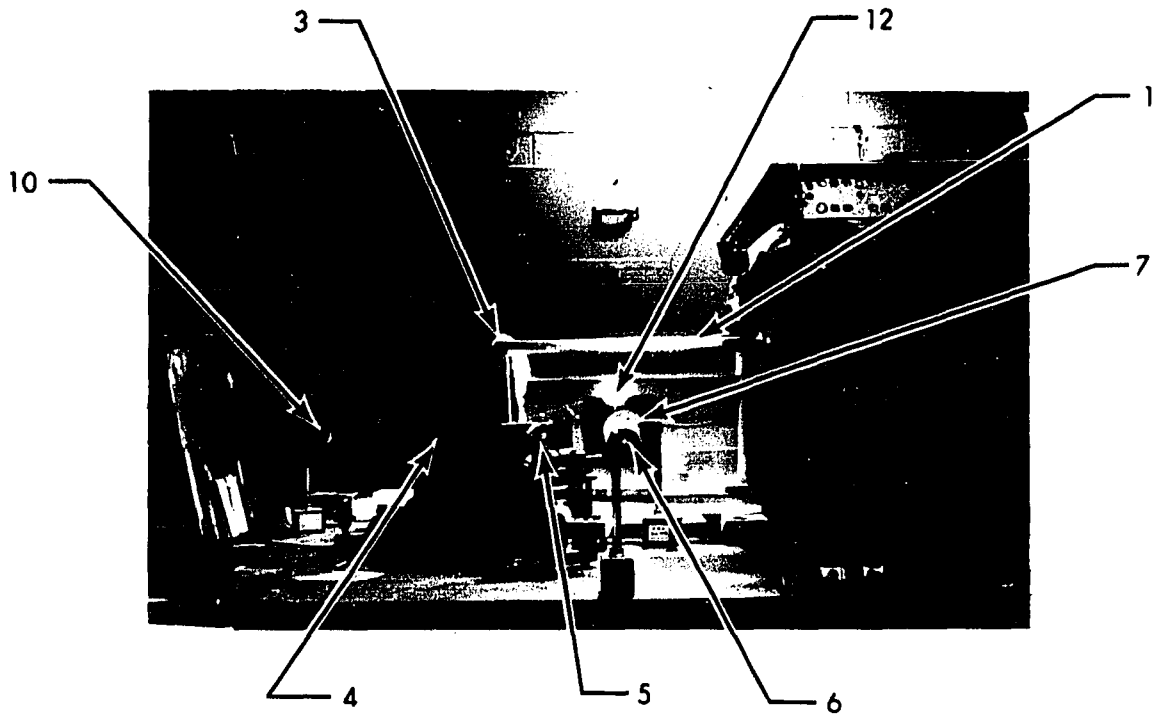


Figure 3-9a One view of the experimental arrangement used to record Schlieren images and holograms with "unshifted" optical reference waves. (The reference numbers correspond to those of Fig. 3-8.)

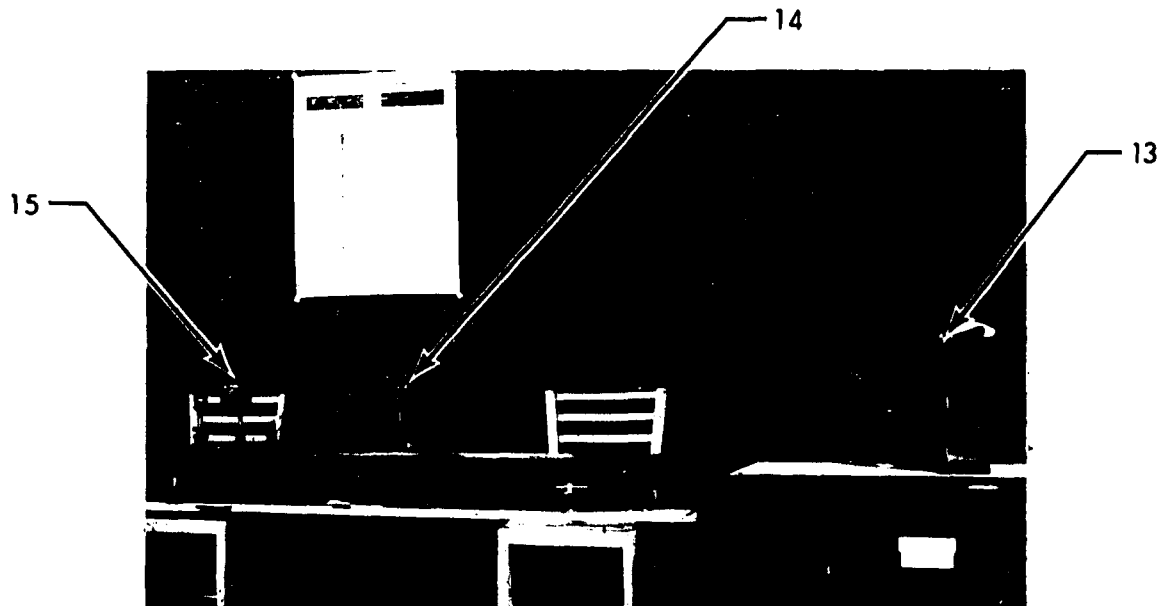


Figure 3-9b A view of the optical components used to obtain Schlieren images. (The reference numbers correspond to those of Figure 3-8.)

sound is present, should appear uniformly dark whereas light regions indicate, in accordance with equation (3-18), the presence of sound.

Figure 3-1a approximately demonstrates these principles. It shows the reflection and some transmission of a (1 MHz) sound wave by a 1/8" thick aluminum plate. The fact that the background in this image is not uniformly dark is due to the incomplete blocking of the zero spectral order. The filtering is difficult at this relatively low frequency because the zero order does not focus to an ideal "point" and because the spectral orders are separated only by about 0.84 mm (see equation (3-15)).

Assuming that the incident (or reflected) sound wave is a plane, progressive wave having a circular cross-section, the radiance distribution over its cross-section is given by equations (3-18) and (3-21); that is

$$\mathcal{R}_{x'} \propto \sum_{r=1}^{\infty} J_r^2(kl_m N) = 1 - J_0^2(kl_m N) \quad (3-24)$$

Referring to Figure 3-7, the distribution given by (3-24) is zero at the edge of the sound beam and also exhibits a series of maxima and minima. However, since the contrast between minima and maxima is small, the radiance over the cross-section of the incident sound beam in Figure 3-1a appears relatively uniform.

It is, of course, possible to measure the radiance distribution over the cross-section of the incident and the reflected waves and to compute from the positions of the maxima and minima (under the plane, progressive wave approximation) the sound intensity of each wave as well as the reflection coefficient of the aluminum plate for this angle of incidence. (An example of such a computation will be presented later.) Another method (and probably the more suitable in this case) of determining the acoustic intensity is to measure the radiance of the individual diffraction orders directly.

Careful examination of the region next to the aluminum plate where the incident and the reflected waves interfere, reveals the presence of nodes and anti-nodes of the resultant standing wave pattern. As known, the loci of these nodes are parallel to the metal plate and are equally spaced - the distance between adjacent nodes being $\lambda/2\cos\theta$, where θ is the angle of incidence. This fact allows one to scale the photograph or to determine the frequency of the sound wave if one or the other quantity is known.

The usefulness of the Schlieren method as an educational tool is clearly demonstrated in Figures 3-10 and 3-11. Figure 3-10 shows the diffraction of a (1 MHz) sound wave by a 1/8" wide x 1" long slot. To the left of the 1/32" thick aluminum plate (which contains the slot)

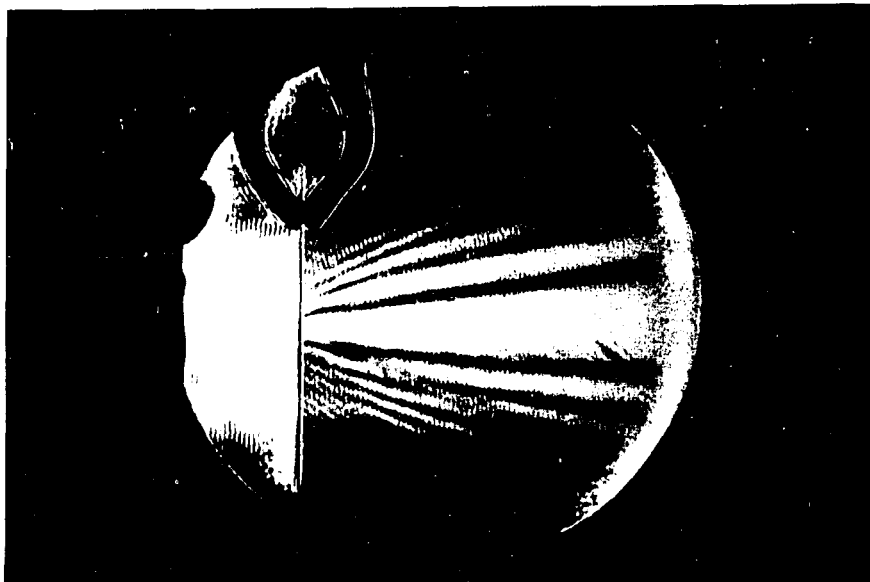


Figure 3-10 A Schlieren image showing the diffraction of a (1 MHz) sound wave by a 1/8" x 1" slot

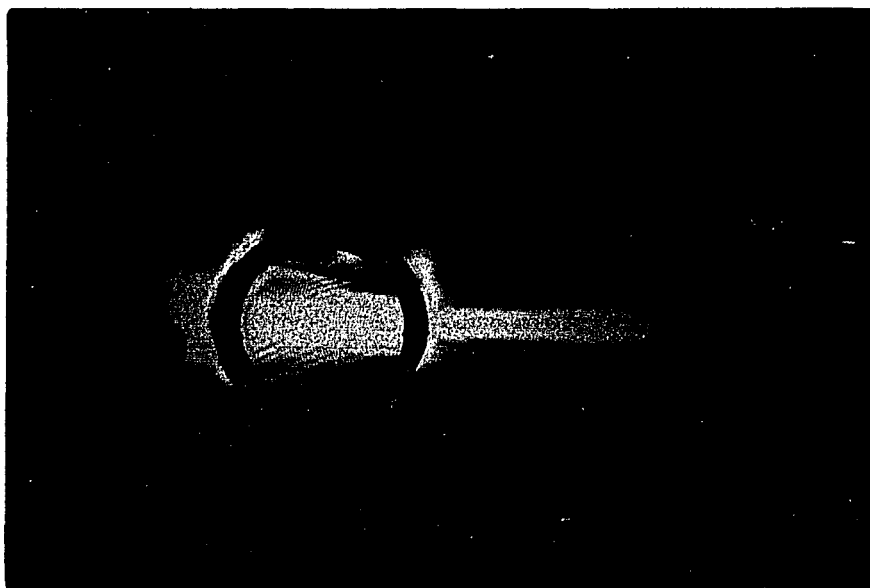


Figure 3-11 A Schlieren image showing the focusing effect of a 1" I.D. plastic cylinder on a (1.64 MHz) sound wave

one obtains, of course, a standing wave pattern as evidenced by the loci of nodes and anti-nodes parallel to the plate. On the other hand, the standing waves to the right of this plate may be due to some reflection from the butyl rubber.

Figure 3-11 shows the focusing effect of a 1" I.D. plastic cylinder on a (1.64 MHz) sound wave. The focusing results from the fact that the speed of sound in plastic is higher than that in the surrounding water medium. (In optics, such a "lens" would tend to diverge the light radiation.) Note also the considerable sound reflection and refraction from the various cylinder surfaces.

Figure 3-1b shows the reconstructed image obtained from a hologram which was recorded as per Figure 3-8 (recorded with the ground glass). As in Figure 3-1a, this image also shows the reflection and some transmission of a (988 KHz) sound wave by a 1/16" thick aluminum plate. The radiance distribution within this image may also be explained on the basis of a plane, progressive sound wave having a circular cross-section. Under this assumption, the discussion on pages 69-73 applies; that is, the radiance over the cross-section of the sound beam is distributed in accordance with $J_0^2(kl_m N)$ (see Figure 3-7). Hence, the brightest regions in this image correspond to areas where no sound is present whereas the darker regions indicate the presence of sound (to be more exact, they

indicate a variation of the refractive index during the exposure time of the hologram). This discussion should be compared to that referring to Figure 3-1a. Hence, as far as the radiance distribution over the cross-section of the sound wave is concerned, Figure 3-1b would be the "negative" of Figure 3-1a if both images had been obtained under the same acoustical conditions.

From the radiance distribution of the incident and reflected sound waves, it is possible to determine the reflection coefficient of the aluminum plate for this angle of incidence. Referring to the incident sound wave in Figure 3-1b, imagine that, starting at the edge of the sound beam, one scans over its cross-section. With reference to Figure 3-7, such a scan corresponds to moving from the origin to the right. Hence, at the position of the first minimum in the radiance, $kl_m N = 2.405$; and as one approaches the center of the sound beam, the radiance approaches its second minimum. Therefore, at the sound beam axis, $kl_m N \approx 5.5$. Continuing the scan from the axis to the other edge of the beam corresponds, in Figure 3-7, to moving from the point at which $kl_m N = 5.5$ to the left; back to the origin. In a similar manner, one obtains that the value of the Raman-Nath parameter at the sound beam axis of the reflected wave is between 2.4 and 5.5. The exact value (4.5) may be determined by actually measuring

the relative radiance distribution. Finally, since the acoustic intensity is proportional to $(kl_m N)^2$, the power reflection coefficient is computed to be $(4.5/5.5)^2 = 0.67$.

Comparing Figures 3-1a and 3-1b, it is noted that the bright background in the reconstructed image appears considerably more uniform than the dark background in the Schlieren image. The reason that one is bright while the other is dark has already been discussed, i.e. it results from the fact that the hologram was recorded with an "unshifted" reference wave (zero order shift) whereas the Schlieren image was recorded with all but the zeroeth spectral order. On the other hand, the more uniform background in the reconstructed image results from the fact that the "filtering" in the holographic method is accomplished by varying the frequency of the optical reference wave and is therefore, not limited by the practical problems associated with the spatial filtering of the diffraction orders that is required in the Schlieren method.

Continuing the comparison, note that the reconstructed image also shows the resultant standing wave pattern next to the aluminum plate. Finally, the striations in the reflected and transmitted sound waves in Figure 3-1b are suspected to be due to unwanted reflections from the tank bottom.

Some of the capabilities of the holographic method to visualize low-frequency sound waves are illustrated in Figures 3-12 and 3-13. Figure 3-12 shows the "near-field" and "far-field" radiation patterns of a 2.2 cm dia. crystal which is vibrating at 328 KHz. Although the side lobes are partially obstructed by the transducer housing, these lobes as well as the main lobe are clearly visible. Note that, in the Fresnel region of this crystal where the sound wave may be considered to be approximately plane, the radiance distribution over its cross-section is similar to that shown in Figure 3-1b. Observe also that the background of this image does not appear uniformly bright. The various dark regions in the background (which may also be observed in other reconstructed images) are caused by slow-moving water currents inevitably generated by the transducer. The resultant variations of the refractive index are detected in the same manner as those produced by the high-frequency pressure fluctuations.

Figure 3-13 shows the standing wave pattern generated by a 2-1/2" dia. crystal which is vibrating at 164 KHz. Although the sound absorber of Figure 3-8 was used, note that the formation of standing waves is almost unavoidable at this low frequency.

In order to examine the contention that, under certain conditions, the radiance within reconstructed and

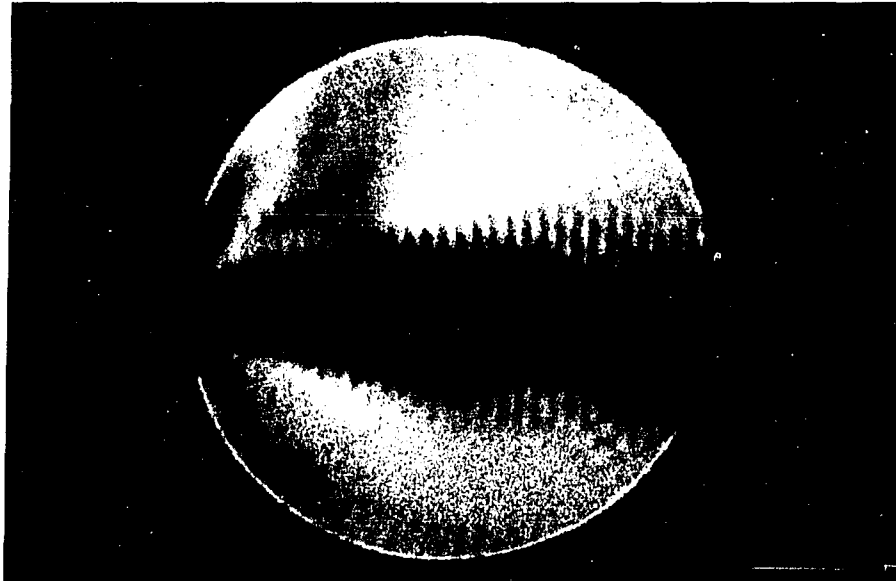


Figure 3-12 Reconstructed image showing the "near-field" and "far-field" radiation patterns of a small crystal vibrating at 328 KHz



Figure 3-13 Reconstructed image of the standing wave pattern generated by a large crystal vibrating at 164 KHz

Schlieren images can be equally distributed (see page 69), the sound frequency was increased to 3.23 MHz (the third harmonic of a 2.2 cm dia., 1 MHz crystal) to facilitate the spatial filtering of the various spectral orders.

Figure 3-14 shows the reconstructed image obtained from a hologram which was recorded as per Figure 3-8. (As shown, the frequency of the optical reference wave was not shifted ($n=0$) and the diffusion screen was used.) Clearly visible on the ground glass is the outline of the sound wave as well as the shadow of a copper wire. This "pointer" is situated approximately 13 cm to the right of the crystal face. Notice that the effect of slow-moving water currents, as discussed previously, has obstructed the right portion of the sound image.

The diffusion screen (8) in Figure 3-8 was then removed and a new hologram was recorded. Figure 3-15 shows the image reconstructed from this hologram with the arrangement shown in Figure 3-4a. (The pictures illustrated in Figure 3-4 were obtained from this hologram.)

A Schlieren system (as per Figure 3-8 with the ground glass and film plate removed) utilizing the same plane wave illuminating source as the above two holograms, was also used to detect the same sound wave. The image of this wave was formed by allowing only the zeroth diffraction order to pass the spatial filter ($r=0$), and since it appeared

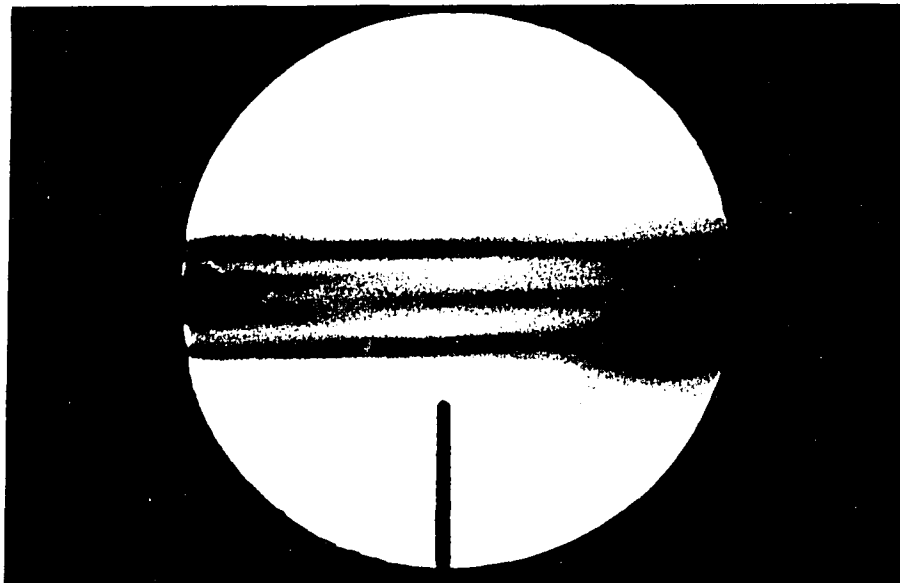


Figure 3-14 Reconstructed image of a diffusion screen showing the outline of a (3.23 MHz) sound wave. The 2.2 cm. dia. crystal is 13 cm. to the left of the wire.

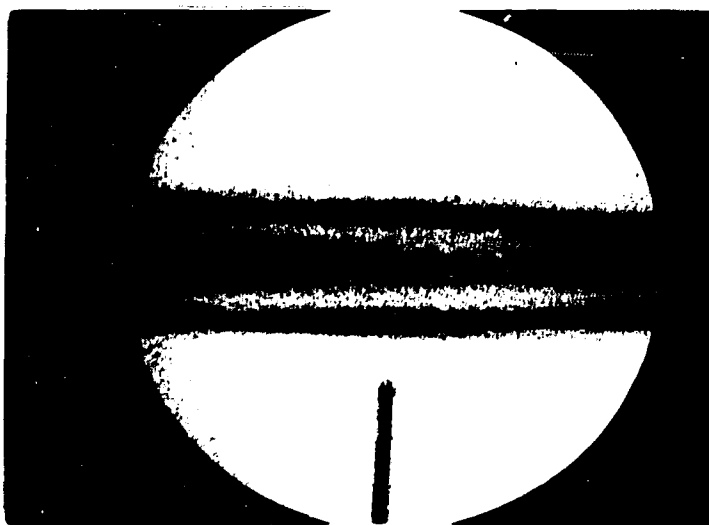


Figure 3-15 Image of the same sound wave as above, but reconstructed from a hologram which was recorded without the use of a diffusion screen

identical to Figure 3-15, the resultant image is not illustrated here.

Finally, the radiance distribution was measured over the cross-section of the sound beam immediately above the "pointer". Figure 3-16 shows the comparison of these measurements for the three images discussed above.

Referring to Figure 3-16, it is evident that the radiance distributions agree well within experimental error. Notice also that the radiance distributions of the reconstructed image (hologram recorded without a diffuser) and of the Schlieren image are somewhat irregular and that their minima approach zero; whereas a smooth distribution of reduced contrast is obtained from the hologram which was recorded with a diffusion screen. As discussed on pages 60 and 69, both of these results are expected.

If it is again assumed that the radiance distributions in Figure 3-16 are due to a plane sound wave having a circular cross-section, then the positions of the minima and maxima allow one to calculate the effective beam diameter L and the Raman-Nath parameter (kLN) at the beam axis. Hence, with reference to Figure 3-16, as the beam is scanned from either edge to its center, the following relations prevail

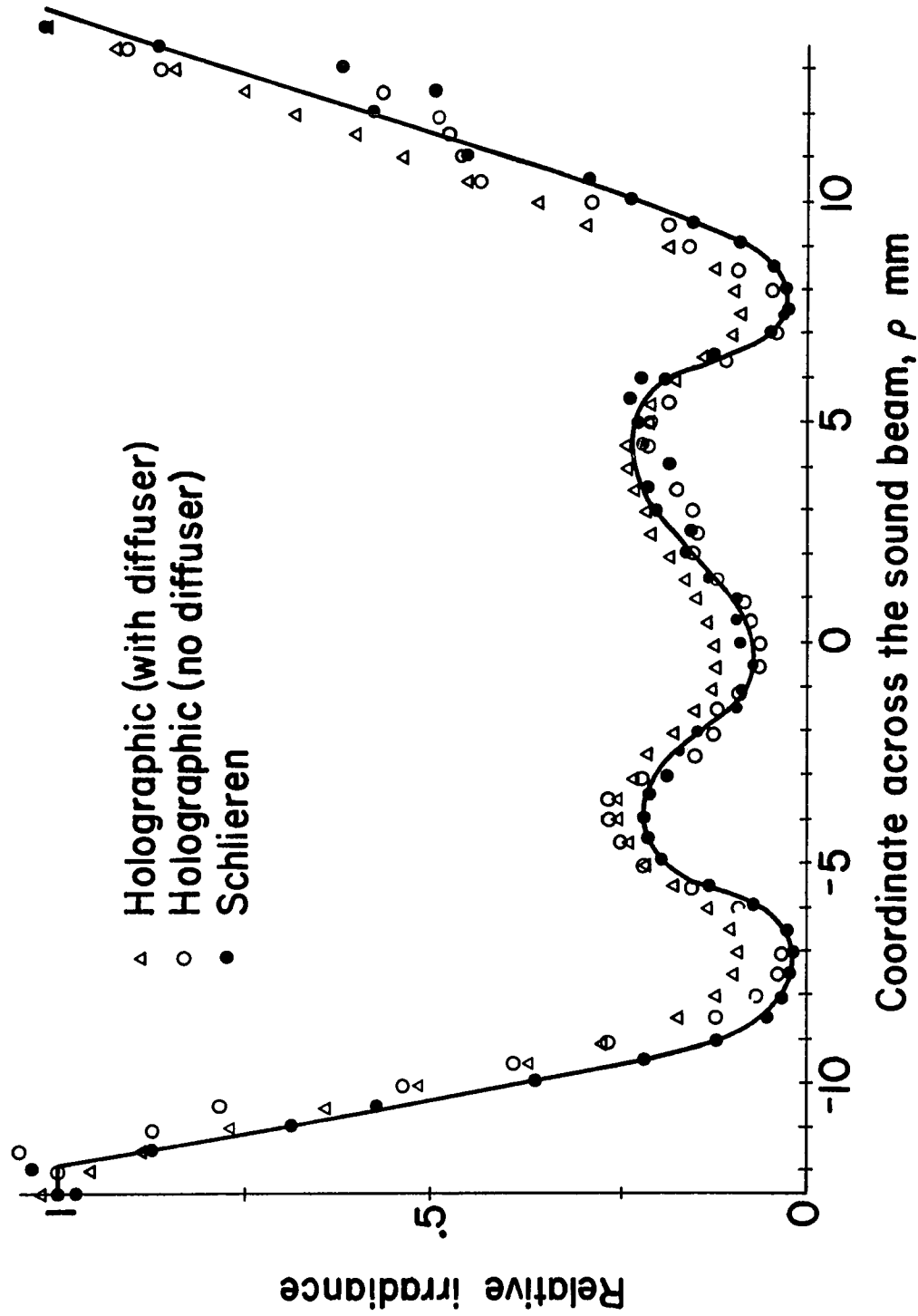


Figure 3-16 Comparison of the radiance distribution in the images formed by a Schlieren system and two holographic methods

$$kN [L^2 - (2\rho_1)^2]^{\frac{1}{2}} = 2.405 \quad \text{at first minimum}$$

$$kN [L^2 - (2\rho_2)^2]^{\frac{1}{2}} = 3.832 \quad \text{at second maximum}$$

where

$$\rho_1 = \text{cross-sectional coordinate at the first minimum,} \\ \approx 7.5 \text{ mm}$$

$$\rho_2 = \text{cross-sectional coordinate at the second maximum,} \\ \approx 4.5 \text{ mm}$$

The above two relations may be solved simultaneously to yield $L \approx 17.9$ mm and $(kLN) \approx 4.4$.

Sound waves were also made visible by the holographic and Schlieren methods when the frequency of the reference wave used to record the hologram as well as the frequency of the light wave allowed to pass the spatial filter (in the Schlieren system) were translated by an integer multiple of the sound frequency.

Figure 3-17 diagrammatically shows the arrangement used to record the hologram. Note that the same acoustic wave which is made visible is also used to translate the frequency of the optical reference wave. As shown, any desired order of shift in the reference frequency can be selected by properly positioning the spatial filter.

Figures 3-18a, b and c are reconstructed images showing a (6.5 MHz) sound wave propagating to the left in a water medium. The holograms corresponding to parts "b" and "c" were recorded in accordance with Figure 3-17 and with $n = 1$ and 2 , respectively. The hologram corresponding

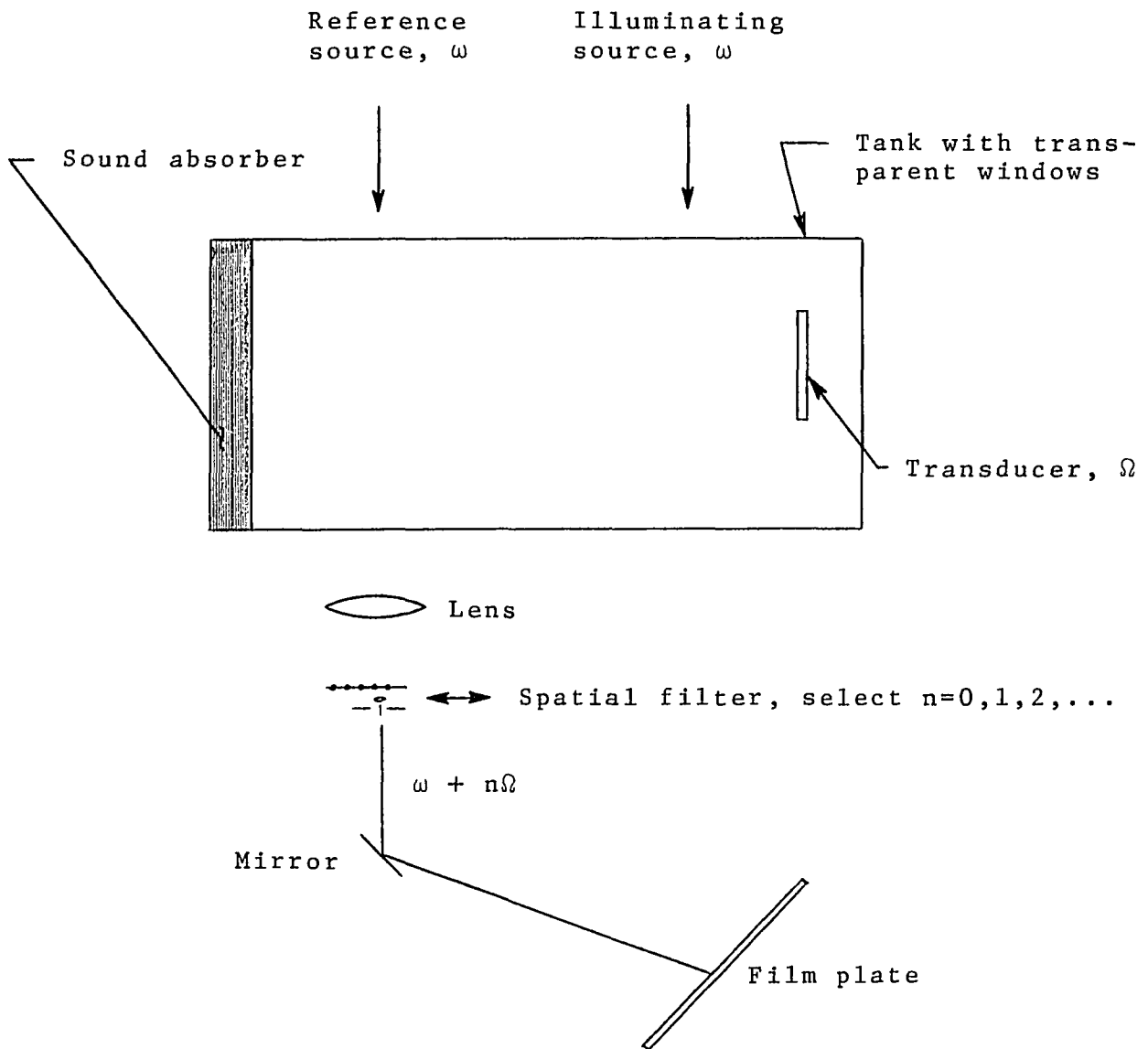


Figure 3-17 Arrangement used to record holograms with a "frequency shifted" reference wave

HOLOGRAPHIC

SCHLIEREN

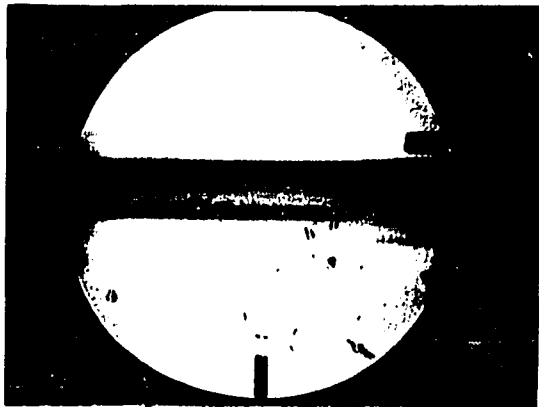
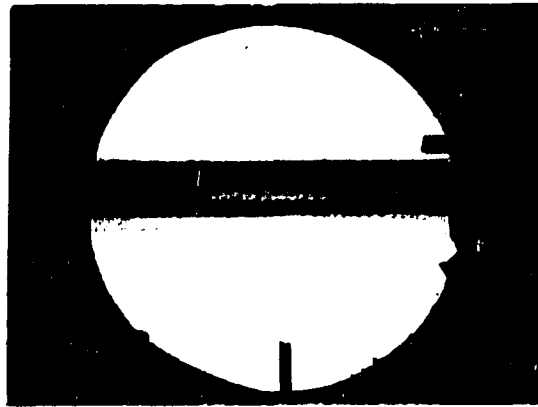
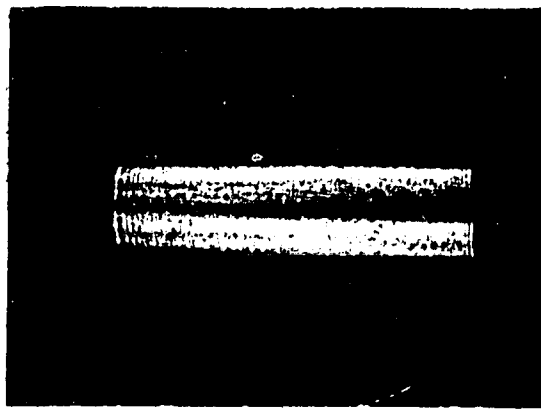
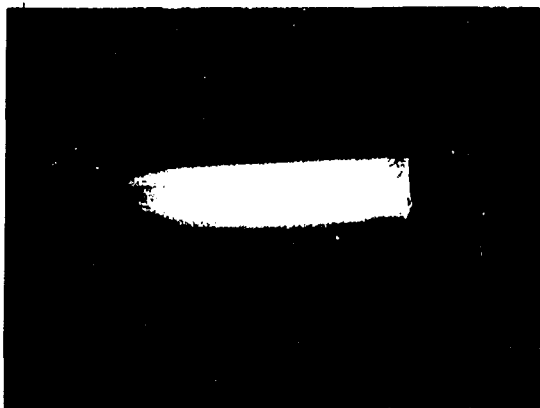
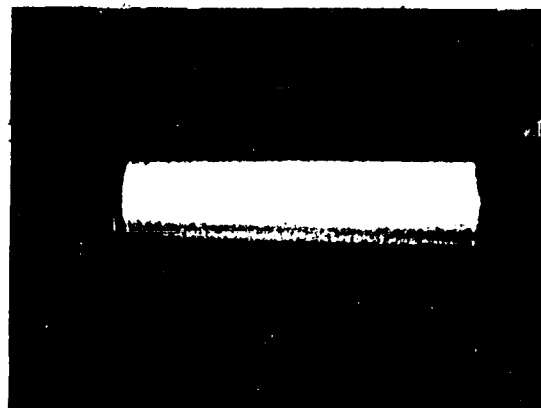
a, $n = 0$ a', $r = 0$ b, $n = 1$ b', $r = 1$ c, $n = 2$ c', $r = 2$

Figure 3-18 Comparison of holographic reconstructed and Schlieren images (see text)

to image "a" was recorded with $n = 0$; but rather than traversing the water medium, as shown in Figure 3-17, the reference wave was routed around the tank (the reason for this action will become apparent shortly). All three images were reconstructed as per the arrangement shown in Figure 3-4b.

A Schlieren system (as per Figure 3-5) utilizing the same plane wave illuminating source as the above holograms, was used to image a similar (but not the same) sound wave. Figures 3-18a', b' and c' show the Schlieren images which were formed when the 0, 1st and 2nd spectral orders were allowed to pass the spatial filter, respectively.

Figure 3-18 illustrates a number of characteristics of both visualization systems. As discussed previously, in images obtained with a "zero-order shift" (Figures 3-18a and a'), the regions where no sound is present (the background) appears uniformly bright; whereas the background in all other images is uniformly dark. This is a direct consequence of equation (3-11); that is

$$\psi_n(\mu=0) = \begin{cases} 0 & \text{when } n \neq 0 \\ 1 & \text{when } n = 0 \end{cases} \quad (3-25)$$

The undesirable effect of slow-moving water currents which results in a loss of coherence and therefore, a loss of image detail, is evident in all of the reconstructed

images. The effect, however, is more pronounced in parts b and c - probably because both the illuminating and reference waves traversed the water medium during the recording of the hologram. (This result suggests one method of minimizing this disturbance; that is, decreasing the total optical path length in the water medium.) Image "a" also exhibits a number of "speckles". These are due to dust particles which were trapped by the swollen emulsion during the photographic processing of the hologram. As discussed on page 60, their effect appears in the reconstructed image because the hologram was recorded with non-diffuse illumination.

Notice that the sound beam appears wider in parts b or b' than in a or a'. This results from the greater sensitivity of each system when the "first-order shift" is utilized. As an example, consider that the sound wave is plane and progressive so that the radiance within each respective image is (see equation 3-22)

$$\mathcal{R} \propto \begin{cases} J_0^2(kl_m N) & \text{zero-order shift} \\ J_1^2(kl_m N) & \text{first-order shift} \end{cases}$$

Since the contrast in the latter is theoretically infinite, i.e. $\left[J_1^2(kl_m N) / J_1^2(0) \right] = \infty$, the edge of the sound beam in this image appears visible for a smaller value of $(kl_m N)$ than in the image obtained with a "zero-order shift". Hence, if the sound beam has a circular cross-section, it

will appear to have a larger diameter in images which are obtained with a "first-order shift."

Comparing the radiance distributions over the cross-section of the sound beam in the corresponding images shown in Figure 3-18, it is noted that those of parts a and a', and c and c' appear almost the same whereas those of parts b and b' differ. (Remember that the contrast in the reconstructed images is reduced somewhat due to the use of a diffusion screen in the reconstruction process.) Since the radiance at the sound beam axis in Figure 3-18b' approaches a minimum whereas that in image b does not, the acoustic intensity of the sound wave imaged with the Schlieren system appears to be higher than that of the sound wave which is made visible with the holographic method.

Comparing the holographic and Schlieren visualization systems, it is evident that, on a theoretical basis, the two systems described in this chapter are equally versatile. On a practical basis, however, one or the other system may be more suitable for a particular application.

The primary advantage of the Schlieren system is that the imaging process is a "real-time" process. Furthermore, it is possible to obtain information about the sound wave by analyzing either the diffraction spectra directly or

the radiance distribution in the image plane. However, for accurate analyses, high quality glass windows and special Schlieren-free lenses are required. Furthermore, the task of separating the spectral orders becomes increasingly more difficult as the sound frequency is decreased (see equation (3-15)) since this requires that the focal length of the lens and the light beam diameter become increasingly larger. Thus, due to practical considerations, it is generally accepted that the Schlieren system cannot be used to image sound waves whose frequency is less than about 500 KHz.

The holographic method, on the other hand, is not affected by this low-frequency restriction. This is illustrated in Figures 3-12 and 3-13 - normally, these images could not be obtained with Schlieren methods. Furthermore, a permanent and accurate record of the distribution of irradiance within the image can be obtained with relatively simple optics, permitting measurements of the Raman-Nath parameter (under plane wave assumptions) even long after the production of the acoustic phenomenon. This, of course, can also be accomplished with the Schlieren method, but it requires special control of the photographic parameters. As a result, the holographic technique is particularly suited for the investigation of acoustic transients.

Chapter IV

DETECTING AND MEASURING THE DISPLACEMENT AMPLITUDE
OF VIBRATING OBJECTS

The work described in Chapters V and VI makes use of devices which permit the detection and measurement of small (fractions of a wavelength) sinusoidal vibration amplitudes. In this chapter, some of the existing interferometric detection methods and modifications thereof are discussed.

Modified Michelson Interferometer

Figure 4-1 shows the diagram of a modified Michelson interferometer. The arrangement is similar to that used by Deferrari¹⁸ except that a spatial filter (see note 1) has been added in order to increase the signal-to-noise ratio.

Referring to Figure 4-1, a monochromatic wave of frequency ω is split into two waves by the beam splitter. One of these waves (reference wave) is reflected from a "fixed" mirror while the other is focused onto the vibrating object by the objective. (By focusing the light onto the object, the system can be used to investigate non-polished objects.) The wave reflected by the object (object wave) and the reference wave are recombined at the beam splitter, spatially filtered, and detected by the photo detector. The function

Note 1. The addition of a spatial filter was originally suggested by M. Lurie of RCA Laboratories, Princeton, N. J., 08540.

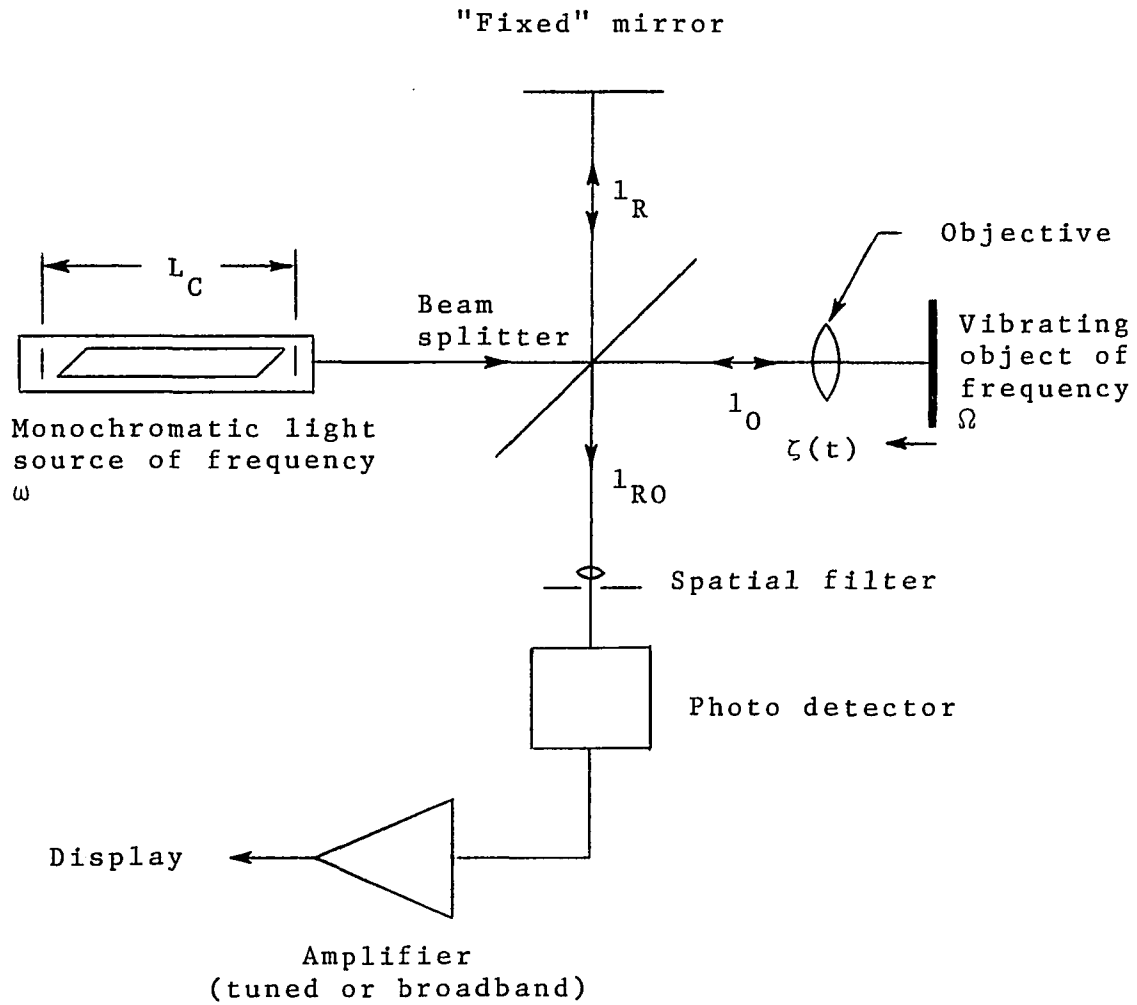


Figure 4-1 Arrangement of the modified Michelson interferometer

of the spatial filter is to select only the plane wave component of each interfering wave so that less than one fringe appears across the aperture of the receiving photo detector.⁸⁹

The irradiance at the photodetector can be expressed as

$$Q \propto \left\{ E_R \cos[\omega t - k(2l_R + l_{RO})] + E_O \cos[\omega t - k(2l_O + l_{RO} - 2\zeta)] \right\}^2 \quad (4-1)$$

where

E_R = electric field amplitude of the reference wave

E_O = electric field amplitude of the object wave

ω = angular frequency of the light source

$k = 2\pi/\lambda$

λ = wavelength of the light source

l_R = optical path length between the beam splitter and the "fixed" mirror

l_O = optical path length between the beam splitter and the mean position of the object

l_{RO} = optical path length between the beam splitter and the photo detector

$\zeta(t)$ = instantaneous vibration amplitude of the object

The photo detector responds to the irradiance expressed in equation (4-1), but since it cannot respond to the high optical frequencies, the resultant current output of the phototube is

$$i(t) \propto \frac{1}{2} E_R^2 + \frac{1}{2} E_0^2 + E_R E_0 \cos \phi(t) \quad (4-2)$$

where

$$\phi(t) = 2k[l_0 - l_R - \zeta(t)] = \theta_0 - 2k \zeta(t)$$

$$\theta_0 = 2k(l_0 - l_R)$$

If the motion of the object is sinusoidal and of frequency

Ω , i.e. $\zeta(t) = A \sin \Omega t$, then

$$i(t) \propto \frac{1}{2}(E_R^2 + E_0^2) + E_R E_0 \cos \theta_0 \sum_{m=0,2,4,\dots} J_m(2kA) \cos m\Omega t \\ + E_R E_0 \sin \theta_0 \sum_{m=1,3,5,\dots} J_m(2kA) \cos m\Omega t \quad (4-3)$$

where $J_m(2kA)$ is the m^{th} order Bessel function of argument $(2kA)$ and A is the peak vibration amplitude of the object. Hence, the photo detector current contains an infinite number of frequency components which are related harmonically to the fundamental frequency of the vibrating object.

Examination of equation (4-3) also shows that the amplitude of each frequency component depends on the vibration amplitude (through the term $J_m(2kA)$) as well as on the mean positions of the object and "fixed" mirror (through the angle θ_0). Specifically, irrespective of the vibrational amplitude A of the object, all even numbered frequency components are zero when $(l_0 - l_R) = (1+2n) \lambda/8$, $n=0,1,2,\dots$; and all odd numbered frequency components are zero when $(l_0 - l_R) = n\lambda/4$, $n=0,1,2,\dots$. Therefore, the amplitude of any one frequency component will vary from

zero to a maximum as the mean position of the object or the position of the "fixed" mirror drifts by $\lambda/8$.

The result of the above discussion is that extreme mechanical stability is required. When small displacement amplitudes are to be measured, it may even be necessary to use a feedback system to vary (electromagnetically or piezoelectrically) the position of either the "fixed" mirror or the object so that $(l_0 - l_R)$ remains constant.

The sensitivity of this interferometer can be maximized by

1. Adjusting the radiance of the reference or object beams so that $E_R = E_0$
2. Adjusting the mean position of the object or fixed mirror so that $\sin \theta_0 = 1$ and $(l_0 - l_R) \approx nL_C$, $n=0,1,2,\dots$ (see Fig. 4-1 and page 108) where L_C is the length of the laser cavity
3. Selecting only the fundamental frequency component ($m=1$ in eq. 4-3) by means of an amplifier tuned to Ω

Under these conditions, the photo detector output signal is

$$\text{output signal} \propto J_1(2kA) \cos \Omega t \quad (4-4)$$

There are several techniques that can be used to calibrate this interferometer.¹⁸ A simple and accurate method is to vary the vibration amplitude of the object and to record the maximum output signal from the amplifier in Figure 4-1 when the amplifier is tuned to the fundamental frequency Ω . Since this point is precisely known, namely

$2kA = 1.841$, the displacement amplitude A of the object can be calculated ($A = 927 \text{ \AA}$ for $\lambda = 6328 \text{ \AA}$). Any other vibration amplitude can be determined absolutely by relating the corresponding amplifier output signal to the "calibrated" signal through the known variation of the first order Bessel function.

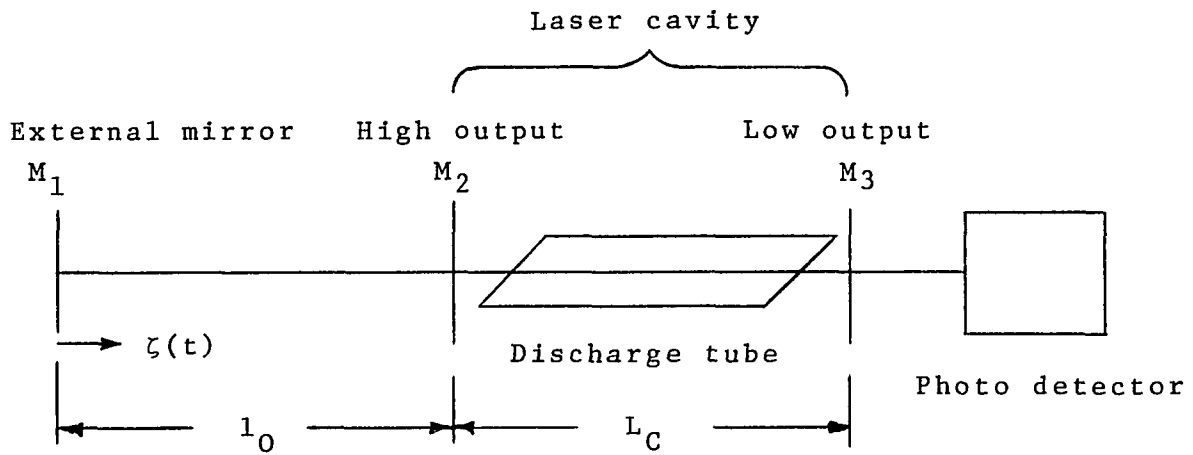
The above absolute vibration amplitude measurement requires that θ_0 remain constant and that a vibration amplitude of at least 927 \AA can be attained. If either one of these two requirements cannot be met, a more satisfactory measurement technique may be to record the amplitudes of the fundamental and third harmonic frequency components simultaneously with a spectrum analyzer. In this manner, absolute vibration amplitudes can be calculated from the ratio $J_1(2kA)/J_3(2kA)$ (for an example of this technique, see the next section). With modern spectrum analyzers having a dynamic range of 80 dB, the interferometer can be calibrated with as little as 50 \AA ($\lambda = 6328 \text{ \AA}$) of displacement amplitude.

Once the interferometer has been calibrated, absolute vibration amplitudes of less than 10 \AA can be measured with ease; in fact, Khanno⁴⁶, using an arrangement similar to that shown in Figure 4-1 (but without the spatial filter) has reported the measurement of a displacement amplitude of 0.03 \AA .

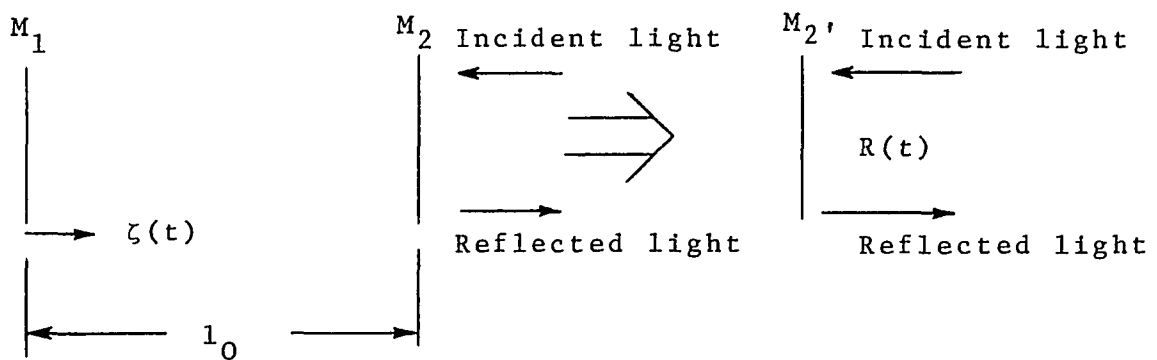
Laser Feedback Interferometer

A laser interferometer which has been used to measure large displacement amplitudes (several wavelengths) and velocities of vibrating objects is shown in Figure 4-2a. An external mirror M_1 is positioned so that nearly all of the light is reflected back into the laser cavity, and a photo detector monitors the light emerging from the other end of the laser cavity. As the external mirror moves along the laser axis, King and Steward⁴⁷ noted that the laser power output at the photo detector may be enhanced or diminished, and that the effect is periodic for each half-wavelength of motion of the mirror M_1 .

Although the laser interferometer shown in Figure 4-2a consists of only a few components, its operation, from an optical point of view is quite complicated since the addition of the external mirror M_1 effectively forms two coupled Fabry-Pérot optical resonators, one of which (the laser cavity) contains an "active" medium. Hence, in order to describe the effect reported by King and Steward most completely, it is necessary to explore the resonant frequencies and eigenfunctions of such a system. To the knowledge of this author, such a general analysis has not been performed, although the system has been discussed under several simplifying approximations.^{15,76}



a) Arrangement of the laser feedback interferometer



b) Replacing the external cavity with an equivalent reflector having reflectance R

Figure 4-2 The laser feedback interferometer and a simple method of analyzing its principle of operation

One such approximate analysis is to consider only the multiple-beam interference of the external cavity formed by mirrors M_1 and M_2 and to treat the laser cavity and its "active" medium as an optical oscillator whose feedback coefficient is appropriately modulated. Referring to Figures 4-2a and 4-2b, the etalon properties of the Fabry-Perot cavity formed by the externally vibrating mirror M_1 and the laser cavity mirror M_2 allow it to be replaced with a fixed reflector M_2' having an equivalent reflectance R , which can be expressed as

$$R = \frac{r_2^2 + r_1^2(1-L_2)^2 - 2r_1r_2(1-L_2)\cos \sigma(t)}{1 + (r_1r_2)^2 - 2r_1r_2\cos \sigma(t)} \quad (4-5)$$

where

$$\sigma(t) = 2k[l_0 - \zeta(t)] = \theta_0' - 2k\zeta(t)$$

R = equivalent reflectance of the external cavity formed by mirrors M_1 and M_2

r_1 = amplitude reflectivity of the external mirror M_1 for light coming from M_2

r_2 = amplitude reflectivity of the laser cavity mirror M_2 for light coming from M_1

L_2 = fraction of the incident energy that is absorbed during each reflection at mirror M_2

$\sigma(t)$ = phase difference between successive interfering waves (see note 2)

Note 2. Strictly speaking, σ is the same only when M_1 is stationary. Furthermore, the frequency of the light reflected back into the laser cavity experiences a Doppler shift which must be less than the bandwidth of the laser oscillator. For these reasons, this analysis applies only for low frequency vibrations of the mirror M_1 .

$$\theta'_0 = 2kl_0$$

$$k = 2\pi/\lambda$$

λ = wavelength of the incident light

$\zeta(t)$ = instantaneous vibration amplitude of the mirror M_1

The equivalent reflector M'_2 and the mirror M_3 are now considered to form the laser cavity. As the external mirror M_1 slowly moves along the laser axis, the reflectance R of M'_2 varies in accordance with equation (4-5) and changes the feedback coefficient of the laser oscillator; with the result that the laser output power is modified. Clunie and Rock¹⁵ experimentally demonstrated that, for low vibrational frequencies of the mirror M_1 , the irradiance at the photo detector and therefore, the photo detector output is proportional to the reflectance R of the equivalent cavity mirror M'_2 .

$$\text{photo detector output} \propto R(t)$$

It should be recognized that the expression for the reflectance R (equation (4-5)) is the Airy function for the light reflected from a Fabry-Perot interferometer having unequal mirror reflectivities. For such a system, the reflectance and therefore, the photo detector output is a minimum whenever $\sigma = n2\pi$, $n=0,1,2,\dots$, i.e. whenever the mirror displacement is $\lambda/2$ from a position of maximum output (tuned Fabry-Pérot cavity). Hence, this result essentially describes the observation made by King.⁴⁷

A discussion of other interesting characteristics of this interferometer and a somewhat different analysis are given by Rudd.⁷⁶ For further information about the operating principle of this interferometer, the reader may consult Kleinman⁴⁹ and Kogelnik⁵⁰ since the arrangement shown in Figure 4-2a can be used for mode suppression and single frequency operation of gas lasers.

To the knowledge of this author, the absolute measurement of small (fractions of a wavelength) vibration amplitudes with the laser feedback interferometer represents a new application of this device. If, in equation (4-5), the product $r_1 r_2$ is small compared to unity, the reflectance and therefore, the photo detector current becomes

$$i(t) \propto R(t) \approx r_2^2 + r_1^2(1-L_2)^2 - 2r_1 r_2(1-L_2)\cos \sigma(t) \quad (4-6)$$

The condition that $r_1 r_2 \ll 1$ is equivalent to stipulating that interference occurs only between the initial waves reflected from mirrors M_1 and M_2 (see Figure 4-2b). Comparing equations (4-6) and (4-2), $i(t)$ is

$$i(t) \propto r_2^2 + r_1^2(1-L_2)^2 - 2r_1 r_2(1-L_2)\cos \theta'_0 \sum_{m=0,2,4,\dots} J_m(2kA)\cos m\Omega t \\ - 2r_1 r_2(1-L_2)\sin \theta'_0 \sum_{m=1,3,5,\dots} J_m(2kA)\cos m\Omega t \quad (4-7)$$

where $J_m(2kA)$ is the m^{th} order Bessel function of argument $(2kA)$ and A is the peak vibration amplitude of the mirror M_1 . Hence, the previous discussion about the variation

of each harmonic frequency component with the mean position of the object (mirror M_1), the mechanical stability requirements, and the calibration procedure applies equally well here when $(l_0 - l_R)$ on page 100 is replaced with l_0 .

Under the condition that $r_1 r_2 \ll 1$, the laser feedback interferometer can be thought of as a Michelson interferometer where the external cavity is considered to be one arm and where the laser cavity is considered to be the reference arm. The laser mirrors M_2 and M_3 provide feedback for the optical oscillator as well as spatial filtering of the resultant beam. The analogy can be carried one step further when one compares the condition for the maximum fringe visibility at the photo detector aperture (assuming that the Michelson interferometer uses a laser as a source of light).

$$\begin{aligned} \text{Michelson interferometer} \quad (l_0 - l_R) &= nL_C \\ \text{Laser feedback interferometer} \quad (l_0 - L_C) &= (n-1)L_C \end{aligned} \quad (4-8)$$

where $n=0,1,2,\dots$ and L_C is the length of the laser cavity.

Absolute vibration amplitudes of a vibrating piezoelectric crystal (150 KHz) were measured with the arrangement shown in Figure 4-3a. The objective was mounted directly on the laser housing so that the optical alignment consisted merely of positioning the laser-lens combination until the light was focused onto the crystal surface. The crystal electrode was not polished so that

the condition $r_1 r_2 \ll 1$ was satisfied.

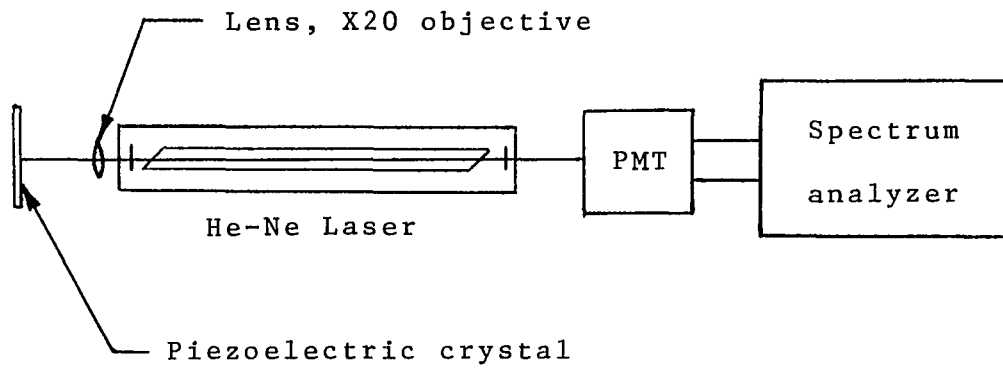
The spectrum (spectra are displayed on a log scale) of the photo-tube current is pictured in Figure 4-3b.

As the crystal voltage was varied, the first maximum and minimum of the amplitude of the fundamental frequency component could be observed. Also observed was the alternate "extinction" of all the even and odd harmonic frequency components as thermal expansion of the crystal changed its average thickness.

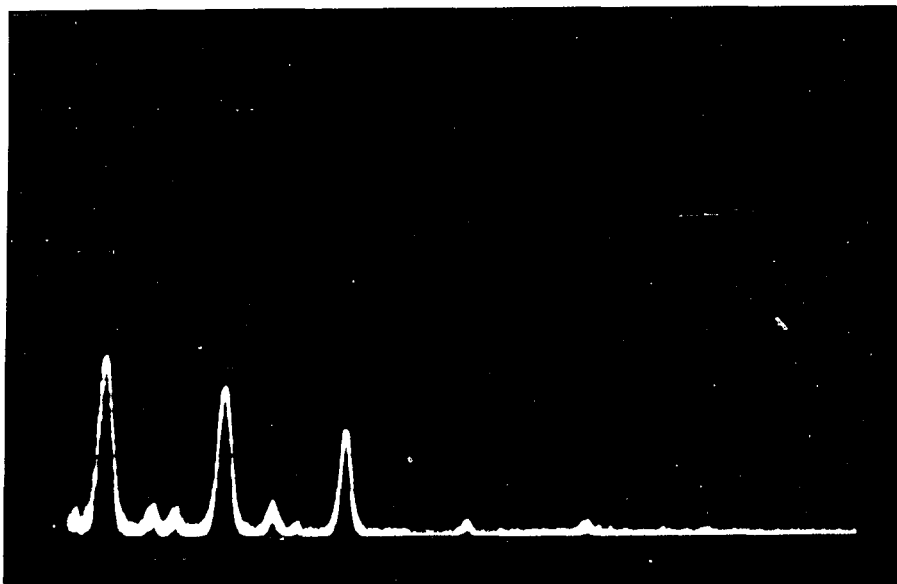
Referring to Figure 4-3b and to the discussion on page 102, the ratio of the amplitude of the first and third frequency components is 3.13, so that $2kA=2.28$ and $A=1150 \text{ \AA}$. The maximum vibration amplitude A can also be obtained by making a similar calculation for the 2nd and 4th frequency components. This provides a check on the absolute measurement of A .

In addition to the five harmonically related frequency components, Figure 4-3b also shows other spectral components. It was observed that the frequency of these spurious components slowly varied throughout the experiment, and for this reason, they are believed to be due to thermal motion of the laser cavity mirrors.

Under the simplifying conditions considered in this section, the performance of the laser feedback and modified



- a) Practical arrangement for investigating the crystal vibrations with a laser feedback interferometer



- b) Resultant spectrum of the laser output

Figure 4-3 Investigating the vibrations of a piezoelectric crystal with the laser feedback interferometer

Michelson interferometers appears to be the same. However, from a practical point of view, the laser feedback interferometer is considerably simpler to align; and, despite the fact that, in this form, the system exhibits a low signal-to-noise ratio because of the requirement that $r_1 r_2 \ll 1$, it is estimated that absolute displacement amplitudes of $30 \overset{\circ}{\text{Å}}$ can be measured with relative ease.

"Holographic Interferometer"

The interferometric properties of holography are, by now, well known. Although there are other techniques such as the "real-time" and "double-exposure" methods, only the "time-averaged" holographic interferometric technique is discussed here, and the system will be referred to as the "holographic interferometer."

Unlike the previously discussed interferometers, the "holographic interferometer" is able to simultaneously record the vibration amplitude of every point of a vibrating object. In order to demonstrate this important feature of the "holographic interferometer", Figure 4-4a shows the reconstructed image of a 1-1/2" dia. piezoelectric crystal which is vibrating in air at 328 KHz. Under the conditions used during the recording of this hologram (to be described later), Zambuto and Lurie⁹⁹ have shown that the radiance of a point m' in the reconstructed image corresponding to the object point m of a sinusoidally vibrating object is

$$R_m \propto J_0^2(2kA) \quad (4-9)$$

where $J_0(2kA)$ is the zeroeth order Bessel function of argument $(2kA)$ and A is the peak vibration amplitude of point m . Hence, by measuring the irradiance at each point in the reconstructed image, it is possible to calculate the peak vibration amplitude from the known variation of J_0^2 (see Figure 3-7).

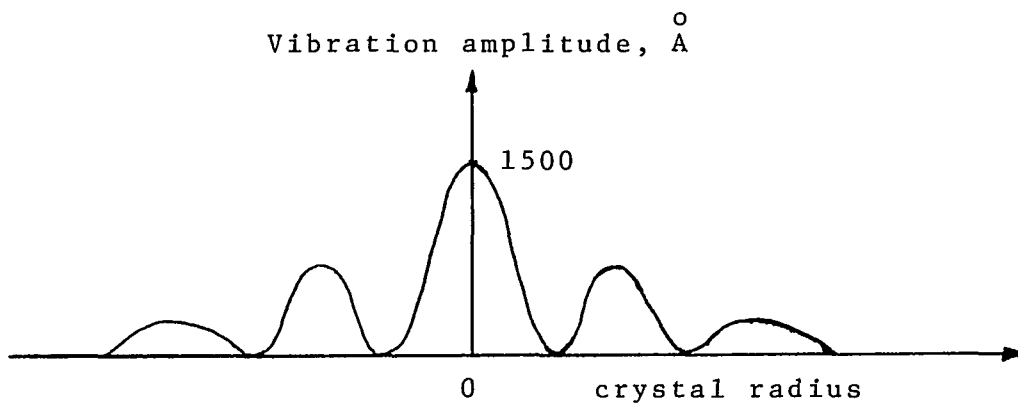
The result of such a computation at each point of the transducer surface is illustrated in Figure 4-4b. The vibration nodes and antinodes of the crystal surface are due to the finite diameter of the crystal. (A more detailed discussion of the various modes of vibration of barium titanate disks is given by Shaw.⁸¹)

Using equation (4-9) and the familiar Rayleigh criterion, it can be shown that the sensitivity of the "holographic interferometer" is approximately 330 \AA ($\lambda = 6328 \text{ \AA}$). Although this sensitivity is adequate for many applications, it does not compare with that of the previously described interferometers. However, by appropriately shifting the frequency of the reference wave used to record the hologram (see note 3), it is potentially possible to obtain a sensitivity approaching that of the Michelson interferometer. This holographic technique is

Note 3. This work is presently being prepared for publication.



a) Reconstructed image of a piezoelectric crystal vibrating in air at 328 KHz



b) Vibration amplitude profile of the above crystal

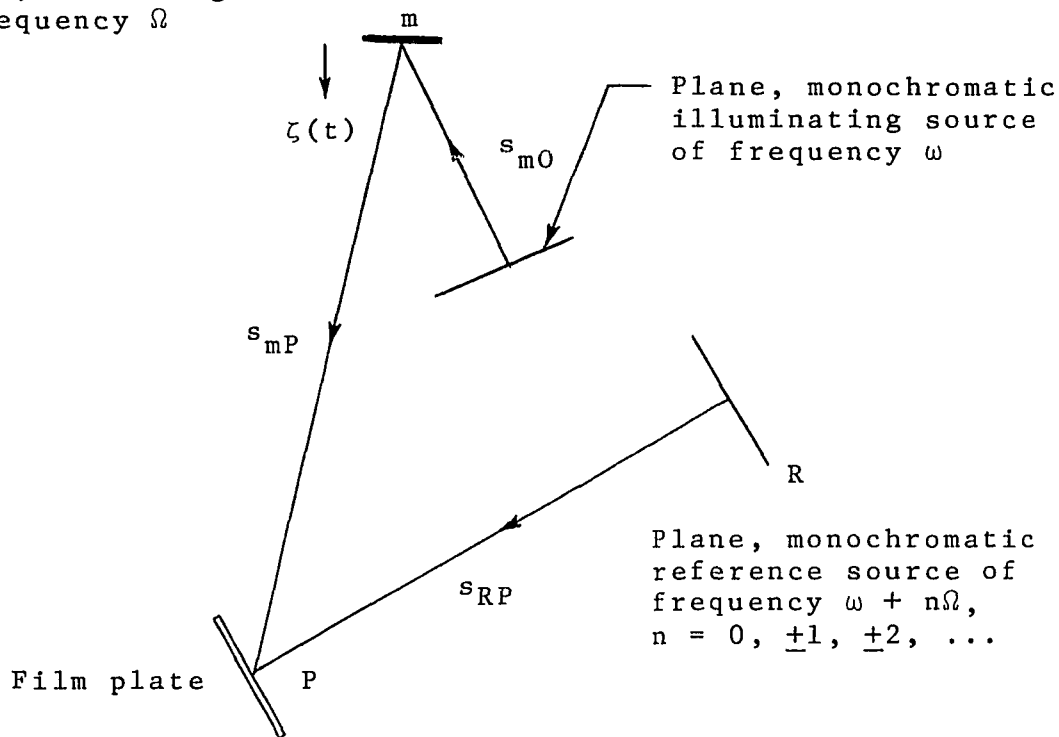
Figure 4-4 Investigating the vibrations of a piezoelectric crystal with the holographic interferometer

very similar to that used in Chapter III to visualize sound waves. Indeed, the only difference is the method by which the object wave is phase modulated.

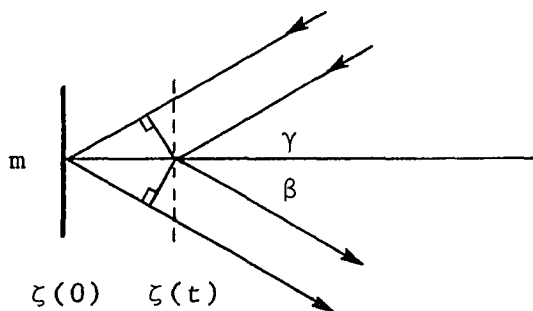
Figure 4-5a shows the geometry of the recording process of the "shifted reference holographic interferometer". It is the familiar arrangement of plane wave, split-beam holography in which the film emulsion records the stationary interference pattern formed by the interference of a phase modulated object wave and a highly coherent reference wave. The modification to the usual holographic technique consists in shifting the frequency of the reference wave by an integral multiple of the frequency of the vibrating object. Note that the arrangement is similar to that shown in Figure 3-2 except that in this case the object wave is phase modulated by varying its geometrical path length, while in Chapter III, the phase is modulated by varying the refractive index of the medium traversed by the object wave.

The method used to determine the radiance in the reconstructed image is identical to that used in Chapter III (based on coherence theory). It is assumed that during the recording process the reference radiation at the film plate is plane and monochromatic and that the object wave uniformly illuminates the film plate. It is further assumed that the hologram is reconstructed with a plane monochromatic wave. Under these conditions, equations

Object, vibrating
at frequency Ω



a) Geometry of the recording process of the "shifted reference holographic interferometer"



b) Geometry for determining the phase shift due to the motion of point m

Figure 4-5 Arrangement of the "shifted reference holographic interferometer" and geometry for determining ξ_{mR}

(3-1) and (3-2) apply so that the problem of calculating the radiance in the reconstructed image reduces to one of determining the modified complex degree of coherence g_{mR} at an arbitrary point P in the hologram plane.

Referring to Figure 4-5a, let \underline{m} be a point on the object and P a point on the film plate. The phases of the two interfering waves at point P can be describes as

$$\phi_R = (\omega + n\Omega)t - (\omega + n\Omega)s_{RP}/c \quad (4-10)$$

$n=0, \underline{+1}, \underline{+2}, \dots$

$$\phi_m = \omega t - ks_{m0}(t) - ks_{mP}(t) - C_1 \quad (4-11)$$

where

ϕ_R = phase at point P of the radiation coming from the reference source R

ϕ_m = phase at point P of the radiation coming from the object point \underline{m}

ω = radial frequency of the illuminating source

c = speed of light in vacuum

$k = \omega/c$

Ω = radial frequency of the vibrating object

$n =$ an integer, $0, \underline{+1}, \underline{+2}, \underline{+3}, \dots$

$(\omega+n\Omega)$ = frequency of the reference radiation

t = time

s_{RP} = optical path length between the reference source and the point P

$s_{m0}(t)$ = optical path length between the illuminating source and the object point \underline{m}

$s_{mP}(t)$ = optical path length between points \underline{m} and P

C_1 = the constant phase shift between the reference and illuminating sources

Referring to Figure 4-5b, the total path length between the illuminating source O and the point P is

$$s_{mO}(t) + s_{mP}(t) = \overline{s_{mO}} + \overline{s_{mP}} - (\cos \gamma + \cos \beta) \zeta(t) \quad (4-12)$$

where

$\overline{s_{mO}}$ = mean optical path length between the object point \underline{m} and the illuminating source O

$\overline{s_{mP}}$ = mean optical path length between the object point \underline{m} and point P

γ = angle of incidence of the light at point \underline{m}

β = angle of the light reflected from point \underline{m}

$\zeta(t)$ = instantaneous displacement amplitude of the vibrating point \underline{m}

Substituting equations (4-10), (4-11), and (4-12) into the expression for the complex degree of coherence g_{mR} (see equation (3-2)), it follows that

$$g_{mR} = \exp i\phi'_0 \frac{1}{T} \int_0^T \exp \left\{ i \left[n\Omega t - k(\cos\gamma + \cos\beta)\zeta(t) \right] \right\} dt \quad (4-13)$$

where

$$\phi'_0 = k(s_{mO} + s_{mP} - s_{RP}) - n\Omega s_{RP}/c + C_1$$

T = exposure time of the photographic emulsion

Comparing now equations (4-13) and (3-6), it is noted that their form is similar. Hence, when $T \gg 1/\Omega$, the radiance $\mathcal{R}_{m'}$ at point m' in the reconstructed image corresponding to the object point \underline{m} can be expressed directly

$$\mathcal{R}_{m'} \propto |g_{mR}|^2 = |\psi_n|^2 \quad (4-14)$$

where

$$\psi_n = \frac{1}{2\pi} \int_0^{2\pi} \exp \left\{ i \left[k(\cos\gamma + \cos\beta)\zeta(t) - n\Omega t \right] \right\} dt$$

Therefore, if the motion of the point \underline{m} is sinusoidal, i.e. $\zeta(t) = A \sin\Omega t$, and $\gamma=\beta=0$, then

$$\mathcal{R}_{m'} \propto J_n^2(2kA) \quad n=0, \pm 1, \pm 2, \dots \quad (4-15)$$

where $J_n(2kA)$ is the n^{th} order Bessel function of argument $(2kA)$, and A is the peak vibration amplitude of point m .

This result is significant because by shifting the optical reference frequency by the n^{th} harmonic of the frequency of the vibrating object, only the n^{th} Fourier coefficient ψ_n of the phase of the object wave is used to modify the radiance of the reconstructed image. Note that, when the reference frequency is not shifted ($n=0$), equation (4-14) reduces to equation (4-9). It was under this condition, with the arrangement shown in Figure 4-5a ($n=0$, $\gamma=\beta=0$), that the hologram which yielded the image shown in Figure 4-4a was recorded. As was mentioned on page 112, the sensitivity of the holographic interferometer for this case ($n=0$, $\gamma=\beta=0$, $\lambda=6328 \text{ \AA}$) is 330 \AA .

However, when the reference frequency is shifted by one order ($n=\pm 1$), the radiance $\mathcal{R}_{m'}$ is proportional to $J_1^2(2kA)$, so that the ratio of the radiance of vibrating and stationary object points is theoretically infinite. Hence, the sensitivity of the modified holographic inter-

ferometer is significantly improved (see note 4) and is only limited by optical noise and fog in the photographic process. Indeed, when considering the fact that the time exposure of the photographic emulsion will tend to "average-out" some of the optical noise, it is expected that the sensitivity of this interferometer will approach that of the Michelson interferometer (see equation (4-4)).

In order to calibrate the "holographic interferometer", the vibration amplitude of at least one point of the vibrating object must be large enough so that $J_n(2kA)$ can be calculated from a known maximum or minimum of $J_n(2kA)$. If this is not possible, the instrument can be calibrated by recording two holograms with reference frequencies which differ by one order, and measuring the ratio of irradiance at corresponding reconstructed image points.

A direct demonstration of the ability of the "shifted reference holographic interferometer" to investigate the displacement amplitudes of vibrating objects is difficult since at high vibrational frequencies (greater than 2 MHz), the acoustical power required to vibrate an object by more

Note 4. The sensitivity of the modified holographic interferometer can be improved (until the noise level is reached) by using a more intense source of light. This, however, is not possible when $n = 0$.

than $50 \overset{\circ}{\text{Å}}$ is high. Although the interferometer is expected to readily detect such motion, the measurement also places a severe requirement on the mechanical system stability. On the other hand, at low vibrational frequencies (less than 1 MHz), it is difficult to efficiently translate the optical frequency of the reference wave. This difficulty is due to the necessary filtering which follows the optical heterodyne process.

Nevertheless, it should be recognized that the two holographic techniques of visualizing sound waves (see Chapter III) and of detecting vibrational displacement amplitudes are the same; only the manner of phase modulating the object wave is different. Hence, the experimental results of Chapter III indirectly demonstrate the success of obtaining a radiance distribution in accordance with equation (4-15) by appropriately translating the frequency of the optical reference wave.

The relative ease of adjusting the optical parameters of the "shifted reference holographic interferometer" as well as its high sensitivity and its ability to detect the displacement amplitude of every point of a vibrating, diffusely reflecting object would seem to make this device suitable for detecting motion induced by acoustic waves. Such an ultrasonic detector and its use in an acoustical imaging system are described in the next chapter.

Chapter V

FOUR-STEP ACOUSTICAL HOLOGRAPHY WITH THE OPTICAL
"HOLOGRAPHIC INTERFEROMETER"

In Chapter III several methods were described which can be used to show a side-view picture of a sound wave propagating in an optically transparent medium. More specifically, these detectors display the distribution of a quantity related to the Raman-Nath parameter in a plane parallel to the direction of sound propagation.

On the other hand, the detectors discussed in Chapter II are able to show the acoustic intensity distribution in a plane nearly normal to the direction of propagation of the sound wave.

In this chapter the techniques used in Chapters II-IV are utilized in a new acoustical holographic imaging system. The proposed method, which can be referred to as four-step acoustical holography, consists of the following processes

1. The generation of an acoustical hologram and its transfer from one medium (water) to another (air)
2. The optical recording of the acoustical hologram. In the proposed system, the resultant, converted acoustical hologram is obtained in two steps by using the holographic interferometer discussed in Chapter IV.

3. The reconstruction of the converted acoustical hologram

Generation and Transference of the Acoustical Hologram

Consider the conventional techniques of constructing an acoustical hologram as shown in Figure 5-1. An acoustical "reference" wave is made to interfere with an "object" wave at a given plane S_1 in the water medium. The resulting acoustical interference pattern at S_1 constitutes the acoustical hologram. For the purpose of eventually reconstructing the original object wave in visible form, it is desired to obtain an optical record of the interference pattern. This optical record of the acoustical hologram constitutes the converted acoustical hologram.

In order to accomplish this, recall from the discussion in Chapter I that such an acoustical diffraction pattern can be characterized by its unique distribution of vibration amplitudes. Hence, it is conceivable that any of the instruments discussed in Chapter IV can be used to record this distribution, provided it is first transferred from plane S_1 in the water medium to a surface S_2 situated in air.

This transference can be achieved by coupling, and a device which performs this task can be called a "coupler". The primary function of the coupler shown in Figure 5-1 is, therefore, to produce on surface S_2 a vibration

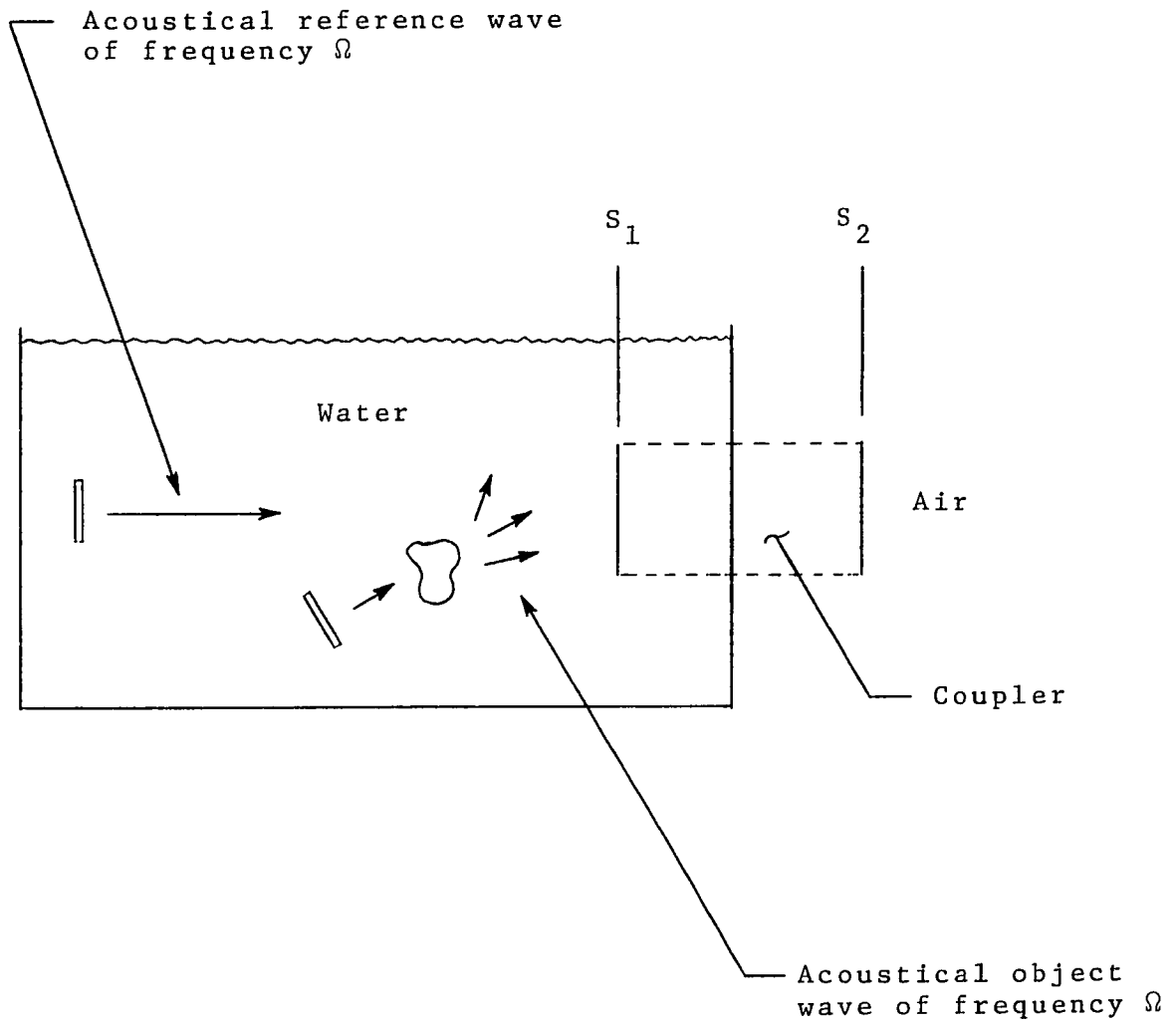


Figure 5-1 Step 1 - Forming the acoustical hologram on surface S₂ (bounded by air)

amplitude distribution whose form is similar to the distribution on S_1 .

Other desirable functions of the coupler as well as some possible, practical devices are discussed on page 132. From that discussion it will become evident that this transference is a critical part of the overall imaging system and that, in practice, the coupler largely determines the system's performance.

Recording the Acoustical Hologram

The purpose of recording the acoustical hologram is to obtain a properly scaled optical representation of the vibration amplitude distribution of S_2 . This optical record, referred to as the converted acoustical hologram, may then be used in the reconstruction process described on page 127.

Any of the interferometers discussed in Chapter IV may be used to record the acoustical hologram. Of these instruments, the ability of the optical "holographic interferometer" to simultaneously detect the vibration amplitude of each and every point on the surface S_2 makes this device most attractive; especially, since its use eliminates the need for scanning S_2 .

Using the "holographic interferometer", the recording of the acoustical hologram can be implemented in two steps

1. Obtain an optical hologram of surface S_2
2. Use this optical hologram to reconstruct and photograph the modified image of S_2

Figure 5-2a shows the arrangement for constructing the optical hologram of S_2 . As shown, the vibrating surface S_2 is the "object" of the "shifted reference optical holographic interferometer" and the frequency of the optical reference wave is shifted by one order ($n=1$) so that the sensitivity of the process is maximized.

The reconstruction process of the optical hologram is shown in Figure 5-2b. Recalling the discussion in Chapter IV, the virtual (or real) image obtained in this process is an optical representation of the vibration amplitude distribution of the surface S_2 and the record (photograph) of this virtual image represents the converted acoustical hologram of the object in the water medium. This latter recording (photographing the virtual image) incidentally affords an opportunity to scale the dimensions of the converted acoustical hologram (see Chapter I).

In the description of these two steps it has been assumed that the vibration amplitude of points on S_2 is sufficiently large to be detected by the interferometer. This important requirement is discussed in greater detail on page 130.

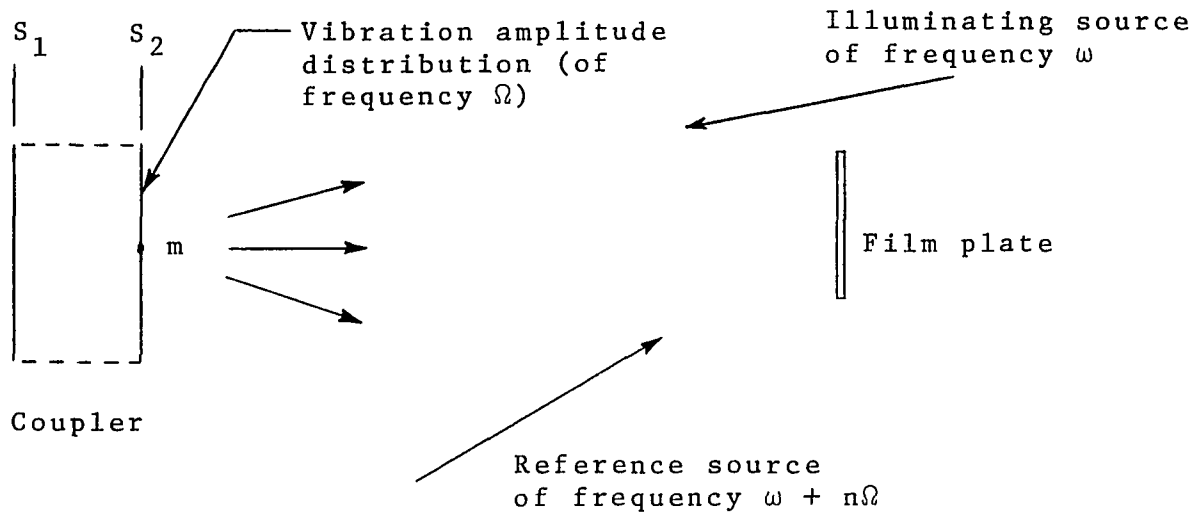


Figure 5-2a Step 2 - Recording an optical hologram of the surface S_2 with a shifted reference frequency

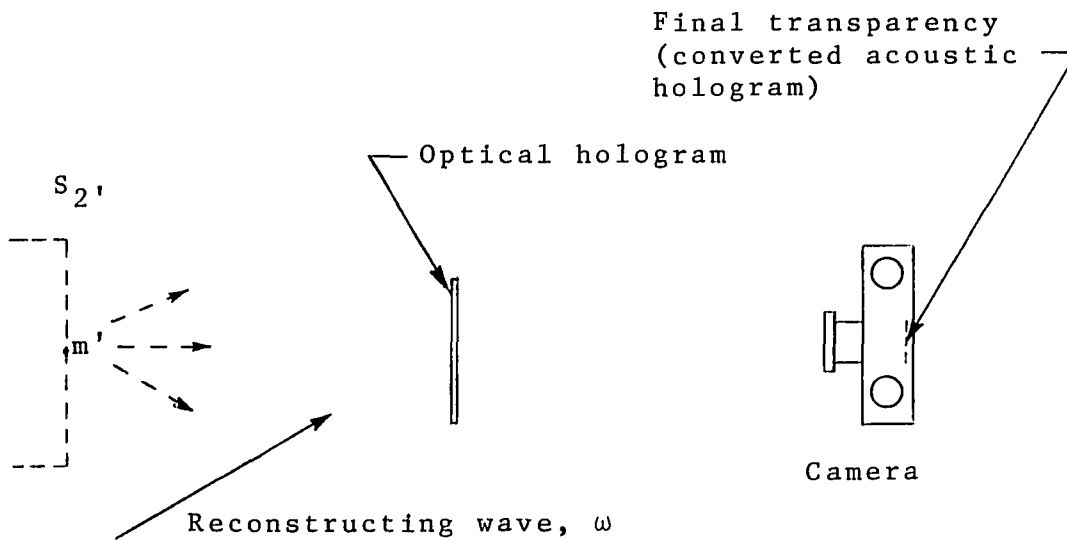


Figure 5-2b Step 3 - Photographing the reconstructed image of the optical hologram to obtain the converted acoustical hologram

Reconstructing the Converted Acoustical Hologram

The final process is the construction of an optical wave bearing similar information about the object in the water medium as does the acoustical object wave. As shown in Figure 5-3, this can be accomplished by treating the converted acoustical hologram (photograph) obtained in the previous step as a normal optical hologram and illuminating it with visible, coherent radiation having a radius of curvature which is properly scaled with respect to that of the original acoustical reference wave.

The use of an optical "reconstructing" wave is, of course, necessary if a visible image of the object in the water medium is to be obtained. Unfortunately, the small wavelength of this radiation as compared to the wavelength of the acoustical recording waves introduces a number of image distortions which, as discussed in Chapter I, can be minimized to some extent by properly scaling the dimensions of the acoustical hologram.

As a result of this wavelength scaling, the resultant image of the original object is usually reduced in size and, as shown in the figure, may require the use of a microscope to view it properly.

The four steps of the proposed acoustical holographic imaging system may now be summarized as follows

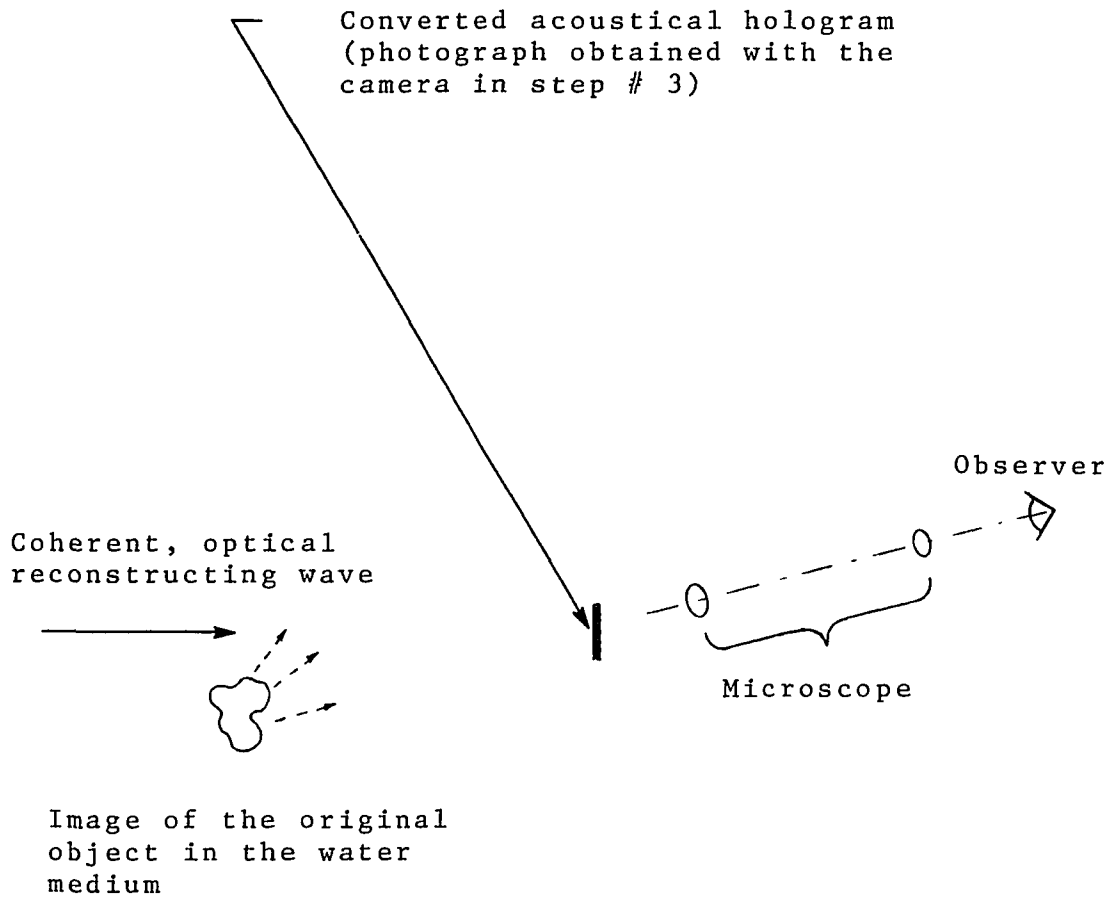


Figure 5-3 Step 4 - Reconstructing the converted acoustical hologram with visible radiation

1. Generating the acoustical hologram (vibration pattern of suitable amplitude) on a surface bounded by air (Figure 5-1)
2. Constructing an optical hologram of this surface with the modified optical holographic technique (Figure 5-2a)
3. Photographing the reconstructed image of the optical hologram obtained in step #2 (Figure 5-2b) — the resultant optical transparency is the converted (and scaled) acoustical hologram
4. Reconstructing the converted acoustical hologram (Figure 5-3)

The devices which can accomplish this, their characteristics, and the resultant characteristics of the overall imaging system will now be discussed in greater detail.

The Optical "Holographic Acoustic Image Converter"

The proposed four-step acoustical holographic imaging system just described is made possible by the use of the "shifted reference optical holographic interferometer" (see Figure 5-2) with an appropriate coupler (see Figure 5-1). Together, these two devices form a subsystem of the overall imaging process and will be referred to as the (optical) "holographic acoustic image converter." This nomenclature is appropriate since the coupler transfers an acoustical image (diffraction pattern, shadowgram, or focused image) from the water medium to a surface bounded by air and the interferometer converts this acoustical image to an optical image.

"Shifted reference holographic interferometer". An important parameter of this device which has already been analyzed in Chapter IV, is its sensitivity.

Recall that when the optical reference frequency is shifted by one order, as shown in Figure 5-2, the radiance $\mathcal{R}_{m'}$ at a point m' in the reconstructed image corresponding to a general point \underline{m} on the surface S_2 is

$$\mathcal{R}_{m'} \propto J_1^2(2kA_m) \quad (5-1)$$

where

$J_1(2kA_m)$ = first order Bessel function of argument $2kA_m$

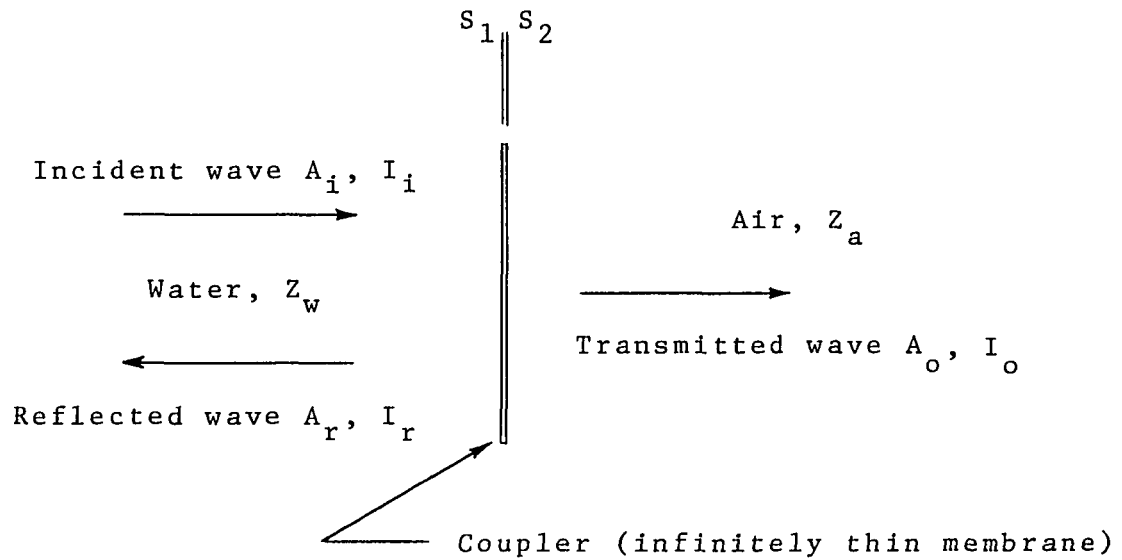
$k = 2\pi/\lambda$

λ = wavelength of the illuminating source

A_m = peak vibration amplitude of point m

Although the ratio of the radiance of vibrating points to stationary points on S_2 is infinite, that is, $[J_1(2kA_m)/J_1(0)]^2 = \infty$, optical noise and photographic fog will ultimately limit the minimum vibration amplitude that can be detected by this instrument. Since this value depends on a number of experimental factors, it is assumed that a reasonable value for the sensitivity of the "holographic interferometer" is 30 $\overset{\circ}{\text{A}}$.

In order to appreciate the amount of acoustic power required to obtain a vibration amplitude of 30 $\overset{\circ}{\text{A}}$, consider the "ideal" case shown in Figure 5-4. A plane sound wave



$$t_d \equiv A_o/A_i$$

A_i = peak vibration amplitude of the incident sound wave

I_i = sound intensity of the incident wave

A_r = peak vibration amplitude of the reflected sound wave

I_r = sound intensity of the reflected wave

A_o = peak vibration amplitude of the transmitted wave

I_o = sound intensity of the transmitted wave

Z_w = characteristic acoustic impedance of the water medium, 1.5×10^6 kgm/m²sec

Z_a = characteristic acoustic impedance of air, 420 kgm/m²sec

Figure 5-4 Performance of an infinitely thin membrane used as a coupler

propagating in a water medium is normally incident on an infinitely thin and supple membrane which couples the water medium to air. Due to nearly 100% reflection at the interface, the peak vibration amplitude A_m of a point on this membrane is

$$A_m = A_o \cong 2A_i = 2/\pi f (I_i/2Z_w)^{\frac{1}{2}} \quad (5-2)$$

where f is the frequency of the sound wave and where the remaining parameters are defined in Figure 5-4. This relation can be used to determine the minimum sound intensity $(I_i)_{\min}$ (threshold intensity) in water that can be detected by the interferometer with this coupler.

$$(I_i)_{\min} = 2Z_w (\pi f A_m / 2)^2 = \begin{cases} 6.7 \text{ mw/cm}^2 @ f=1 \text{ MHz} \\ 670 \text{ mw/cm}^2 @ f=10 \text{ MHz} \end{cases}$$

The above example essentially demonstrates that, for those frequencies (1-10 MHz) commonly used for acoustic imaging, some means should be provided for increasing the vibration amplitude. This consideration places an additional requirement on the coupler, i.e. it should couple the vibration amplitude distribution from the water to air and augment it.

Some practical couplers. The previous discussion has shown that the primary function of the coupler is to couple an arbitrary acoustic image from a surface S_1 bounded by water to a surface S_2 bounded by air. However, it should also

1. be able to augment the vibration amplitudes without introducing any additional distortions
2. be able to resolve all of the interference fringes of the acoustic image
3. not be sensitive to the incident angle of the sound wave(s)

How well practical couplers simultaneously satisfy these requirements will be discussed on page 141.

The discussion at this time is concerned primarily with the first two requirements; that is, coupling and augmenting the vibration amplitude distribution. Devices which can perform these two functions can be classified as

1. Velocity transformers - "free" resonant vibrators and acoustic matching plates
2. Velocity amplifiers - conversion-amplification-conversion

Before some of these couplers are described, a "figure of merit" which is applicable to any coupler will be defined. Referring to Figure 5-4, imagine the thin membrane to be any coupler whose surfaces S_1 and S_2 are bound by water and air, respectively. Under the condition of normal sound incidence as shown in the figure, let $t_d \equiv A_o/A_i$ = displacement amplitude transmission coefficient. If no ambiguity exists, the magnitude of this (complex) coefficient shall also be referred to as the "advantage" or the "gain" of the coupler.

One type of a velocity transformer is a structure vibrating in such a manner that it has a pair of strain-free surfaces. Such "free" resonance is possible when, among other considerations, the lateral dimensions of the structure are small (less than $\Lambda/4$) compared to the wavelength Λ of sound in the material. If, in addition, the two surfaces have unequal areas, velocity amplification is possible by virtue of the law of conservation of momentum.

As an example of such a mechanical transformer, consider the familiar "stepped horn" which is diagrammatically shown in Figure 5-5a. This system is in "free" resonance when the length of each step is $\Lambda/4$, and its mechanical advantage is

$$MA = u_2/u_1 = D_1/D_2$$

where

u_2 = velocity of surface 2

u_1 = velocity of surface 1

D_2 = diameter of surface 2

D_1 = diameter of surface 1

Although other transformer profiles²² can be used such as the exponential horn, "Fourier" horn, inverted cone, etc., the construction of such small, complex devices may be impractical, especially since the ratio D_1/D_2 for these latter profiles is higher for a given mechanical advantage.

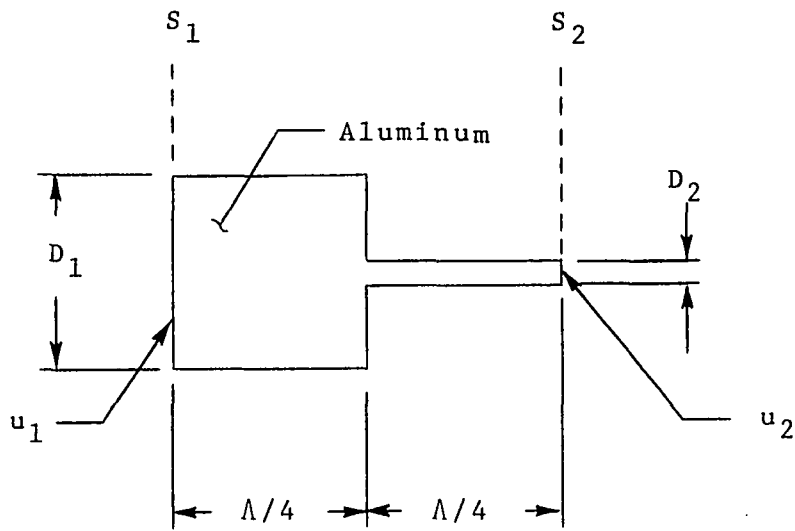


Figure 5-5a The "stepped horn" velocity transformer. The complete coupler would consist of a mosaic of such devices.

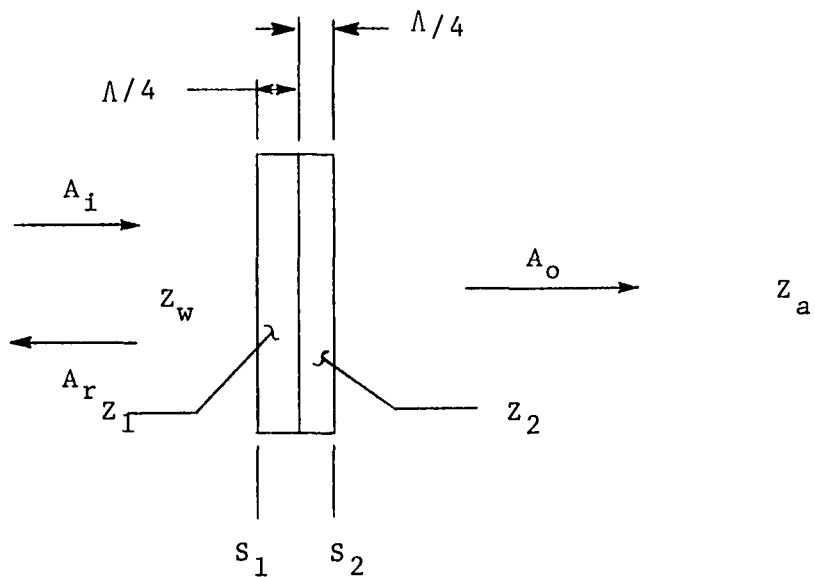


Figure 5-5b The two quarter-wave mechanical, velocity transformer

In addition, the conditions for "free" resonance may be difficult to attain at these high frequencies.

One may think of these devices as mechanical impedance transformers (mechanical impedance = area x specific acoustic impedance) and as such, they couple a differential area of the total surface S_1 to a corresponding differential area of surface S_2 . Hence, the complete coupler must consist of a mosaic of such transformers.

The transmission coefficient t_d defined on page 133 has no meaning when it is applied to a single cell of the coupler, but it does when it is applied to a mosaic of such transformers. It is shown in Appendix I that the gain of such a coupler is

$$\text{gain} = |t_d| = MA|1 + r_d| = (D_1/D_2)|1 + r_d| \quad (5-4)$$

where $r_d = A_r/A_1$ (see Figure 5-4).

A somewhat different type of impedance transformer (one which transforms specific acoustic impedances) is a sandwich of extended, resonant "matching" plates. This type of transformer, particularly the two quarter-wave "matching" system shown in Figure 5-5b is discussed in considerable detail in Chapter VI and in Appendix I. It is shown in the latter that, for this device, the pertinent parameters are

$$|t_d| = 2Z_1Z_2Z_w / (Z_aZ_1^2 + Z_wZ_2^2) \quad \text{and} \quad MA = Z_1/Z_2 \quad (5-5)$$

where Z_1 and Z_2 are the characteristic acoustic impedances of plates 1 and 2, respectively. Note that the gain is a maximum when the impedance of water is matched to that of air (see note 1); that is

$$|t_d|_{\text{matched}} = (Z_w/Z_a)^{\frac{1}{2}} \quad \text{when} \quad (Z_1/Z_2)^2 = Z_w/Z_a \quad (5-6)$$

≈ 60

This value represents the highest theoretical gain that any velocity transformer can achieve under these conditions.

(See Chapter VI for values of experimental gains.)

As a matter of interest, consider the case for which, in Figure 5-5b, $Z_1 = Z_2$, ie. when the system is a single half-wave plate. Under this condition, equation (5-5) reduces to

$$|t_d| = 2Z_w / (Z_a + Z_w) \approx 2 \quad \text{since} \quad Z_a \ll Z_w \quad (5-7)$$

In other words, as far as the gain is concerned, the half-wave resonant plate is a practical realization of the infinitely thin membrane discussed on page 131.

Velocity amplification can also be achieved by converting the acoustical vibration at S_1 (see Figure 5-1) to some other form of energy, amplifying this signal and

Note 1. In order to obtain a total match between water and air, it is possible to control the acoustic impedance of the air medium by, for example, varying its static pressure (see Chapter VI).

reconverting the amplified signal to an acoustical vibration at S_2 .

A possible arrangement of such a velocity amplifier is shown in Figure 5-6. Each cell of the mosaic that comprises the complete coupler consists of a small, half-wave thick, piezoelectric receiving transducer which converts the instantaneous pressure (averaged over its surface) to an electrical signal. This voltage is then added to an appropriate electrical reference voltage which, as discussed in Chapter II, can simulate a corresponding acoustical reference wave. Finally, the sum of these two voltages is amplified and reconverted by the transmitting transducer to an acoustical vibration at S_2 .

If the receiving and transmitting transducers of each cell are the same and if the voltage gain of each summer is unity, the displacement amplitude transmission coefficient t_d for the overall coupler can be expressed as ³⁹

$$|t_d| = (Z_w/2Z_a)^{\frac{1}{2}} (V_2/V_1) \approx 41 (V_2/V_1) \quad (5-8)$$

where V_2/V_1 is the voltage gain of each electrical amplifier.

It will become apparent from the discussion of the next section that the attractive features of this coupler are its selectivity, its ability to amplify a given vibration pattern without sacrificing resolution and its ability to electronically simulate (with relative ease) an appropriate

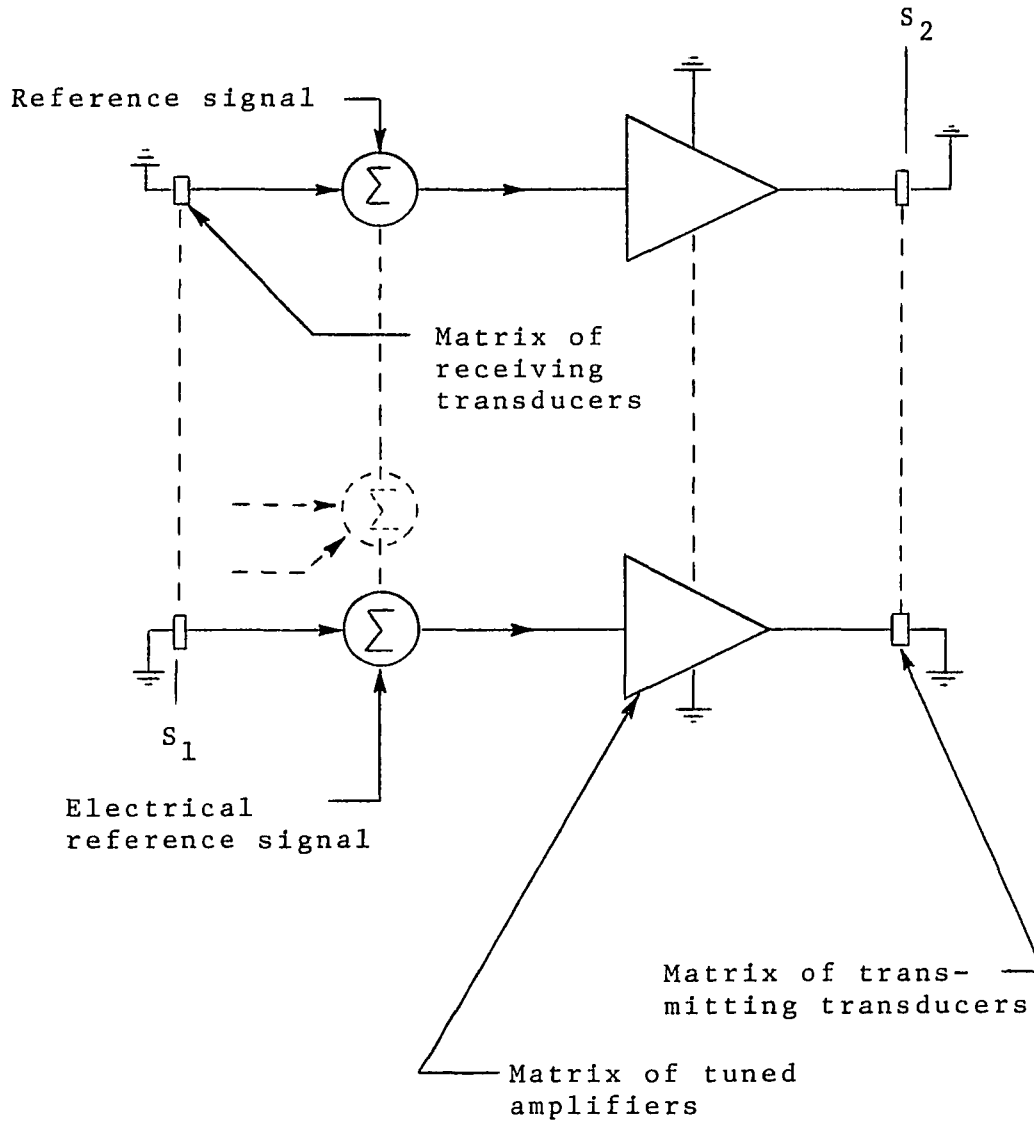


Figure 5-6 A mechanical-electrical-mechanical velocity amplifier (coupler) suitable for use with the holographic sound image converter

acoustical reference wave. In special cases, amplification can also be combined with frequency conversion. Among the advantages of this technique can be a relaxation of the required sensitivity of the optical system (see also Chapter VII).

Having considered some possible couplers and their velocity amplification factors, the sensitivity of the "holographic sound image converter" may be determined. The sound intensity I_i of a sound wave propagating in water and normally incident on the coupler surface S_1 is

$$I_i = 2Z_w(\pi f A_i)^2 = 2Z_w(\pi f A_o/|t_d|)^2 \quad (5-9)$$

where the definition $t_d = A_o/A_i$ has been used. For $f = 1$ MHz, $A_o = 30 \text{ \AA}$ (the sensitivity of the interferometer), and coupling across the water/air interface (air at ambient pressure), the threshold intensity $(I_i)_{\min}$ of the converter can be expressed as

$$(I_i)_{\min} = 26.6/|t_d| \text{ mw/cm}^2 \quad (5-10)$$

As an example, the sensitivities of the "holographic converter" using the various couplers discussed in this section are as follows

Threshold intensity watts/cm ²	Coupler
6.7×10^{-3}	$\Lambda/2$ plate or thin membrane
1.0×10^{-3}	mosaic of stepped horns, $D_1 = .645$ mm, $D_1/D_2 = 5$

Threshold intensity	Coupler
7.4×10^{-6}	matching plates (total match)
1.6×10^{-11}	velocity amplifier, $V_2/V_1 = 1000$

Characteristics of the "holographic converter." Generally speaking, the "holographic acoustic image converter" combines some of the characteristics of both linear and non-linear ultrasonic detectors discussed in Chapter II due to the use of a coupler and the "holographic interferometer", respectively. As a result, this device is a simple, relatively sensitive, frequency selective, non-scanned image converter whose receiving aperture is not limited to any particular size (a $1/2 \text{ m}^2$ aperture size appears feasible) and which is suitable for underwater use.

Depending on the type of coupler used, the conversion sensitivities that can be achieved in practice, may range from 6.7×10^{-3} to 10^{-11} watt/cm² at a frequency of 1 MHz (see page 140). However, it must be remembered that these values are given for normal sound incidence (for which threshold intensities are usually reported) and that, as demonstrated in Chapter VI, an angle of 5° off-axis can reduce the sensitivity by one half.

The interdependence between the angular sensitivity, threshold intensity, and resolution of the converter is due essentially to the use of a coupler whose receiving

surface S_1 is a part of a mechanical resonant device. This interdependence is most readily determined experimentally and, to the knowledge of this author, it has only been reported quantitatively for some extended, half-wave thick, piezoelectric transducers.

For example, recall from the discussion of the ultrasonic camera in Chapter II, that the ability of a half-wave quartz plate to transform a given pressure distribution at its receiving surface to a similar charge pattern on its other surface depends on the inherent image "spreading" which results from mode coupling within the crystal. It has been determined experimentally that this lateral "spreading" is least (approximately equal to the crystal thickness) when the sound wave is normally incident, but it can double if the sound wave is approximately 5° off-axis.

Speaking qualitatively, one would expect the variation of the lateral spreading with the angle of incidence to be related to the mechanical Q of the faceplate. That is, although the inherent lateral spreading (at normal incidence) may be lower for a high Q system, its rate of increase with the angle of incidence is expected to be higher. The net result is that if incidence is not strictly normal, the resolution of a high Q coupler may be lower than that of a low Q coupler. For this reason, the increase

in sensitivity that can be obtained with extended matching plates of high Q may, in some degree, be at the expense of resolution. Hence, the "holographic converter" using such a coupler would be suitable for imaging a single, nearly plane, normally incident sound wave. (Note that the Pohlman cell discussed on page 18 has a similar restriction and that its sensitivity ($3 \times 10^{-7} \text{ w/cm}^2$) is comparable to that of the holographic converter ($7.4 \times 10^{-6} \text{ w/cm}^2$) using a coupler which matches air to water.

On the other hand, those couplers comprised of a mosaic of small, uncoupled, resonant cells do not suffer from this lateral image spreading (although there may be mode coupling within each cell, the effect of this is to decrease the threshold intensity). Hence, these couplers can decrease the angular sensitivity without affecting the resolution. When designing such a system, the primary concern is that the receiving area of each cell be sufficiently small and that adjacent cells be sufficiently close so that all of the acoustic interference fringes can be resolved. If the interfering sound waves are plane, this consideration will then determine the maximum angle that can be subtended by the two sound waves.

The "holographic acoustic image converter" whose coupler is a mosaic of "stepped horns" having $D_1 = 0.645 \text{ mm}$ and $D_1/D_2 = 5$ (see Figure 5-5a), would have a threshold

intensity of 10^{-3} w/cm² (see page 140) and would allow two plane interfering sound waves to subtend a maximum angle of approximately 20°. In some respects, the performance of this converter can be compared to that of the liquid-surface-levitation imaging method described on pages 20-26 in that both are non-scanned, have similar sensitivities and can be used to perform conventional (split-beam, off-axis) acoustic holography. Although the "holographic converter" cannot be used for "real-time" imaging, it is a frequency selective device and its use is not restricted to the water surface. Furthermore, whereas the optical system of the levitation technique responds to the spatial derivative of the surface levitation and thus suppresses low spatial frequencies, the "holographic converter" is a true intensity device. That is, for $(2kA_m) < 1$, the radiance $\mathcal{R}_{m'}$ at a point m' in the reconstructed image is approximately directly proportional to the acoustic intensity at the corresponding point \underline{m} on the coupler surface S_2 (see equation (5-1)).

The "holographic sound image converter" which uses a mosaic of very small velocity amplifiers as shown in Figure 5-6 would display similar resolution characteristics as the above converter. In addition, a higher sensitivity can be achieved as well as the electronic simulation of an acoustic reference wave. Referring to Chapter II, the performance of such a converter compares favorably with that

of any of the electronically scanned or optically scanned detectors (see, for example, Figures 2-10 to 2-13). In fact, for a given array of receiving transducers, the "holographic converter" has a potentially higher resolution capability. This is possible because the "holographic converter" is not affected by any decrease in resolution due to the display system, scanning electron beam diameter, etc.

Chapter VI

TWO QUARTER-WAVE VELOCITY TRANSFORMER(ACOUSTIC MATCHING PLATES)

The discussion of Chapter V has shown that the "holographic ultrasonic image converter" using a coupler which matches air to water can be a simple and sensitive system which does not require scanning.

In this chapter, the use of two, nearly quarter-wave plates to partially or completely match air to water is further investigated. In particular, the design, construction and performance of such acoustic "matching" plates is discussed in some detail.

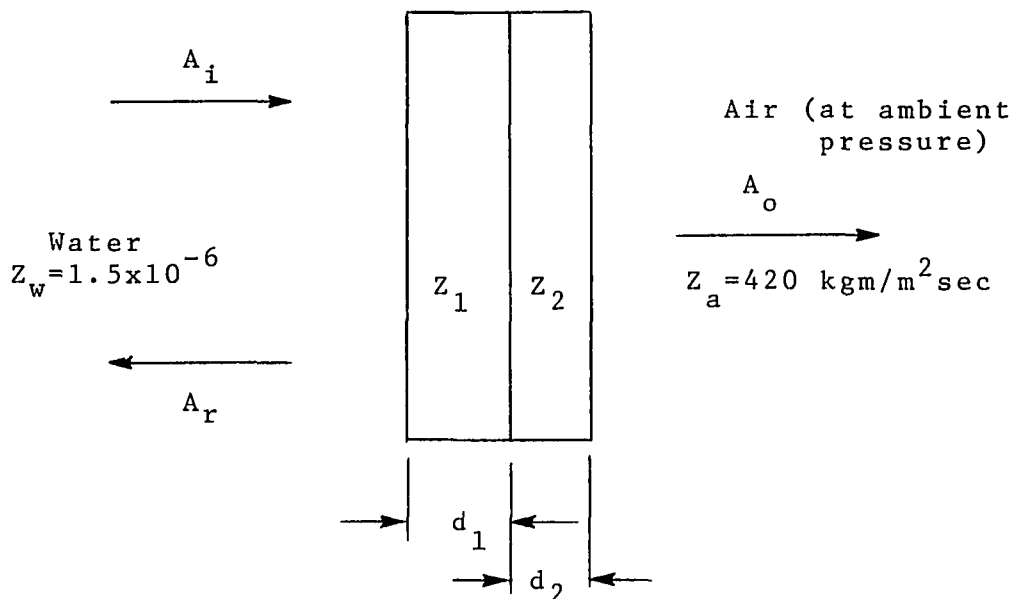
General Remarks

Under the condition of plane, normally incident sound waves, it is well known that, theoretically, a single, lossless quarter-wave plate can match any two media. If these media are water and air at ambient pressure the acoustic impedance of the matching plate must be $2.5 \times 10^4 \text{ kgm/m}^2 \text{ sec}$. Possibly some rubber-like materials exhibit such low impedances, but generally, their losses are prohibitively high so that velocity augmentation can only be achieved at very low (sonic) frequencies.⁹¹ Because of the lack of suitable materials, it is more expedient therefore, to use two or more quarter-wave plates in order to obtain velocity augmentation at those frequencies

commonly used for acoustic imaging (1-10 MHz).

The two quarter-wave resonant coupler which is investigated in this chapter is shown in Figure 6-1. It is assumed that a plane sound wave propagating in water and having a maximum displacement amplitude A_i is normally incident on plate 1. Of this incident energy, a part is reflected back into the water and a part is transmitted to the air. It is further assumed that the air medium extends to infinity so that no reflected wave exists in the air. Under these conditions, the displacement amplitude transmission coefficient t_d (the magnitude of this quantity will also be referred to as the "gain") of the system is defined as $t_d = A_o/A_i$, where A_o is the maximum vibration amplitude of the transmitted wave.

The analysis of the system shown in Figure 6-1 basically consists of determining the transmission coefficient t_d for various specific conditions. This analysis can be achieved with the use of standard transmission-line theory; in particular, with the use of the theory of multilayer films (commonly used in optics) as applied to acoustic plates. This technique is particularly convenient since, as shown in Appendix I, each individual plate can be described by a unique transfer matrix, and therefore, the method is readily applicable to the investigation of systems consisting of several resonant plates.



$$t_d = \frac{A_o}{A_i} = \frac{2Z_w}{(A \cos \gamma_1 \cos \gamma_2 - B \sin \gamma_1 \sin \gamma_2) + i(C \cos \gamma_1 \sin \gamma_2 + D \sin \gamma_1 \cos \gamma_2)}$$

$$A = Z_a + Z_w$$

$$C = Z_2 + Z_a Z_w / Z_2$$

$$B = Z_1 Z_a / Z_2 + Z_w Z_2 / Z_1$$

$$D = Z_1 + Z_a Z_w / Z_1$$

$$\gamma_1 = K_1 d_1 - i \alpha_1 d_1$$

$$\gamma_2 = K_2 d_2 - i \alpha_2 d_2$$

$$K_1 = 2\pi f / c_1$$

$$K_2 = 2\pi f / c_2$$

$$c_1 = \text{speed of sound in plate 1 (m/sec)}$$

$$c_2 = \text{speed of sound in plate 2 (m/sec)}$$

$$\alpha_1 = \text{attenuation coefficient of plate 1 (neper/m)}$$

$$\alpha_2 = \text{attenuation coefficient of plate 2 (neper/m)}$$

$$d_1 = \text{thickness of plate 1 (meters)}$$

$$d_2 = \text{thickness of plate 2 (meters)}$$

Figure 6-1 A resonant mechanical transformer used for velocity augmentation across the air/water interface

It should be noted that some control of the matching characteristic of the transformer shown in Figure 6-1 can be achieved by varying the acoustic impedance Z_a of the terminating medium, for example, by controlling the static pressure of the air medium. As discussed in Chapter VII, one practical advantage of this optimization method is the reduction of the coupler's reflection coefficient, and consequently, the minimization of standing waves within the water medium.

Design of Two, Lossy, Nearly Quarter-Wave Plates

It is shown in Appendix I that, under the condition of normal incidence, the displacement amplitude transmission coefficient t_d of two arbitrarily thick plates is

$$t_d = \frac{2Z_w}{(A \cos \gamma_1 \cos \gamma_2 - B \sin \gamma_1 \sin \gamma_2) + i(C \cos \gamma_1 \sin \gamma_2 + D \sin \gamma_1 \cos \gamma_2)} \quad (6-1)$$

where Z_w , Z_1 , Z_2 and Z_a are the characteristic acoustic impedances of water, plate 1, plate 2 and air, respectively; and where the remaining parameters are defined in Figure 6-1.

Referring to Figure 6-1, the transmission coefficient shall be determined under the following, additional conditions

1. The plates are homogeneous and of uniform thickness

2. The losses of each plate are small so that $\text{Cosh } \alpha d \approx 1$ and $\text{Sinh } \alpha d \approx \alpha d$.
3. The plates are nearly a quarter-wave thick so that $K_1 d_1 \approx \pi/2$ and $K_2 d_2 \approx \pi/2$ (see Figure 6-1)
4. Plate 1 is assumed to be a metal and plate 2 is assumed to be a plastic-like material so that the acoustic impedances exhibit the following relationship

$$Z_1 > Z_2 \text{ or } Z_w \quad \text{and} \quad Z_2 \text{ or } Z_w \gg Z_a$$

Under this condition, the parameters A, C and D defined in Figure 6-1 are approximately

$$A \approx Z_w \quad C \approx Z_2 \quad D \approx Z_1$$

Using the small loss approximation listed above, it follows from equation (6-1) that

$$2Z_w/t_d = (A' \cos \theta_1 \cos \theta_2 - B' \sin \theta_1 \sin \theta_2) + i (D' \sin \theta_1 \cos \theta_2 + C' \cos \theta_1 \sin \theta_2) \quad (6-2)$$

where

$$\theta_1 = K_1 d_1$$

$$\theta_2 = K_2 d_2$$

$$A' = A + DL_1 + CL_2 + BL_1 L_2$$

$$B' = B + CL_1 + DL_2 + AL_1 L_2$$

$$C' = C + BL_1 + AL_2 + DL_1 L_2$$

$$D' = D + AL_1 + BL_2 + CL_1 L_2$$

$$L_1 = \alpha_1 d_1$$

$$L_2 = \alpha_2 d_2$$

This equation and the Taylor series expansion of $\cos^2 \theta$ and $\sin 2\theta$ about $\pi/2$ may be used to determine the following expression

$$4Z_w^2/|t_d|^2 = B'^2 + a(f/f_1 - 1)^2 + b(f/f_2 - 1)^2 \quad (6-3)$$

$$+ 2c(f/f_1 - 1)(f/f_2 - 1) - d(f/f_1 - 1)^2(f/f_2 - 1)^2$$

where

$$a = (\pi/2)^2(C'^2 - B'^2)$$

$$b = (\pi/2)^2(D'^2 - B'^2)$$

$$c = (\pi/2)^2(D'C' - A'B')$$

$$d = (\pi/2)^4(C'^2 + D'^2 - A'^2 - B'^2)$$

$$f_1 = c_1/4d_1 = \text{frequency at which plate 1 is a quarter-wave thick}$$

$$f_2 = c_2/4d_2 = \text{frequency at which plate 2 is a quarter-wave thick}$$

$$f = \text{frequency of the incident sound wave}$$

Strictly speaking, the parameters A', B', C' and D' and therefore a, b, c, and d vary with frequency since the attenuation coefficient and, to some extent, the speed of sound in a particular medium are frequency dependent. However, for small frequency variations (nearly quarter-wave plates), one may consider these parameters to be constant. It should also be mentioned that, under the conditions listed on page 150, the following inequality is observed

$$d \text{ or } b > c \quad \text{and} \quad c > a \gg B'^2 \quad (6-4)$$

Equation (6-3) will now be examined for two specific conditions, namely the "tuned" and "untuned" case.

Tuned plates ($f_1 = f_2$). The system shown in Figure 6-1 is considered to be "tuned" when the two plates are

a quarter-wave thick at the same frequency, i.e. when $f_1 = f_2 = f_0$. Under this condition, equation (6-3) can be re-written as

$$t_d = \frac{2Z_w}{[B'^2 + (a + b + 2c)(f/f_0 - 1)^2 - d(f/f_0 - 1)^4]}^{\frac{1}{2}} \quad (6-5)$$

Since $(a + b + 2c) \gg B'^2$, it is expected that the gain exhibits a sharp maximum at $f = f_0$ and that it is relatively small at all other frequencies. Figure 6-2 shows a typical variation of $|t_d|$ with frequency. Referring to this figure, one may define the following important parameters

$$\begin{aligned} |t_d|_{\max} &= \text{maximum gain (at } f_0) \\ \Delta f &= \text{bandwidth (half-power points)} \\ \Delta |t_d|_{\max} &= \text{gain-bandwidth product} \\ Q &= f_0/\Delta f = \text{mechanical } Q \text{ of the system} \end{aligned}$$

The above parameters may be determined from equation (6-5). At $f = f_0$, the maximum gain $|t_d|_{\max}$ is

$$|t_d|_{\max} = 2Z_w/B' = 2Z_w/(B + CL_1 + DL_2 + AL_1L_2) \quad (6-6)$$

Substituting the appropriate expressions for A, B, C and D listed on page 148 and assuming small losses, equation (6-6) becomes

$$|t_d|_{\max} \approx 2Z_w/[Z_1Z_a/Z_2 + Z_wZ_2/Z_1 + Z_2L_1 + Z_1L_2] \quad (6-7)$$

Since the impedance of material 1 is larger than that of material 2, this expression shows that the losses of the

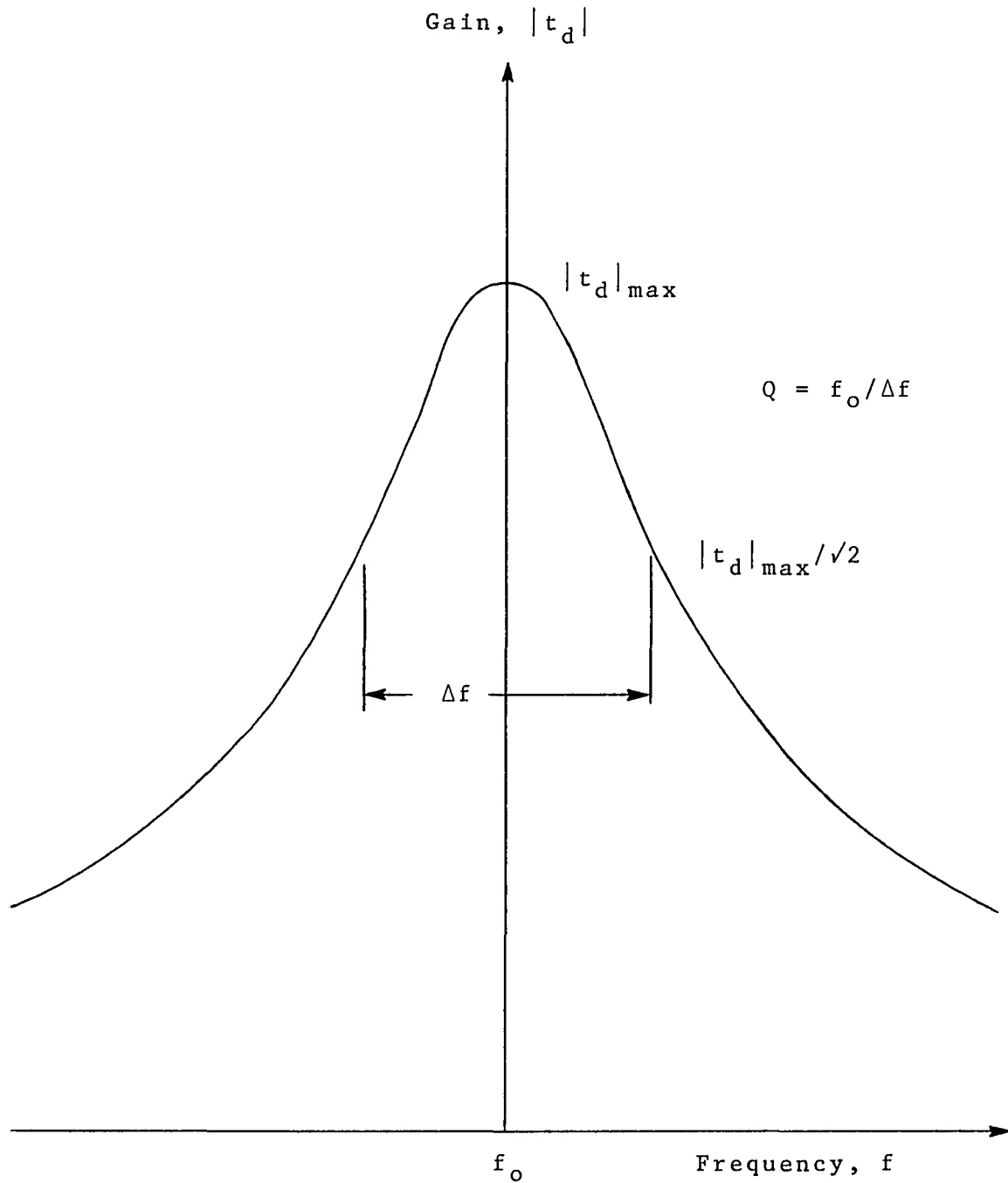


Figure 6-2 Typical frequency response of the displacement amplitude transmission coefficient

plastic-like medium (plate 2) affect the maximum gain to a considerably greater extent than do the losses of material 1.

Upon identifying the half-power points in Figure 6-2, equation (6-5) may also be used to determine the bandwidth of the system. Neglecting the fourth-order term in the denominator of this expression, the bandwidth Δf becomes

$$\Delta f \approx \frac{4f_0 B'}{\pi [(C' + D')^2 - 2B'(A' + B')]} \frac{1}{2} \quad (6-8)$$

where the relation $(a+b+2c) = (\pi/2)^2 [(C'+D')^2 - 2B'(A'+B')]$ has been used. It follows from equations (6-6) and (6-8) that the gain bandwidth product $\Delta f |t_d|_{\max}$ is

$$\Delta f |t_d|_{\max} \approx \frac{8f_0 Z_w}{\pi [(C' + D')^2 - 2B'(A' + B')]} \frac{1}{2} \quad (6-9)$$

and the mechanical Q is

$$Q \approx \frac{\pi}{4B'} [(C' + D')^2 - 2B'(A' + B')] \frac{1}{2} \quad (6-10)$$

In order to predict the performance of a lossy system, $\frac{1}{2}$ it will be useful to evaluate the term $[(C'+D')^2 - 2B'(A'+B')] \frac{1}{2}$. Substituting the approximate relations for A', B', C' and D', this term reduces to

$$[(C'+D')^2 - 2B'(A'+B')] \frac{1}{2} \approx Z_1 (1 - L_2^2) \approx Z_1 \quad (6-11)$$

Considering the previous discussion, the fact that this term is approximately constant and equal to Z_1 for $L_1 \ll 1$,

means that the losses of plate 2 essentially determine the performance of the "tuned" system and that, for small losses, the gain-bandwidth product is relatively constant and equal to $8f_0Z_w/\pi Z_1$. Furthermore, substituting relation (6-11) into (6-8) and using the expression for B' , the bandwidth Δf of a lossy, "tuned" system may be expressed as

$$(\Delta f)_{\text{lossy}} \cong (\Delta f)_{\text{lossless}} (1 + Z_1^2 L_2 / Z_w Z_2) \quad (6-12)$$

As will be demonstrated later, this relationship can be used to experimentally determine the approximate attenuation coefficient α_2 of plate 2.

Having developed the mathematical expressions for the parameters indicated in Figure 6-2, it will be useful to examine some numerical examples using existing materials. Table 6-1 lists the design parameters for the system shown in Figure 6-1 when media 1 and 2 are quarter-wave plates (at $f_0 = 140$ KHz) of steel and epoxy, respectively. (The reason for using epoxy is explained on page 163.)

Referring to this table, note that these plates only partially match water to air since a total match requires that the lossless system have a gain of about 60. As the materials are made lossy, both the maximum transmission coefficient $|t_d|_{\text{max}}$ and the Q decrease in such a manner that, as expected, the gain-bandwidth product remains relatively constant. (The acoustic impedance and sound velocity of each plate, as listed on the bottom of Table

TABLE 6-1

TUNED RESONANT PLATES

Water-Steel-Epoxy-Air

$f_o = 140 \text{ KHZ}$

α_1	$ \tau_d _{\max}$	Δf	$\Delta f \tau_d _{\max}$	Q
α_2				
nep/m		KHz	$\times 10^3$	
0.00	30.63	0.40	12.30	350
0.00				
0.01	30.55	0.40	12.30	348
0.00				
0.01	11.31	1.09	12.31	128.5
1.00				
0.01	3.21	3.84	12.33	36.5
5.00				
0.01	1.69	7.27	12.33	19.3
10.00				
$Z_1 = 41.2 \times 10^6 \text{ kgm/m}^2\text{sec}$		$Z_2 = 2.5 \times 10^6 \text{ kgm/m}^2\text{sec}$		
$c_1 = 5.29 \times 10^3 \text{ m/sec}$		$c_2 = 2.27 \times 10^3 \text{ m/sec}$		
$d_1 = 9.45 \times 10^{-3} \text{ m}$		$d_2 = 4.05 \times 10^{-3} \text{ m}$		

6-1, are measured values and were obtained from the data which is presented later.)

The results listed in Table 6-1 may also be translated to any other base frequency provided that the parameters A', B', C' and D' remain the same. For example, when $f_0 = 1.4$ MHz and $\alpha_1 = 0.1$ nepers/meter and $\alpha_2 = 10$ nepers/meter, then

$$\begin{array}{ll} d_1 = 0.065 \text{ mm} & d_2 = 0.405 \text{ mm} \\ |t_d|_{\max} = 30.55 & \Delta f = 4.03 \text{ KHz} \\ \Delta f |t_d|_{\max} = 12.3 \times 10^4 & Q = 348 \end{array}$$

Table 6-2 lists the parameters of a "tuned", aluminum-epoxy resonant system for the same attenuation coefficients that were used in Table 6-1. Comparing these two tables, it should be noted that, for lossy media, the actual gain of an initially low Q system (aluminum-epoxy) may be higher than that of an initially high Q system (steel-epoxy). One would also expect that the tolerance requirement of the low Q system is less stringent. As a result, in practice (and particularly at high frequencies), it may be more advantageous to construct a low Q rather than a high Q system.

Untuned plates ($f_1 \neq f_2$). The situation that is usually encountered in practice is that plates 1 and 2 are a quarter-wave thick at different frequencies. It

TABLE 6-2

TUNED RESONANT PLATES

Water-Aluminum-Epoxy-Air

$$f_o = 140 \text{ KHz}$$

α_1	$ t_d _{\max}$	Δf	$\Delta f t_d _{\max}$	Q
α_2				
nep/m		KHZ	$\times 10^3$	
0.00	12.65	2.29	29.0	61.1
0.00				
0.01	12.64	2.29	29.0	61.0
0.00				
0.01	9.93	2.92	29.0	48.0
1.00				
0.01	5.34	5.44	29.1	25.7
5.00				
0.01	3.29	9.10	30.8	15.4
10.00				

$$Z_1 = 16 \times 10^6 \text{ kgm/m}^2 \text{ sec}$$

$$Z_2 = 2.5 \times 10^6 \text{ kgm/m}^2 \text{ sec}$$

$$c_1 = 5.4 \times 10^3 \text{ m/sec}$$

$$c_2 = 2.27 \times 10^3 \text{ m/sec}$$

$$d_1 = 9.65 \times 10^{-3} \text{ m}$$

$$d_2 = 4.05 \times 10^{-3} \text{ m}$$

remains, therefore, to examine the frequency response of $|t_d|$ when $f_1 \neq f_2$.

Assuming that the attenuation coefficient α_1 and α_2 remain frequency independent in the frequency range of interest, numerical substitution into the general expression (6-1) shows that the frequency response of $|t_d|$ of slightly "untuned" plates (as long as $0.9f_1 \leq f_2 \leq 1.1f_1$) is very similar to that of "tuned" plates (see Figure 6-2) - in the sense that the shape of the curve and the maximum gain are almost the same. However, the frequency f_0 at which the transmission coefficient is a maximum, is shifted. In general, f_0 is between f_1 and f_2 and, due to the low loading of plate 2, f_0 is very close to f_2 .

The frequency f_0 at which the gain of "untuned" plates is a maximum may be determined quantitatively by differentiating equation (6-3) with respect to f (under the assumption that A' , B' , C' and D' are independent of frequency), equating the resultant expression to zero, and solving for its roots. Such a calculation shows that $f_0 = f_2(1 + \eta)$ where, to a good approximation

$$\eta \approx \frac{(f_2 - f_1)(af_2 + cf_1)}{[(d - a)f_2^2 + (d - b)f_1^2 - 2(d + c)f_1f_2]} \quad (6-13)$$

Numerical substitution into this expression confirms that η is very small, implying that $f_0 \approx f_2$ and that its sign is always such that f_0 is between f_1 and f_2 . Furthermore, as the impedance ratio Z_1/Z_2 is increased, f_0 approaches more closely f_2 .

An analytical expression for $|t_d|_{\max}$ of "untuned" plates may also be determined by substituting f_0 into equation (6-2). The resultant expression, however, is rather involved and, for engineering purposes, it is of minor use. (Although (6-13), which is obtained from the approximate relation (6-3), accurately predicts f_0 , the gain at this frequency must be obtained from the more exact relation (6-1) or (6-2).)

The above frequency shift of "untuned" plates is expected, but the fact that the maximum gain and the bandwidth of such plates is nearly that of "tuned" plates, is not at all obvious, a priori. The extent of this variation of the design parameters is tabulated in Table 6-3 for the previously discussed aluminum-epoxy system when $f_2 = 0.92f_1$ (top) and $f_2 = 1.08f_1$ (bottom).

Comparing Tables (6-2) and (6-3), as f_2 is increased from $0.92f_1$ to $1.08f_1$, the following are observed

TABLE 6-3

"UNTUNED" ALUMINUM-EPOXY PLATES

$$f_1 = 140 \text{ KHz}, f_2 = 128.8 \text{ KHz}$$

α_1	$ t_d _{\max}$	Δf	$\Delta f t_d _{\max}$	Q	f_o
α_2		KHz	$\times 10^3$		KHz
nep/m					
0.00					
0.00	12.58	2.15	27.0	60.7	130.2
0.01					
0.00	12.57	2.15	27.0	60.6	130.2
0.01					
1.00	9.72	2.78	27.0	46.8	130.2
0.01					
5.00	5.09	5.32	27.1	24.5	130.2
0.01					
10.00	3.19	8.45	27.1	15.3	130.2

$$f_1 = 140 \text{ KHz}, f_2 = 151.2 \text{ KHz}$$

0.00					
0.00	12.58	2.46	31.0	60.8	149.6
0.01					
0.00	12.57	2.46	31.0	60.7	149.6
0.01					
1.00	10.05	3.08	31.0	48.5	149.6
0.01					
5.00	5.58	5.57	31.1	26.9	149.6
0.01					
10.00	3.59	8.67	31.1	17.2	149.6

1. When the plates are lossless, Δf and $\Delta f |t_d|_{\max}$ increase monotonically while $|t_d|_{\max}$ and Q peak when the system is "tuned."
2. For small losses, all four parameters increase monotonically.
3. For large losses, Δf peaks when the system is "tuned" while the remaining parameters increase monotonically.
4. Only the gain-bandwidth product increases for all of the above conditions and registers the greatest change (13%).

Although one is tempted to draw appropriate conclusions from these results, it must be recalled that these were obtained for constant attenuation coefficients and that, in practice, these coefficients often are linearly related to the frequency. Consequently, practical plates are expected to exhibit the characteristics described in #1 above.

Summarizing the results of the discussion thus far, it is apparent that the performance of the two, nearly quarter-wave plates shown in Figure 6-1 is essentially determined by plate 2 (plastic-like material) in the following way

1. The absolute thickness d_2 of medium 2 virtually determines the "resonant" frequency f_0 of the overall system.
2. Under the previously stated conditions, the maximum gain of the overall system is limited mainly by the attenuation coefficient α_2 of material 2.

The previous discussion has also shown that substantial sound transmission to the air can be obtained even when the plates are "untuned" ($f_1 \neq f_2$) by as much as $\pm 10\%$.

Heuristically, it may also be argued that, due to #1 above, the thickness tolerance of material 2 is more critical than that of medium 1. However, the actual tolerance is difficult to calculate since this requires, among other things, a knowledge of the lateral coupling between adjacent, differential elements.

Construction of Two Quarter-Wave Plates

As a result of the previous discussion, the choice of media 1 and 2 for the system shown in Figure 6-1 is based, theoretically, on their attenuation coefficients at the frequency of interest, as well as on the ratio of their acoustic impedances. However, in practice, an important additional consideration is the availability of a suitable adhesive in order to form a strong, lossless, mechanical bond between these two materials.

In reference to this latter consideration, the undesirable effects of the adhesive, particularly at high frequencies where its thickness (relative to that of the plates) cannot be neglected, has led to the use of epoxy; that is, of constructing plate 2 entirely of epoxy. In this manner, efficient use is made of both the adhesive

and acoustic properties of epoxy.

Since the object is to construct high-gain plates and since this requires that $Z_1 \gg Z_2$ (medium 1 must be an acoustically "hard" material), restricting medium 2 to be epoxy limits the choice of material 1. Hence, materials such as glass, common metals, etc. appear to be an appropriate choice for plate 1.

The following discussion describes the general construction and tuning techniques used to obtain both high-frequency and low-frequency, metal-epoxy, quarter-wave plates.

Construction techniques. With reference to the previous theoretical discussion, the metal substate (plate 1) is prepared in the following manner

1. The metal plate is hand-ground to the desired thickness which should be maintained as uniform as experimental conditions will permit. (The thickness was maintained within ± 3 microns.)
2. The surface which will face the epoxy is partially polished. This is desirable since the thickness tolerance of the epoxy is expected to be more critical than that of the metal.
3. The plate is now immersed in water and, using the pulsed sound method described in Appendix II, the frequency f_1' at which the plate is a half-wave thick, is recorded. (The purpose of this step will become apparent later.)

4. The metal is chemically cleaned and degreased with trichlorethylene vapor. This step is rather important since the bond of a number of plates weakened or broke completely - presumably because of improper degreasing.
5. A teflon or lucite mask which will serve as a mold for the epoxy, is attached to the polished surface.

The epoxy is prepared in accordance with two specific purposes - homogeneity of the mixture and minimization of the attenuation coefficient. The latter indirectly implies that all gaseous impurities be removed from the mixture. For this reason, the casting of the epoxy is performed in the following way

1. Epon resin 828 and curing agent V-40 are degassed separately in vacuum (5mm Hg) at an elevated temperature (80°C) for approximately five hours. The components are then allowed to cool to 50°C.
2. The degreased metal plate with its mask is placed in a vacuum chamber, leveled and preheated to 50°C.
3. Equal parts (by weight) of the above resin and curing agent are carefully and thoroughly mixed by hand in a preheated bowl (50°C) at ambient pressure. (See note 1).
5. The mixture is again degassed by rapidly decreasing the pressure to about 5 mm Hg. During this critical step, the temperature is allowed to rise to 60°C in order to facilitate the removal of any gaseous

Note 1. Ideally, the degassing of the epoxy components, the mixing of these components and the casting of the epoxy should be done in a vacuum environment. Since this was not possible with present facilities, the compromise procedure, as described in steps 3 through 6, was used.

impurities which may have been trapped during mixing. A mechanical "manipulator" may also be used to burst any particularly large gas bubbles. (see note 1).

6. Step #5 may be continued as long as the viscosity of the epoxy remains sufficiently low (about 25 minutes). At this time, the volume, and therefore, the adverse acoustical effect of any remaining surface bubbles, may be reduced by removing the vacuum. (see note 1).
7. The epoxy is cured at 60°C for approximately three days. (However, a faster curing schedule did not appear to affect the performance of the completed system.)

Figure 6-3 illustrates a completed cast (steel-epoxy plates) while in the curing process. Clearly visible are the vacuum collar (1) with its manipulator (2), the heater (3) with its electrical connections (4) and the masked, steel plate (5) onto which the epoxy (6) has been cast.

Preliminary tuning of metal-epoxy plates. From the previous, theoretical discussion of nearly quarter-wave plates it is apparent that maximum gain is obtained when the two plates are "tuned". For the metal-epoxy plates whose construction details are described above, this tuning is accomplished by grinding the epoxy to its proper thickness. (Frequency f_1 is assumed to be the design frequency.)

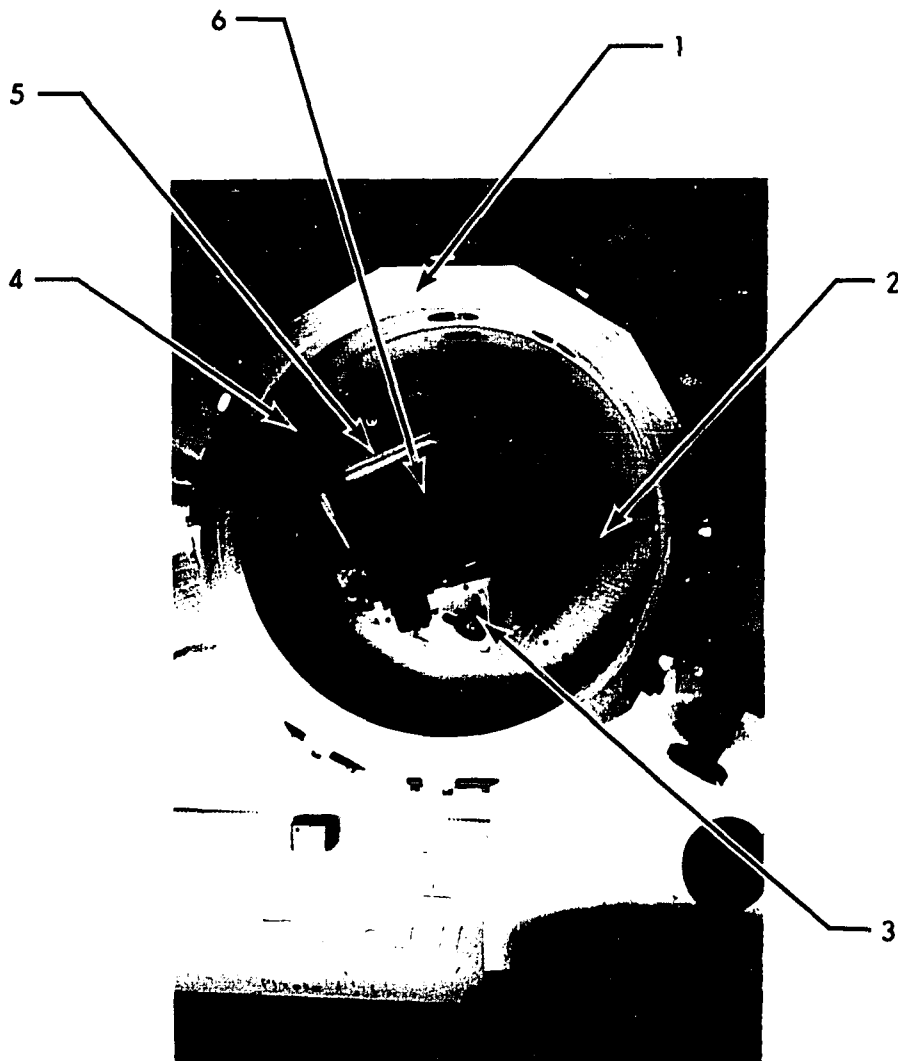


Figure 6-3 A completed steel-epoxy casting shown in its curing stage. The glass dome which completes the vacuum chamber has been removed. (see text)

During the tuning process, a convenient technique for monitoring the extent to which the plates are tuned, is based on the shift in frequency at which the transmission coefficient of a "loaded" half-wave plate is a maximum. In particular, consider the resonant system shown in Figure 6-1 when $Z_a = Z_w$ (plates immersed in water) and when the frequency f of the sound wave is doubled, i.e. when each plate is nearly a half-wave thick. Using an analysis very similar to that discussed on pages 149 - 161, it can be shown that the frequency f'_0 at which $|t_d|$ of the overall system is a maximum (for $Z_a = Z_w$, $|t_d|_{\max} \approx 1$), lies between the frequencies at which either plate is a half-wave thick. Furthermore, f'_0 is very nearly equal to f'_1 , where f'_1 is the half-wave frequency of plate 1 (metal). Although the frequency shift $|f'_1 - f'_0|$ is small and decreases as Z_1/Z_2 is increased, it is sufficiently large to be detected with the pulsed sound method described in Appendix II.

As a result of the above discussion, a metal-epoxy system which is designed for a base frequency f_0 (that is, the thickness of each plate is nearly a quarter-wave thick at f_0), may be "tuned" at a frequency which is approximately equal to $2f_0$. This is accomplished by immersing the bonded plates in water as shown in Figure II-1 and determining, in accordance with the discussion

of Appendix II, the frequency f'_0 at which the sound transmission through the system is a maximum. This frequency is then compared to f'_1 , i.e. the half-wave frequency of the metal plate alone (before the epoxy has been cast on it). If the epoxy thickness is initially too thick, then $f'_0 < f'_1$ and as the epoxy thickness is reduced, f'_0 will approach f'_1 until, when $f'_0 = f'_1$, the plates are "tuned". Of course, further reduction of the epoxy thickness will make $f'_0 > f'_1$. (Specific data is presented on page 177.)

With the above, simple tuning procedure, the quarter-wave frequency f_2 of the epoxy can readily be adjusted to within 5% of f_1 . Final tuning, however, is performed under actual loading conditions; that is, with the epoxy bounded by air.

Testing and final tuning of metal-epoxy plates. The performance of the metal-epoxy resonant system may be determined from the frequency response of the relative vibration amplitude of the epoxy surface and from the relations developed on pages 149-161. One arrangement which may be used to obtain the frequency response is diagrammatically shown in Figure 6-4 and illustrated in Figure 6-5.

Referring to Figure 6-4, the partially tuned plates (1) are mounted to the wall of a tank (2) which is filled with water. A broadband transducer, mounted on a movable carriage to provide a vernier adjustment of the distance D between its surface and that of the metal, is made to generate a continuous, approximately plane sound wave which is normally incident on the metal surface. Finally, the resistor R tends to maintain a constant acoustic output as the sound frequency is varied.

The optical system shown in this diagram is identical to that described in Chapter II (see page 44). A laser (3) generates a collimated light wave which is reflected from the epoxy surface. Due to the sinusoidal vibrations of this surface, the reflected light beam suffers a periodic lateral displacement which is converted to an amplitude modulation by the knife edge (4). The resultant amplitude modulated wave is detected by the photo multiplier tube (5) and is converted to an electrical signal whose frequency is that of the sound wave. This signal is then amplified and displayed on an oscilloscope (6). Assuming that the epoxy surface vibrates as a piston, the electrical signal amplitude is directly proportional to the surface vibration amplitude.

Figure 6-5 illustrates the actual optical arrangement used. (The reference numbers shown in this figure

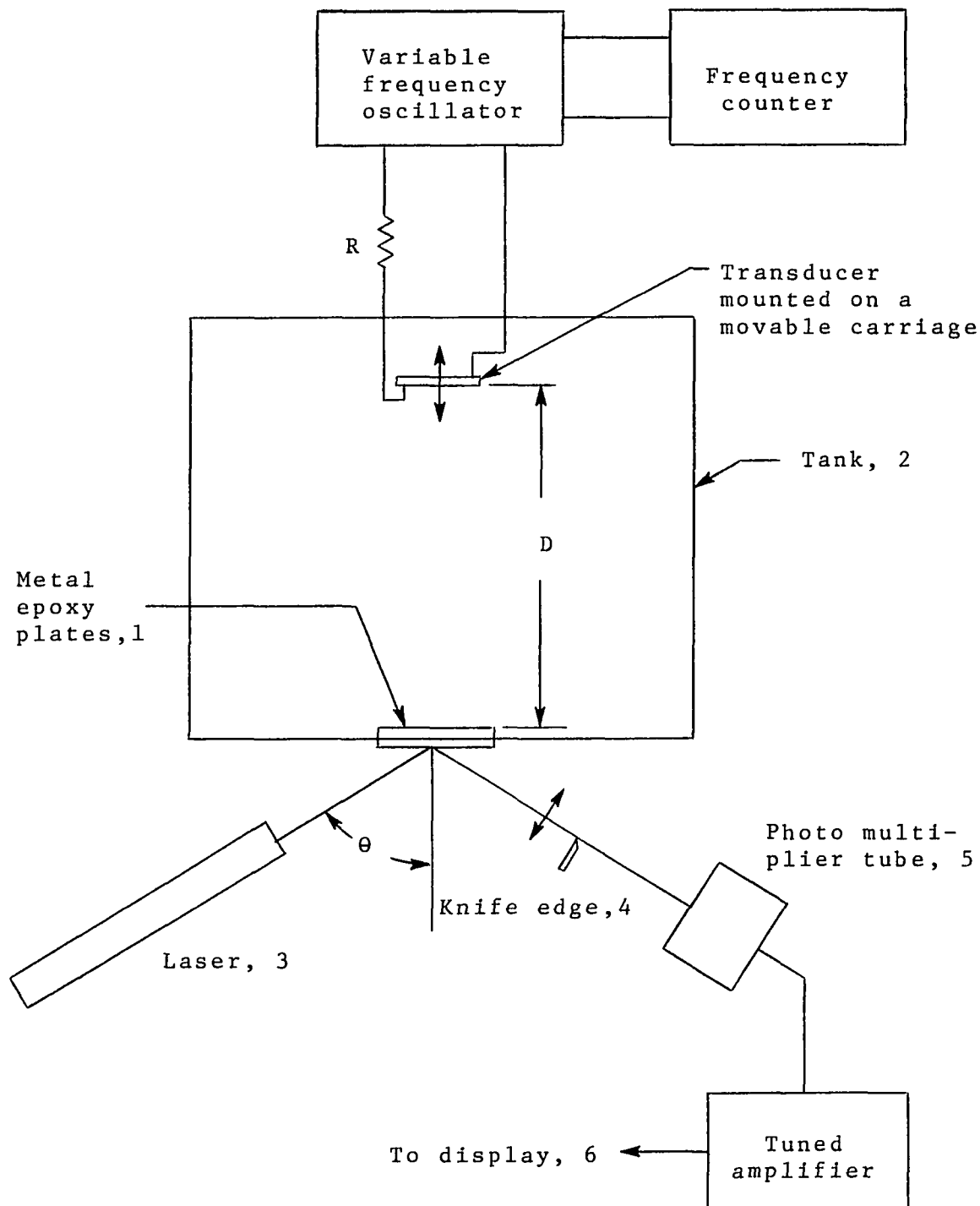


Figure 6-4 An arrangement which may be used to test the performance of metal-epoxy resonant plates

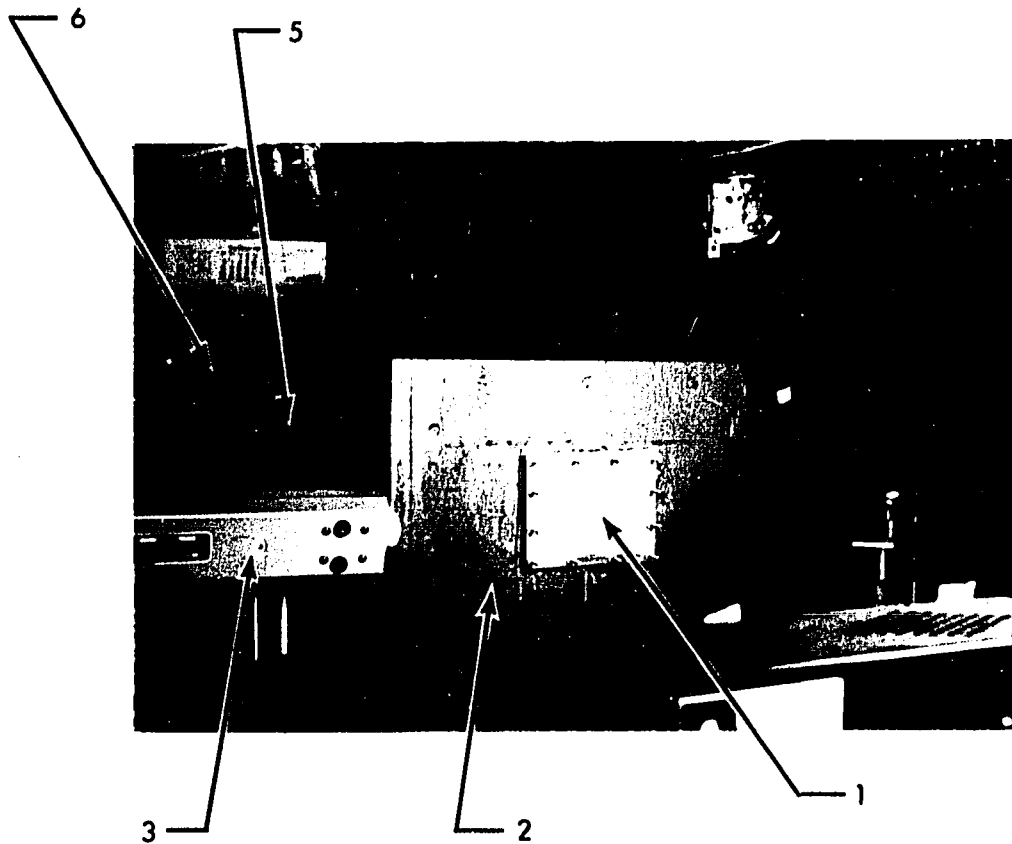


Figure 6-5 Illustration of the actual reflection method used to measure the relative vibration amplitude of the epoxy surface. (The reference numbers correspond to those of Figure 6-4.)

correspond to those used in Figure 6-4.) As can be seen, a mirror directs the reflected laser beam past the knife edge (not visible) and to the photo detector (5). Note also that the angle of incidence of the light beam (angle θ in Figure 6-4) is relatively large (75°). This increases the sensitivity of the optical system and tends to average the vibration amplitude over a larger area (instead of measuring it at one point).

It is worth noting that the method described above detects the vibration amplitude A_o of the epoxy surface; not the displacement amplitude transmission coefficient t_d . Since $t_d = A_o/A_i$, it is imperative, therefore, that the acoustic intensity of the incident sound wave be constant with frequency.

With the experimental arrangement shown in Figure 6-4, the following general procedure is used to determine the frequency response of A_o

1. In order to minimize diffraction effects, particularly at low frequencies, the nominal distance D is adjusted to be as large as possible (approximately 24 cm).
2. The transducer is first aligned to a "dummy" quarter-wave plate with the use of pulsed sound, i.e. its angular orientation is adjusted to yield the strongest echoes. By measuring the magnitude of the first echo, this arrangement may also be used to determine the frequency response of the transducer output. The "dummy" plate is then replaced with the metal-epoxy system which is to be tested.

3. The optical system, especially the position of the knife edge, is adjusted to yield the highest signal-to-noise ratio.
4. Having aligned the acoustical and optical system, the transducer is excited with a sinusoidal voltage of variable frequency, and for each frequency, the distance D and the resonant frequency of the tuned electrical amplifier is adjusted to yield a maximum output signal. Finally, each measurement is corrected to account for the variation with frequency of the transducer output and the gain of the electrical amplifier.

Experimental Results

Metal-epoxy plates were constructed, tuned and tested in accordance with the previous discussion (pages 164-174); and the performance of the overall system was evaluated from the resultant mechanical Q - the only parameter that could be determined absolutely from the relative frequency dependence of $|t_d|$.

A detailed description of the techniques used to obtain and to evaluate a low-frequency, steel-epoxy system will now be presented. The performance of this system will then be compared to that of other metal-epoxy plates.

A low carbon steel plate, having the following characteristics and dimensions

Composition - 0.18% Carbon, 0.50% Manganese,
0.20% Silicon, 0.04% Phosphor
and Sulphur

Specific gravity - 7.79

Nominal dimensions - 4" x 5" x 3/8"

was prepared in accordance with the procedure described on page 164; its final thickness was ground to 9.470 mm \pm 3 microns. The half-wave resonant frequency of this plate was obtained with the pulsed sound immersion technique discussed in Appendix II and shown in Figure II-1. In this arrangement, the transducer was a 1-1/2" dia., water-backed, piezoelectric crystal having a resonant frequency of 323 KHz. With the crystal separated 28 cm from the steel plate, the half-wave frequency f_1' of this plate was 305.8 KHz. Theoretically, this measurement implies that the quarter-wave frequency f_1 is approximately 153 KHz and that the speed of sound in this steel plate is 5.97×10^5 cm/sec.

In order to determine the amount of epoxy required for this system, a small epoxy disk was cast and tested separately. The following characteristics were measured

Specific gravity = 1.10

Speed of sound = 2.30×10^5 cm/sec (average value obtained with the pulsed sound immersion technique using frequencies between 1 and 2.2 MHz)

Using this data, a total of 41 grams of epoxy was cast upon the polished steel surface (as per the procedure outlined on page 165), and resulted in a plate having dimensions of approximately 6.3 cm x 10 cm x 5.09 mm. Although this casting process did not yield a "bubble-free"

plate, the gas bubbles were primarily confined to the epoxy surface. Figure 6-3 shows the completed steel-epoxy system.

The system was then tuned with the same arrangement that was used to obtain the half-wave resonant frequency of the steel plate. Table 6-4 shows the resultant data compiled during the tuning process. In this table, f'_0 represents the frequency obtained with the pulsed sound immersion technique at which the pressure transmission coefficient $|t_p|$ is a maximum or at which the reflection coefficient $|r_p|$ is a minimum. As can be seen, after coating the steel plate with an epoxy layer (5.09 mm thick), no resonance could be detected. However, after the removal of 0.45 mm of the epoxy, a broad resonance was observed between 302.2 and 302.6 KHz. Further grinding of the epoxy plate produced more clearly defined resonant points until, at 4.07 mm (305.8 KHz), the pulsed sound method indicated that the two plates were tuned to the same frequency. Figure 6-6 shows the oscillogram obtained for this condition.

Normally, this completes the tuning process; however, for illustrative purposes, the thickness of the epoxy was further reduced to 3.79 mm. As expected, the resonant frequency of the system was then greater than f'_1 .

TABLE 6-4
TUNING DATA FOR A STEEL-EPOXY SYSTEM

d_1	d_2	f'_o	f_o	Comments
mm	mm	KHz	KHz	
9.47	0.00	305.8	139.5	single steel plate
9.47	5.09	-	-	no resonance observed
9.47	4.64	≈ 302.4	-	
9.47	4.63	302.7	123.2	
9.47	4.40	303.5	130.0	see response #1, Figure 6-8
9.47	4.22	305.1	134.9	
9.47	4.07	305.8	139.5	tuned, see response #2, Figure 6-8
9.47	3.79	307.5	149.0	see response #3, Figure 6-8

d_1 = thickness of the steel plate

d_2 = thickness of the epoxy plate

f'_o = frequency at which $|r_p|$ nulls (determined with the pulsed sound immersion technique discussed in Appendix II)

f_o = frequency at which $|t_d|$ is a maximum (obtained graphically from the frequency dependence of $|t_d|$)

During the above tuning process, the frequency dependence of $|t_d|$ was also obtained for various epoxy thicknesses with the arrangement shown in Figures 6-4 and 6-5. Referring to these figures, the following components were used

Tank - 3/4" plywood with reinforced corners,
14" x 19" x 14" high

Laser - University Lab, model LH 351, 3 mw,
6328 Å

Knife edge - razor blade taped to the photo
detector aperture

Photo detector - RCA 6217 multiplier phototube,
peak response at 4500 Å

Oscillator - Tech. Inst. Corp., model 410-A

Tuned amplifier - single pentode, plate tuned,
voltage gain \approx 200

Transducer - 2-1/2" dia., air-backed, ceramic
crystal (see Figure 6-7) driven by a
class B power amplifier (not shown in
Figure 6-4)

R = 390 ohms, carbon type

D = 24.4 cm

$\theta = 75^\circ$

Following the procedure described on pages 173-174, the frequency dependence of the relative gain was obtained for epoxy thicknesses of 4.63, 4.40, 4.22, 4.07 and 3.79 mm. Three of these response curves, namely those for 4.40, 4.07 and 3.79 mm are shown in Figure 6-8. Finally, the frequency f_0 at which, for each response curve, $|t_d|$ is a maximum,

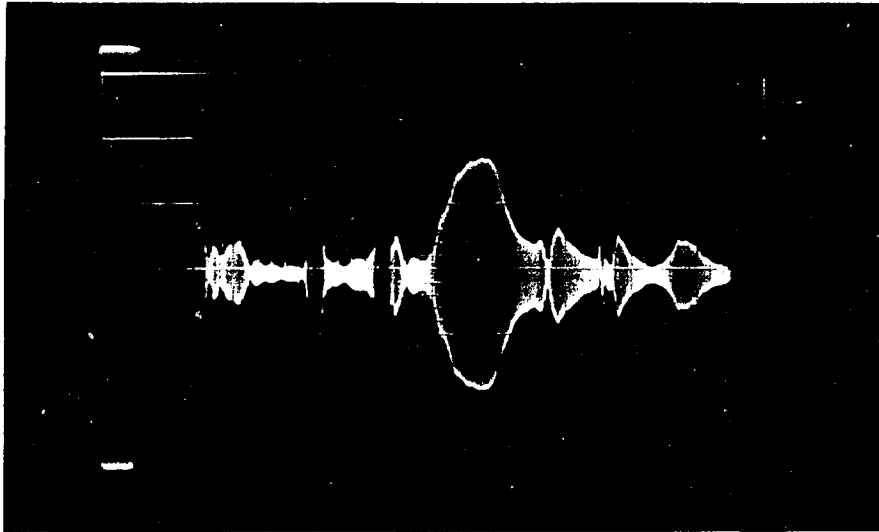


Figure 6-6 Oscillogram obtained as per Figure II-1 for a low frequency, steel-epoxy system. Note that the reflected pulse nulls almost completely at resonance.

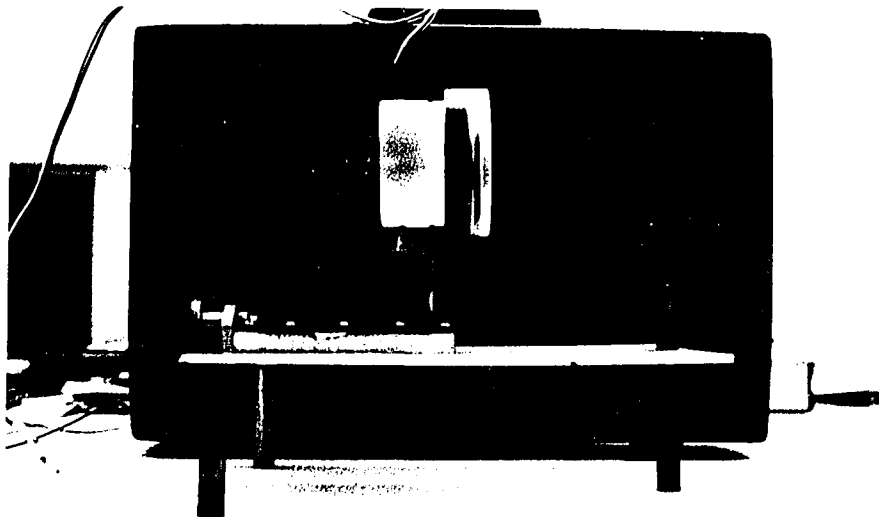


Figure 6-7 Transducer used in Figure 6-4 to determine the frequency dependence of $|t_d|$

is recorded in Table 6-4.

The interpretation of the experimental data presented in Table 6-4 and Figure 6-8 is as follows

1. It is noted that the data obtained with the pulsed sound method (column 3 in Table 6-4) appears self-consistent. That is, the variation of f'_0 with respect to f_1 and the increasing "sharpness" of the nulls as the epoxy thickness is decreased, confirm that the system is tuned when $d_2 = 4.07$ mm.
2. This implies that response curve #2 in Figure 6-8 corresponds to that of tuned plates. Since for this condition $f_1 = f_2 = 139.5$ KHz, it follows that the speed of sound in steel and epoxy (as determined from response curve #2) is 5.29×10^5 cm/sec and 2.27×10^5 cm/sec, respectively. (These values should be compared with those obtained previously with pulsed sound, i.e. 5.97×10^5 and 2.30×10^5 cm/sec, respectively.)
3. Using these newly determined sound velocities, it is possible to compute the epoxy quarter-wave frequency f_2 for other thicknesses at which the frequency dependence of $|t_d|$ was determined. Hence, as shown in Figure 6-8, $f_2 = 129.0$ KHz for curve #1 and $f_2 = 149.9$ KHz for response #3.
4. Referring to the "untuned" response curve #1 and #3 in Figure 6-8, it is evident that f_0 is nearly equal to f_2 but is always between f_2 and f_1 . Hence, the variation of the "resonant" frequency f_0 of the composite system as the epoxy thickness is reduced, is consistent with theoretical expectations. Furthermore, Figure 6-8 also shows the expected relative frequency independence (of nearly quarter-wave plates) of Q and Δf .

In addition to the apparent discrepancy in the value of the sound velocities obtained with pulsed sound and the above analysis, the occurrence of a secondary maximum in the frequency response of "untuned" plates (see curves

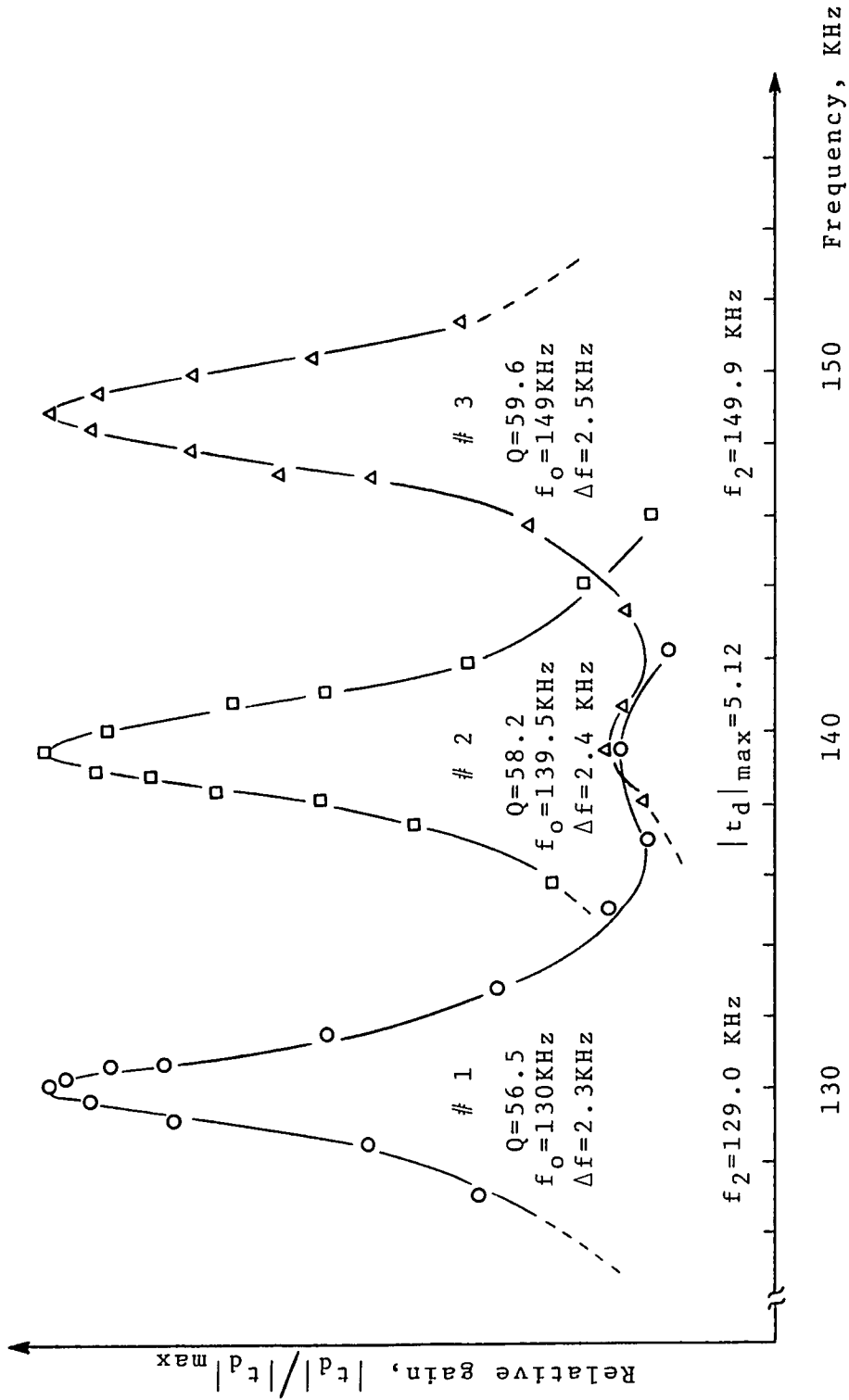


Figure 6-8 Frequency response of the relative gain of a steel-epoxy system for the epoxy thicknesses indicated in Table 6-4

#1 and #3 in Figure 6-8) is not predicted by the previously discussed theory. Although the reason for the occurrence of the secondary peak has not been thoroughly investigated, it is interesting to note that this maximum occurred at 139.5 KHz which, from the previous discussion, is the quarter-wave frequency of the steel plate (see note 2). It was also found that the magnitude of the secondary maximum relative to that of the expected, dominant peak, increased in weakly bonded plates. Hence, these results suggest that diffraction effects or mode coupling within the plates may be responsible for this unexpected behavior.

From the experimental data presented thus far, the following conclusions may be formulated

1. Except for the occurrence of a secondary peak in the frequency dependence of $|t_d|$, the shift of f_0 and the relative invariance of Q and Δf as the epoxy thickness is decreased, confirm the basic theory discussed on pages 164-174.
2. The pulsed sound, immersion method used to tune these plates gives reliable information about the extent to which the plates are tuned to each other. However, the computation of the sound velocity in thin plates, as determined from the measured half-wave resonant

Note 2. Further evidence, supporting the contention that the secondary peak corresponds with f_1 , was obtained by decreasing the steel thickness by 0.076 mm. As would be expected, the frequency at which the secondary peak occurred, shifted to 140.6 KHz.

frequency, may lead to considerable error - especially at low frequencies. This error probably results from the diffraction of the incident sound wave.⁶¹

3. Although the occurrence of a secondary maximum in the frequency response of "untuned" plates remains unexplained, it serves as an additional indicator of the degree to which the plates are tuned. Hence, with reference to Figure 6-8, the plates are tuned when the two peaks overlap.

Two important computations may be made with the aid of response curve #2 in Figure 6-8. The maximum gain $|t_d|_{\max}$ of this steel-epoxy system can be determined from the bandwidth Δf and from the fact that the gain-bandwidth product of "tuned" plates remains relatively constant as the plates are made lossy (see Table 6-1). Hence, using expression (6-9) and the measured acoustic impedances Z_1 and Z_2 indicated in Table 6-1, the maximum gain for this system is

$$\begin{aligned}
 |t_d|_{\max} &= \frac{(\Delta f |t_d|_{\max})_{\text{lossless}}}{(\Delta f)_{\text{lossy}}} & (6-16) \\
 &= \frac{12.3 \times 10^3}{2.4 \times 10^3} = 5.12
 \end{aligned}$$

This value should be compared with 30.63 which is the maximum theoretical gain for lossless steel-epoxy plates (see Table 6-1).

Assuming that the acoustic losses in steel are small compared to those in epoxy, equation (6-12) may be used to

calculate the attenuation coefficient α_2 of the epoxy. Substituting the appropriate values obtained from Figure 6-8 and Table 6-1, $\alpha_2 = 2.72$ nepers/meter at 140 KHz.

Because of this relatively large attenuation coefficient, it would appear, from the discussion on page 157, that a higher gain can be achieved with aluminum-epoxy plates. In order to explore this possibility, an aluminum-epoxy system was constructed and tuned to 140 KHz.

Figure 6-9 shows the experimental and ideal (lossless) frequency dependence of $|t_d|$ of this system. Performing a calculation similar to that of the previous system, one obtains that $|t_d|_{\max} = 8.28$ and $\alpha_2 = 1.89$ nepers/meter. Hence, compared to the steel-epoxy system, a dramatic improvement in the gain has been achieved by constructing an inherently low-Q system. Of course, this improvement is only expected when using lossy materials.

The apparent discrepancy in the value of the epoxy attenuation coefficient obtained in this ($\alpha_2 = 1.89$ nep./m) and the steel-epoxy system ($\alpha_2 = 2.72$ nep./m) is believed to be due to the assumption in equations (6-11) and (6-12) that L_1 is small compared to L_2 . Since this assumption is more accurate for aluminum than for steel, it is assumed

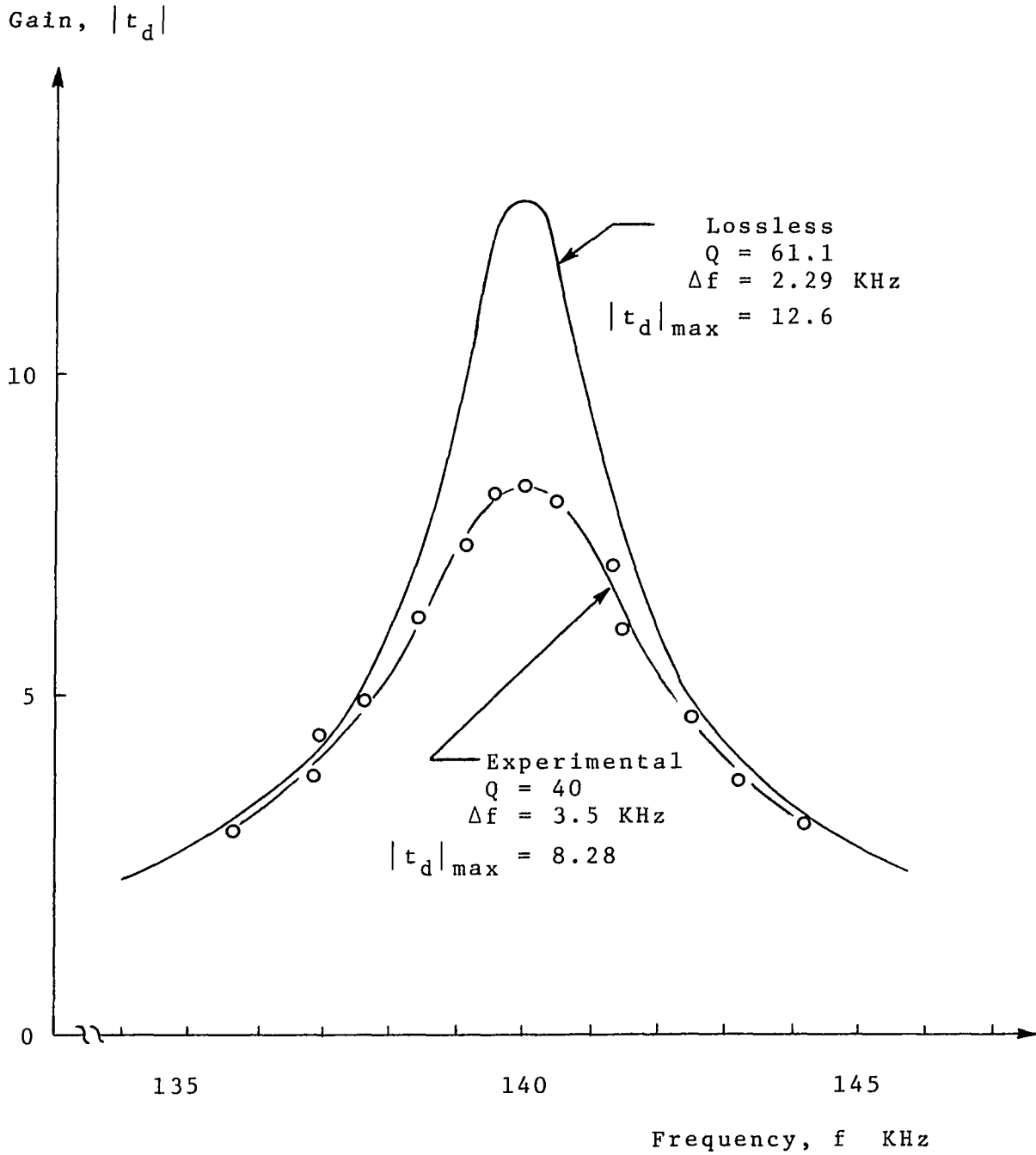


Figure 6-9 Frequency response of a "tuned" aluminum-epoxy system

that the attenuation coefficient of the epoxy used is approximately 1.9 nepers/meter at 140 KHz.

Metal-epoxy plates were also constructed for higher frequencies (0.9 - 1.0 MHz). In some respects these plates were easier to construct since the degassing of the epoxy during the casting process was more complete. This also permitted the casting of the epoxy plate to nearly the required thickness and therefore, it reduced the amount of grinding which was later necessary in order to tune the plates. On the other hand, since the dimensional tolerance requirements at the higher frequencies are expected to be more critical, the plates were entirely hand-ground. (Low-frequency plates were initially (coarse) ground with a surface grinder.)

The plates were tested with the same arrangement used for testing the low-frequency plates (see Figures 6-4 and page 178) except for the following modifications

Transducer - 1-1/2" diameter, water-backed,
ceramic crystal excited directly
by the oscillator (max. output at
 \approx 935 KHz)

R = 200 ohms, carbon type

The procedure used to test the high-frequency plates was also modified from that described on page 173. Rather than adjusting the position of the transducer in order to obtain a maximum in the output signal, it was more

expedient to change the frequency of the sound wave. This is possible because the bandwidth of the plates increases at higher frequencies (see equation (6-8)) whereas the frequency difference between maxima in the output signal remains approximately equal to $c/2D$. In this manner, the frequency response could be sampled at a number of frequencies without disturbing the geometry between measurements.

Although nine different high-frequency plates were tested, each consisting of a quarter-wave plate of steel, brass or aluminum and a quarter-wave plate of filled or unfilled epoxy (see note 3), only the experimental results of unfilled epoxy systems are shown in Table 6-5. This table lists the gain, Q and the attenuation coefficient α_2 computed from the experimental data of high-frequency steel-epoxy, aluminum-epoxy and brass-epoxy plates and shows the comparison with those values computed from the previously discussed low-frequency plates.

In general, the same behavior exhibited by the previously discussed low-frequency plates was also

Note 3. In order to make the epoxy opaque to laser light, a number of systems were constructed with filled epoxy. Typical fillers were 1% to 2% of red dye and iron oxide. In each instance, very low gains were obtained.

TABLE 6-5
PERFORMANCE COMPARISON BETWEEN
HIGH AND LOW-FREQUENCY PLATES

		lossless	experimental		
	f_o	$ t_d _{max}$	$ t_d _{max}$	Q	α_2
	KHz				nep/m
Steel-epoxy	140	30.63	5.12	58.2	2.72
Aluminum-epoxy	140	12.65	8.28	40.0	1.89
Steel-epoxy	960	30.63	5.43	61.9	15.4
Aluminum-epoxy	916	12.65	9.50	48.2	9.89
Brass-epoxy	961	28.90	7.00	71.2	13.3

observed in the high-frequency plates. That is, the pulsed sound immersion technique proved to be a reliable indicator of the degree to which the plates were tuned; and sound velocity computations made from pulsed sound data were consistently higher than the values obtained from the frequency response curves of "untuned" plates, i.e. from the frequency at which the secondary peak occurred.

Referring to Table 6-5, it is noted that, with the same materials, consistently higher gains were obtained at the higher frequencies. Since the diameter of the transducer used to test the high-frequency plates was approximately 24 wavelengths (of sound in water) whereas that of the low-frequency transducer was 5.3, it is reasonable to assume that the apparent increase in gain at higher frequencies is due to less diffraction of the incident sound wave (see note 4). It is also noted that the highest gain was obtained with an aluminum-epoxy system (9.5 at 916 KHz).

With reference to Table 6-5 and the discussion on page 184, the attenuation coefficient of the epoxy is

Note 4. This conclusion is further supported by data obtained when D (in Figure 6-4) was reduced from 24.4 cm to 14.3 cm. For the high-frequency steel-epoxy plate in Table 6-5, Q decreased from 61.9 to 57.3.

approximately 10 nepers/meter at 916 KHz. This value should be compared with 68 nepers/meter at 910 KHz for Epon adhesive #946 (a similar material) as reported by McSimin and Andreath.⁶² The dramatic reduction of the acoustic losses of the epoxy (Epon resin 828 and Epon curing agent V-40; equal parts by weight) used in these experiments is believed to be due primarily to the proper degassing of the mixture during the casting process as described on page 165. Incidentally, different curing schedules or the reduction of internal stresses within the epoxy (accomplished by heating the specimen beyond its heat deflection temperature and then reducing the temperature at a rate of 2°C per hour) did not appear to affect the attenuation coefficient to any observable extent.

Some experiments were also conducted in order to (qualitatively) demonstrate the thickness tolerance requirement of materials 1 and 2. Using the high-frequency steel-epoxy system whose $Q = 61.9$ as shown in Table 6-5, the exposed steel surface was coated with a protective paint approximately 20 microns thick. The result of this action produced no measurable change in Q . However, when the exposed epoxy surface was painted similarly the Q of the overall system was reduced to less than 10.

Finally, with reference to Chapter 5, an important characteristic of metal-epoxy plates is the angular sensitivity. In order to obtain some indication of this sensitivity, the incident angle of the sound wave in Figure 6-4 was off-set by approximately 5° from normal and the relative frequency dependence of $|t_d|$ for the previously described high-frequency steel-epoxy plates was determined. As would be expected, the maximum value of the output signal obtained with the arrangement shown in Figure 6-4 decreased to about 0.4 of the value obtained under normal sound incidence and Q decreased from 61.9 to 34.3. By themselves, little meaning can be attached to either one of these measurements since the elimination of standing waves at non-normal incidence is expected to yield a reduced output and the meaning of Q at non-normal incidence is questionable. Nevertheless, this and other data, obtained by pulsing the transducer (to eliminate standing waves for both normal and non-normal incidence), suggest that the output is decreased to about $1/2$ when the incident sound angle is off-set by approximately 5° .

In summary, it may be stated that simple transmission-line theory predicts reasonably well the performance of actual, two quarter-wave plates.

It has been determined that the maximum displacement

amplitude transmission coefficient obtainable with metal-epoxy plates is limited by the acoustic losses within the epoxy and that, as a consequence, higher gains can be obtained with systems having an inherently lower Q than with inherent high-Q systems. (This is demonstrated in Table 6-5; as can be seen, a gain of 9.50 has been achieved with aluminum-epoxy plates as compared to 5.43 with steel-epoxy plates.) For this reason, the importance of properly eliminating all gaseous impurities from the epoxy mixture cannot be overemphasized. With the procedure described on page 165, epoxy plates have been constructed having an attenuation coefficient of approximately 1/6 of that reported for a similar material.

Finally, the expected sensitivity of the two-quarter-wave velocity transformer to the angle of sound incidence has been demonstrated qualitatively.

Chapter VII

CONCLUSIONS AND RECOMMENDATIONS

The novel "four-step acoustical holographic imaging system", as proposed and described in this dissertation (see Chapter V) consists of

1. The generation of an acoustical hologram and its transference from one medium (water) to another (air)
2. The optical recording of the acoustical interference pattern. In the proposed method, the resultant, converted acoustical hologram is obtained in two steps by using optical holographic techniques.
3. The reconstruction of the converted acoustical hologram

Implementation of the system has been proved possible, and several means for its implementation have been analyzed both theoretically and experimentally.

To this end, a study on the use of optical holographic techniques to convert an arbitrary acoustic image to a visible image (as required in #2 above) has been conducted. This has resulted in the introduction and analysis of the "holographic sound image converter." This device consists of the optical "holographic interferometer" and an appropriate "coupler" whose primary function is to transfer the acoustical energy from a surface bounded by water to a surface bounded by air.

Advantages of this converter over other existing systems (as described in Chapter II) are

1. its simplicity
2. its ability to simultaneously detect a quantity related to the vibration amplitude at each and every point of the acoustical diffraction pattern
3. the subsequent elimination of the need for scanning
4. its frequency selectivity
5. the ease with which amplification can be achieved
6. the possibility of using "reference wave simulation"

The first three advantages are generally characteristic of non-scanned detectors whereas the latter three advantages are usually associated with scanned, linear detectors. The "holographic converter" appears, therefore, to be the first-to-date that exhibits the favorable characteristics of both scanned and non-scanned imaging systems.

The above study has also yielded the new technique of "shifted reference holographic interferometry" (see Chapter IV) which is shown to permit increasing the sensitivity of conventional, time-averaged, optical holographic interferometry by approximately one order of magnitude (that is, from 330 \AA to 30 \AA). This technique is based on shifting the frequency of the optical reference wave by an amount equal to the frequency of the

vibrating "object" (which is assumed to be vibrating sinusoidally at the frequency of the sound wave). Experimental verification of this technique was provided in connection with a different study (as mentioned later).

Even if the motion of the object is not sinusoidal, the "shifted reference holographic interferometer" may be used to investigate, usually with increased sensitivity, the displacement amplitude of every point of the object's surface, provided that a sufficient amount of light reflected from the object experiences a "Doppler shift" comparable to that of the reference wave. However, since it is more difficult to shift the frequency of the reference wave by a small amount as opposed to several megahertz (due to the necessary filtering following the homodyne process), the latter consideration may limit this application of the "shifted reference holographic interferometer" to the study of "fast-accelerating" objects.

Holographic techniques were also applied to the measurement of acoustic parameters and several ways of implementing this relatively new application were proposed and investigated (see Chapter III). By phase modulating the optical "object" wave with an acoustic wave whose propagation vector is normal to that of the

"object" wave, it was shown that a "side-view" of that sound wave can be obtained. Under certain conditions, the distribution of irradiance within the reconstructed image may then be used to determine the Raman-Nath parameter of the sound wave. In a number of experiments, the advantages of this application of holography in the field of ultrasonics were demonstrated and discussed. In particular, a theoretical relation comparing this method to the well known Schlieren method was developed and experimentally verified.

The results of this experimentation also included an experimental verification of the shifted reference holographic technique which was described previously.

A theoretical and experimental study of some possible couplers was also conducted in some detail. Each of the couplers considered proved capable of augmenting the displacement amplitude of the acoustical diffraction pattern as it is transferred from a surface bounded by water to a surface bounded by air. The couplers proposed and investigated range from a simple, specific acoustic impedance transformer (with or without control of the acoustic impedance of the terminating medium) to a mosaic of velocity amplifiers where each cell consists of a receiving crystal, followed by

appropriate electronic circuitry and a transmitting transducer.

A particularly detailed study was conducted on the development and testing of a mechanical velocity transformer consisting of two resonant quarter-wave plates. To this end, the theoretical relations describing the behavior of a system of two lossy, nearly quarter-wave plates were developed (Chapter VI and Appendix I). As discussed later, this study resulted in a practical, working system - a realization which is due, in part, to the novel use of epoxy as one of the resonant materials.

In the course of this experimentation, a useful method for "tuning" quarter-wave metal-epoxy plates was devised. As described in Chapter VI, coarse "tuning" was accomplished with a pulsed sound, (water) immersion technique, whereas final "tuning" was achieved by monitoring the frequency dependence of the displacement amplitude transmission coefficient of the overall system. An examination of experimental "tuning" data obtained by the latter method shows that

1. This method appears to be a promising tool for the accurate measurement of the speed of sound in either resonant plate. This measuring technique may be especially useful at lower frequencies where diffraction effects can adversely affect the accuracy of other methods.

2. This technique may be used to determine the attenuation coefficient of epoxy.

Experimental verification of the theoretical relations describing the behavior of metal-epoxy plates (as developed in this dissertation) was provided (see Chapter VI). In particular, a velocity augmentation of 9.5 at 916 KHz was achieved with aluminum-epoxy plates (loaded with water and air, respectively). The resultant gain (19.6 dB) across the water/air interface represents a significant improvement over the gains reported at considerably lower frequencies. Higher gains, expected with steel-epoxy or brass-epoxy plates, were not realized primarily because of the large acoustic losses within the epoxy.

The theoretical and experimental investigation of other (than holographic) interferometric methods (see Chapter IV), yielded a new application of the laser feedback interferometer to the detection and measurement of small (fractions of a wavelength) vibration amplitudes. It was analytically shown and experimentally verified that, under certain conditions, the laser feedback and the Michelson interferometers can yield similar results.

As a result of the various studies described above, a "holographic sound image converter" having a threshold

intensity of 2.8 mw/cm^2 at 1 MHz appears feasible. Such a converter would be comprised of the "shifted reference holographic interferometer" having a sensitivity of 30 \AA and the aluminum-epoxy, two quarter-wave coupler (loaded with water and air) having an advantage of 9.5.

Experimental data has shown that, with the acoustical arrangement illustrated in Figure 6-4, the exposed epoxy surface experiences a total deformation consisting of the following components

1. A large, static displacement (detected and measured with conventional, "double exposure" holographic techniques)
2. A relatively large, spatially random, slow-time varying deformation (detected with conventional "time-averaged" holographic techniques and the laser feedback interferometer)
3. A small, spatially varying, high-frequency deformation, occurring at the sound frequency (detected and measured with the laser feedback interferometer)

The static deformation is due to the radiation pressure and, as determined experimentally, is similar to that which would result from a concentrated force exerted on the metal plate at the sound beam axis. The radiation pressure as well as the formation of standing waves within the water medium is also believed to be responsible for the second component. Hence, any small change of the sound frequency or of the transducer position

relative to that of the plates, can result in a slow time variation of the radiation pressure, and consequently, of the deformation of the epoxy surface. Because this component can be considerably larger than the desired, high-frequency vibrational amplitudes, the "holographic converter" should be used with pulsed sound (and light). This would eliminate the formation of standing waves. Another possibility for preventing standing waves in this system is to improve the match of water to air by controlling the acoustic impedance of the terminating medium (see Chapter VI).

The various studies conducted and described in this dissertation have resulted in a number of recommendations pertaining to further work.

- a. With reference to the "shifted reference optical holographic interferometer" it would be useful to experimentally determine what is the minimum vibrational amplitude that can be detected with this instrument. Besides providing a further demonstration of the shifted reference technique, such an experiment would permit the determination of the practical sensitivity of this interferometer, and therefore, of the "holographic acoustic image converter". The arrangement of such an experiment could make use of a single transducer mounted in the wall of a water tank. In this manner, the sound wave generated in the water medium may be used to shift the optical frequency of the reference wave and a hologram can be recorded of the other transducer face which is bounded by air. A suitable sound frequency can be 2-3 MHz. This choice insures

sufficient separation of the spectral orders, as well as sufficiently large vibrational amplitudes (for reasonable acoustic intensities) of the transducer face.

- b. The experimental results of Chapter VI indicate that a further increase of the displacement amplitude transmission coefficient is primarily limited by the acoustic losses of the plate which is bounded by air, i.e. the epoxy. It would seem, therefore, that a study of the loss mechanism of epoxy or of any other suitable material and the subsequent reduction of its attenuation coefficient, could greatly increase the gain of two quarter-wave plates. For the purpose of such an investigation, the attenuation coefficient of the material could be conveniently determined using the pulsed sound immersion method described in Appendix II.
- c. There are also indications which suggest that a four layer, resonant system consisting of alternating aluminum and epoxy quarter-wave plates can have, in practice, a higher gain than that obtained with the two quarter-wave plates discussed in Chapter VI. Since this structure may be thought of as two aluminum-epoxy systems in series, it is expected that the frequency dependence of the transmission coefficient of the overall system will behave in a manner similar to that of lumped cascaded tuned filter systems (single tuned, double tuned, stagger tuned, etc.). The experimental portion of such a study could also include a means for controlling the acoustic impedance Z_a of the terminating medium (by increasing or decreasing the air pressure from ambient) in order to achieve a total match.
- d. The previous recommendations refer to the holographic converter using a quarter-wave coupler. Evidently, as discussed in Chapter V, more sophisticated couplers also appear quite feasible. Of these, the velocity amplifier shown in Figure 5-6 or variations thereof, seem to be the most promising. With the use of modern integrated circuits, this coupler can be relatively compact, and when

further used with the holographic detector, the resulting image converter offers all of the advantages stated on page 194; including an improved resolution capability. In addition, the extreme mechanical stability that is required during the recording of the hologram, presents no particular difficulty with this converter since the receiving transducers are mechanically isolated from the transmitting crystals.

The resultant system might also incorporate some form of frequency conversion; that is, the transmitting transducer may be made to vibrate at a lower frequency than the receiving transducer. As discussed in Chapter V, such a technique could result in an increased sensitivity of the overall image converter.

- e. It should also be noted that, if the frequency and the vibration amplitude of the transmitting transducers in Figure 5-6 are sufficiently large, the acoustic image may be formed directly (without using the "holographic interferometer") by an appropriate Schlieren method. The optical arrangement may be similar to that used in the surface levitation system, that is, the (polished) surface of the transmitting transducers is used to phase modulate a coherent optical wave (see Chapter III). The obvious advantage of this technique is that it allows real-time acoustic imaging.

The general applications and advantages of acoustic holography have already been widely (and sometimes optimistically) discussed in the literature. Non-destructive testing, short-range underwater imaging and medical diagnosis are some areas where the application of acoustic holography can afford distinct advantages over present imaging methods. These advantages are often a

result of the increased information that can be obtained about an object (e.g. improved images can also be obtained through turbid media). Although the image of a near object is usually distorted (depth dimension is magnified), useful depth information can be deduced by focusing on different planes of the object. Depth information can also be obtained about distant objects by recording two, separate converted acoustic holograms - each showing, upon reconstruction, a slightly different view of the same object. In this manner, a stereoscopic image of the object can be formed.

It is expected that the proposed four-step acoustic holographic imaging system can be successfully employed in these applications, but result in a simpler more reliable device. The final image is expected to be of a quality equal or superior to that afforded by present acoustic holographic imaging systems.

Appendix I
THEORY OF MULTILAYER FILMS
FOR LONGITUDINAL ACOUSTIC WAVES

Consider the propagation of a plane sound wave through three different media under the condition of normal incidence. Assume that the initial wave is propagating in medium "w" in the positive x direction, that the boundary between media "w" and "l" is located at $x=0$, and that the boundary between media "l" and "a" is located at $x=d$ as shown in Figure I-1. Assume further that medium "a" extends to infinity.

Due to the transmission and reflection of sound at each boundary, a wave propagating in the positive and negative x directions will result in each medium except medium "a" which will only contain a transmitted wave (see Figure I-1). Under steady state conditions, the pressure of each of these waves may be represented as follows

$$\begin{aligned}
 p_w &= P_w \exp [i(\Omega t - k_w x)] \\
 p_w' &= P_w' \exp [i(\Omega t + k_w x)] \\
 p_l &= P_l \exp [i(\Omega t - k_l x)] \\
 p_l' &= P_l' \exp [i(\Omega t + k_l x)] \\
 p_a &= P_a \exp \{i[\Omega t - k_a(x - d)]\}
 \end{aligned}
 \tag{I-1}$$

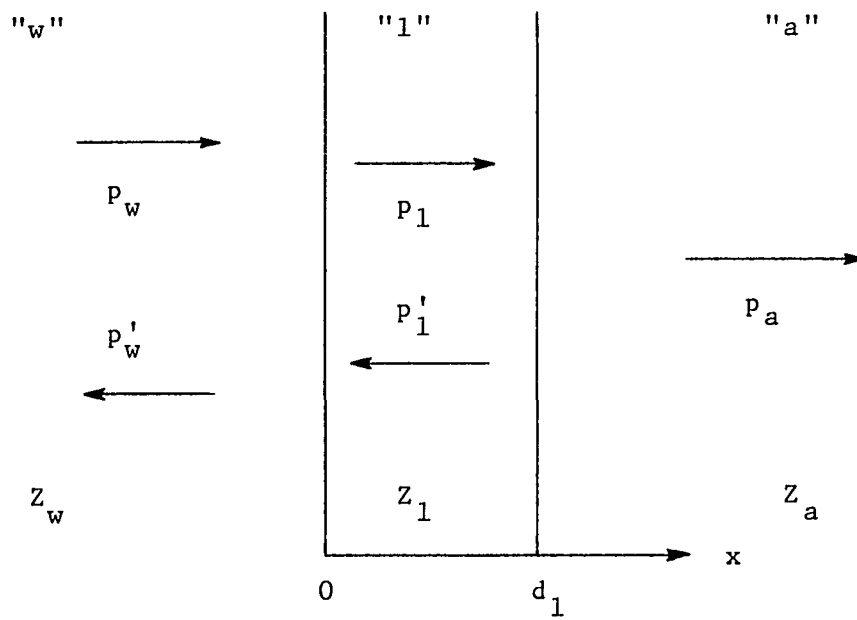


Figure I-1 The propagation of a sound wave through three different media (normal incidence)

where

P is the respective complex amplitude of the pressure of waves travelling in the positive x direction

P' is the respective complex amplitude of the pressure of waves travelling in the negative x direction

k is the magnitude of the propagation vector in each respective medium; in attenuating media, this quantity is complex

Ω = angular frequency of the incident sound wave

d_1 = thickness of medium "1"

t = time

The boundary conditions require that both the pressure and the velocity be continuous. Since the velocity u can be expressed in terms of the pressure p and the characteristic impedance Z in the following manner

$$u = +p/Z \quad \text{for waves propagating in the positive } x \text{ direction}$$

$$u' = -p'/Z \quad \text{for waves propagating in the negative } x \text{ direction}$$

the boundary conditions at $x = 0$ yield

$$\begin{aligned} P_w + P'_w &= P_1 + P'_1 && \text{pressure continuous} \\ \frac{P_w}{Z_w} - \frac{P'_w}{Z_w} &= \frac{P_1}{Z_1} - \frac{P'_1}{Z_1} && \text{velocity continuous} \end{aligned} \tag{I-2}$$

while the boundary conditions at $x = d_1$ yield

$$P_1 \exp(-i\gamma_1) + P_1' \exp(i\gamma_1) = P_a \quad \text{pressure continuous} \quad (\text{I-3})$$

$$\frac{P_1}{Z_1} \exp(-i\gamma_1) - \frac{P_1'}{Z_1} \exp(i\gamma_1) = \frac{P_a}{Z_a} \quad \text{velocity continuous}$$

where $\gamma_1 = k_1 d_1$ (in general, a complex quantity) and where Z_w , Z_1 and Z_a are the characteristic impedances of media "w", "1" and "a", respectively.

Solving simultaneously for P_1 and P_1' from the expressions (I-3) yields

$$\begin{aligned} P_1 &= (Z_a + Z_1)/(2Z_a) P_a \exp(+i\gamma_1) \\ P_1' &= (Z_a - Z_1)/(2Z_a) P_a \exp(-i\gamma_1) \end{aligned} \quad (\text{I-4})$$

Substituting (I-4) into (I-2) and using the following definitions,

$$\begin{aligned} r_p &= P_1'/P_w = \text{pressure reflection coefficient} \\ t_p &= P_a/P_w = \text{pressure transmission coefficient} \end{aligned}$$

the relations of (I-2) become

$$1 + r_p = \left(\cos\gamma_1 + i \frac{Z_1}{Z_a} \sin\gamma_1 \right) t_p \quad (\text{I-5})$$

$$\frac{1}{Z_w} - \frac{r_p}{Z_w} = \left(\frac{\cos\gamma_1}{Z_a} + i \frac{1}{Z_1} \sin\gamma_1 \right) t_p \quad (\text{I-6})$$

These two relations may also be expressed in matrix form in the following way

$$\begin{bmatrix} 1 \\ 1/Z_w \end{bmatrix} + \begin{bmatrix} 1 \\ -1/Z_w \end{bmatrix} \begin{bmatrix} r_p \end{bmatrix} = \begin{bmatrix} M_1 \end{bmatrix} \begin{bmatrix} 1 \\ 1/Z_a \end{bmatrix} \begin{bmatrix} t_p \end{bmatrix} \quad (I-7)$$

where the transfer matrix M_1 of medium "1" is

$$\begin{bmatrix} M_1 \end{bmatrix} = \begin{bmatrix} \cos\gamma_1 & iZ_1 \sin\gamma_1 \\ (i/Z_1) \sin\gamma_1 & \cos\gamma_1 \end{bmatrix} \quad (I-8)$$

Referring to Figure I-1, if media "w" and "a" are separated by more than one layer, for instance N layers, then each layer may be described by a unique transfer matrix of the form (I-8). Furthermore, with an analysis similar to that described on the preceding pages, one can obtain an equation of the form (I-7), where M_1 is replaced by the overall, equivalent transfer matrix M_{eq} . This equivalent transfer matrix is the product of all the individual transfer matrices $M_1, M_2, M_3 \dots M_N$, i.e.

$$\begin{bmatrix} M_{eq} \end{bmatrix} = \begin{bmatrix} M_1 \end{bmatrix} \begin{bmatrix} M_2 \end{bmatrix} \begin{bmatrix} M_3 \end{bmatrix} \dots \begin{bmatrix} M_N \end{bmatrix} = \begin{bmatrix} m_1 & m_2 \\ m_3 & m_4 \end{bmatrix} \quad (I-9)$$

Once M_{eq} has been determined, the pressure transmission and reflection coefficients of the overall system can be determined. With reference to equations (I-5) and (I-6), simultaneously solving for r_p and t_p yields

$$r_p = \frac{m_1 Z_a + m_2 - m_3 Z_w Z_a - m_4 Z_w}{m_1 Z_a + m_2 + m_3 Z_w Z_a + m_4 Z_w} \quad (\text{I-10})$$

$$t_p = \frac{2Z_a}{m_1 Z_a + m_2 + m_3 Z_w Z_a + m_4 Z_w} \quad (\text{I-11})$$

where m_1 , m_2 , m_3 and m_4 are the elements of the equivalent matrix as defined in relation (I-9).

Other reflection and transmission coefficients may be determined from r_p and t_p . Hence, remembering the expressions for the velocity u on page 206, the various coefficients are

for velocity

$$r_u = -r_p \quad t_u = (Z_w/Z_a)t_p$$

for displacement

$$r_d = -r_p = r_u \quad t_d = (Z_w/Z_a)t_p = t_u$$

for power

$$r_{\text{power}} = |r_p|^2 \quad t_{\text{power}} = (Z_w/Z_a)|t_p|^2$$

(A point worth noting is that all of these reflection and transmission coefficients are defined with respect to the incident wave at $x=0$ - not the total, resultant wave!)

When the layers are lossy, as is generally the case, the phase angle γ is complex and may be expressed as

$$\gamma = kd = Kd - i\alpha d$$

where

$$K = 2\pi f/c = 2\pi/\Lambda$$

c = speed of sound in the particular medium

Λ = wavelength of sound in the layer

α = attenuation coefficient of the layer

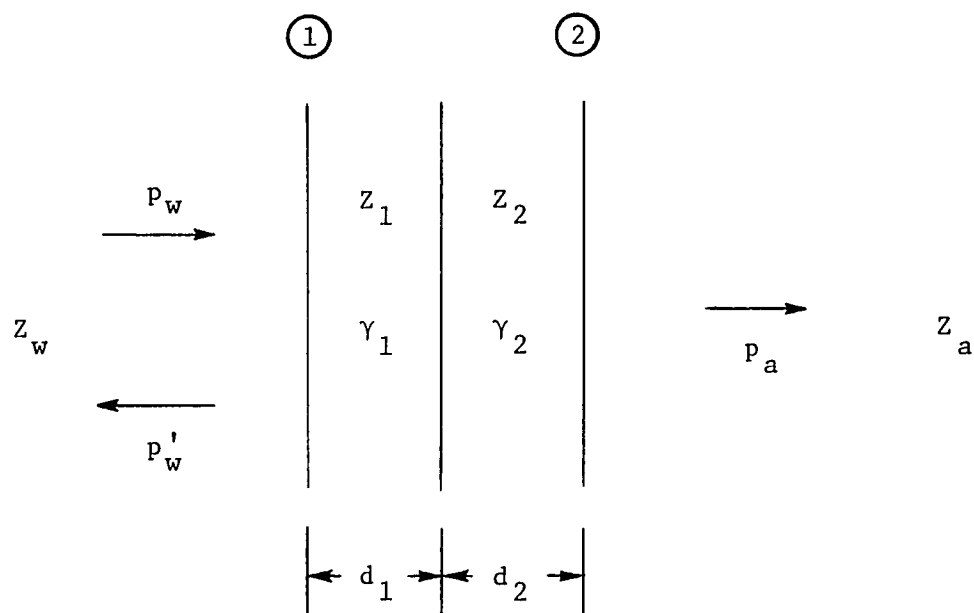
d = thickness of the layer

If, on the other hand, the intervening layers are lossless, then γ is real and the elements of the equivalent transfer matrix are related in such a way that $m_1 m_4 - m_2 m_3 = 1$.

As an example of the application of this theory, consider the two layer system shown in Figure I-2. If Z_1 and Z_2 , and γ_1 and γ_2 are the respective characteristic impedances and phase angles of the two intervening media, then the equivalent transfer matrix for the overall system is

$$\begin{aligned} [M_{eq}] &= [M_1] [M_2] = \begin{bmatrix} \cos\gamma_1 & iZ_1 \sin\gamma_1 \\ (i \sin\gamma_1)/Z_1 & \cos\gamma_1 \end{bmatrix} \begin{bmatrix} \cos\gamma_2 & iZ_2 \sin\gamma_2 \\ (i \sin\gamma_2)/Z_2 & \cos\gamma_2 \end{bmatrix} \\ [M_{eq}] &= \begin{bmatrix} (\cos\gamma_1 \cos\gamma_2 - \frac{Z_1}{Z_2} \sin\gamma_1 \sin\gamma_2) & i(Z_2 \cos\gamma_1 \sin\gamma_2 + Z_1 \sin\gamma_1 \cos\gamma_2) \\ i \left(\frac{\sin\gamma_1 \cos\gamma_2 + \cos\gamma_1 \sin\gamma_2}{Z_1} \right) & \left(\cos\gamma_1 \cos\gamma_2 - \frac{Z_2}{Z_1} \sin\gamma_1 \sin\gamma_2 \right) \end{bmatrix} \quad (I-12) \end{aligned}$$

Comparing the above relation with (I-9) and using equation (I-10) in conjunction with $t_d = (Z_w/Z_a)t_p$, the displacement amplitude transmission coefficient t_d is



$$\gamma_1 = k_1 d_1 = K_1 d_1 - i\alpha_1 d_1$$

$$\gamma_2 = k_2 d_2 = K_2 d_2 - i\alpha_2 d_2$$

Figure I-2 Sound transmission from medium "w" to medium "a" through two intervening layers

$$t_d = 2Z_w \left[(A \cos \gamma_1 \cos \gamma_2 - B \sin \gamma_1 \sin \gamma_2) + i (C \cos \gamma_1 \sin \gamma_2 + D \sin \gamma_1 \cos \gamma_2) \right]^{-1} \quad (\text{I-13})$$

where

$$A = Z_a + Z_w$$

$$B = Z_1 Z_a / Z_2 + Z_w Z_2 / Z_1$$

$$C = Z_2 + Z_a Z_w / Z_2$$

$$D = Z_1 + Z_a Z_w / Z_1$$

This expression is further analyzed in Chapter VI for the case when the intervening media "1" and "2" are lossy and nearly a quarter-wave thick.

If, on the other hand, the layers are lossless and exactly a quarter-wave thick, then (I-13) reduces to

$$t_d = (-2Z_1 Z_2 Z_w) / (Z_a Z_1^2 + Z_w Z_2^2) \quad (\text{I-14})$$

since $\gamma_1 = \gamma_2 = \pi/2$.

Another interesting parameter of a system such as that shown in Figure I-2 is its mechanical advantage MA. For the multilayer system discussed in this appendix, the mechanical advantage may be defined, irrespective of the number of layers, in the following way (see Figure I-2)

$$\text{MA} = \left| \frac{\text{total amplitude of the velocity at plane } \textcircled{2}}{\text{total amplitude of the velocity at plane } \textcircled{1}} \right| \quad (\text{I-15})$$

$$\text{MA} = \left| \frac{P_a / Z_a}{P_w / Z_w - P_w' / Z_w} \right|$$

Remembering the definitions of the reflection and trans-

mission coefficients on pages 207 and 209, MA may be expressed in terms of these coefficients

$$MA = \left| \frac{Z_w}{Z_a} \frac{t_p}{(1 - r_p)} \right| = \left| \frac{t_d}{1 + r_d} \right| = \left| \frac{t_u}{1 + r_u} \right| \quad (I-16)$$

or directly in terms of the elements of the equivalent transfer matrix

$$MA = \left| 1 / (m_3 Z_a + m_4) \right| \quad (I-17)$$

where relations (I-10) and (I-11) have been used.

Hence, for the two, lossless quarter-wave plates discussed on page 212, the mechanical advantage is Z_1/Z_2 .

Appendix II

A LIQUID IMMERSION, PULSED SOUND TECHNIQUE FOR MEASURING
THE SPEED OF SOUND IN THIN PLATES

The design and tuning of the quarter-wave resonant plates discussed in Chapter VI require a knowledge of the speed of sound in thin plates; or more precisely, their quarter-wave resonant frequency.

A simple and relatively accurate method for measuring the speed of sound in thin plates is the liquid immersion technique shown in Figure II-1. Referring to this figure, a gated, sinusoidal voltage whose frequency can be controlled, is applied to a piezoelectric crystal and monitored with an oscilloscope. If normal incidence is observed, the voltage pattern on the CRT will show the initial sound pulse and its echoes which, for the geometry indicated ($d + x_2 < x_1$), arrive in the following sequence

1. Pulse reflected from the front surface of the plate - this pulse has travelled a distance equal to $2x_1$
2. Pulse transmitted through the plate, almost totally reflected from the tank wall, and transmitted a second time through the plate - this pulse has travelled a total distance equal to $2(x_1 + d + x_2)$
3. Further echoes - exactly which echo arrives depends on the relationship between x_1 , d and x_2

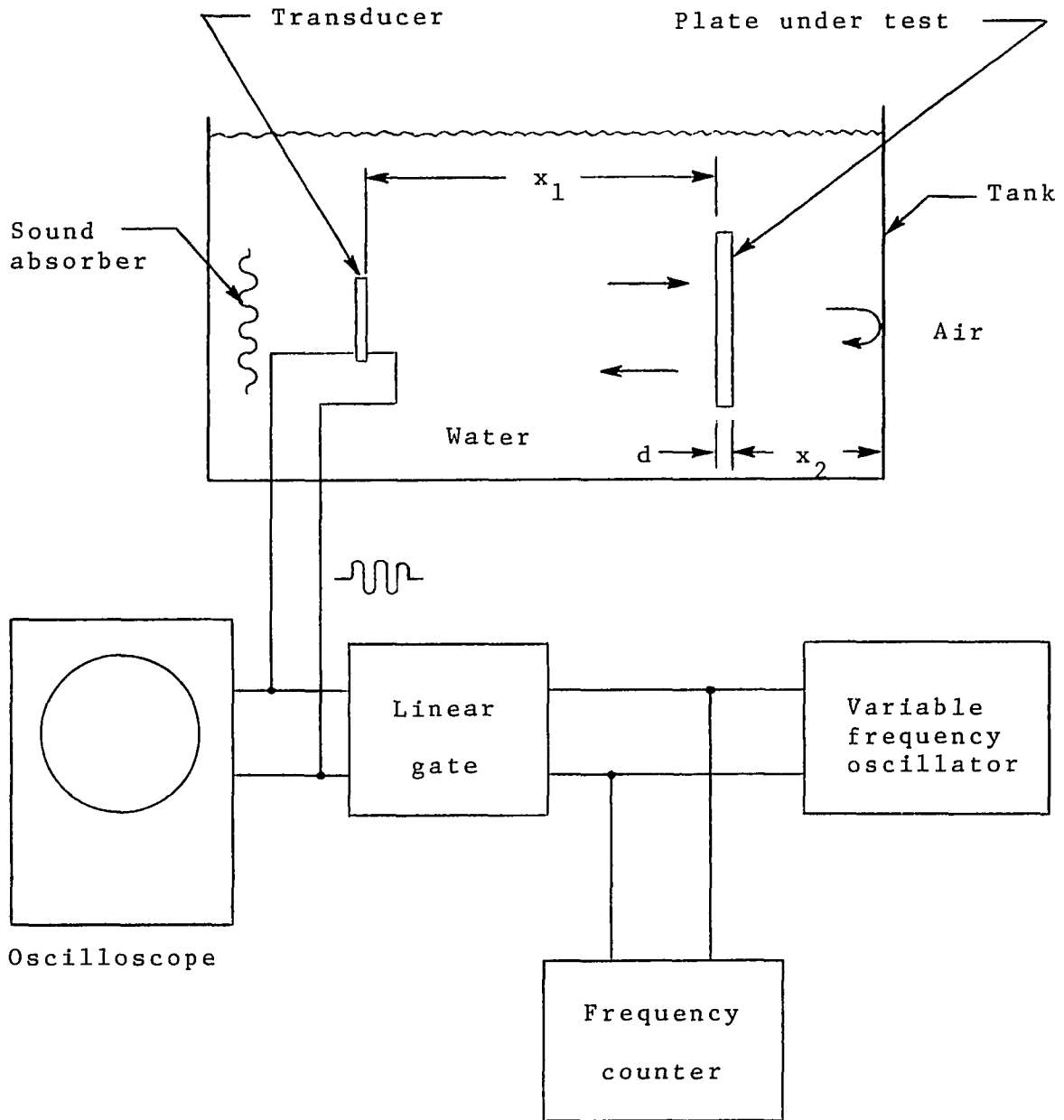


Figure II-1 The pulsed sound, immersion technique for determining the half-wave resonant frequency of thin plates

Assuming that the duration of each pulse is sufficiently long to establish steady-state conditions within the plate, the frequency f'_0 at which, simultaneously, the reflected pulse is a minimum and the transmitted pulse is a maximum indicates that the plate is in resonance and that its thickness d is an integer multiple of $\Lambda/2$ where Λ is the wavelength of sound in the material.

In order to obtain satisfactory results with this method, it is required that, with reference to Figure II-1

1. The bandwidth of the transducer be large - This is desirable in order to obtain a smooth response, minimize "ringing" of the crystal and reduce the number of crystals required to span a given frequency band. Water-backed, ceramic crystals were found to be adequate to measure the half-wave resonant frequency of both metal and plastic plates.
2. The pulsewidth be sufficiently long to establish steady-state conditions within the plate under test - The actual width depends, of course, on the thickness of the plate and the geometry.
3. The gate have low leakage to prevent interference between the leakage signal and the various echoes - A shunt-series-shunt transistor "chopper", driven by a variable pulsewidth, blocking oscillator has given satisfactory performance.

Figure II-2 shows various oscillograms obtained as per Figure I-1 for resonant and non-resonant steel and high-impact polystyrene plates. With reference to this

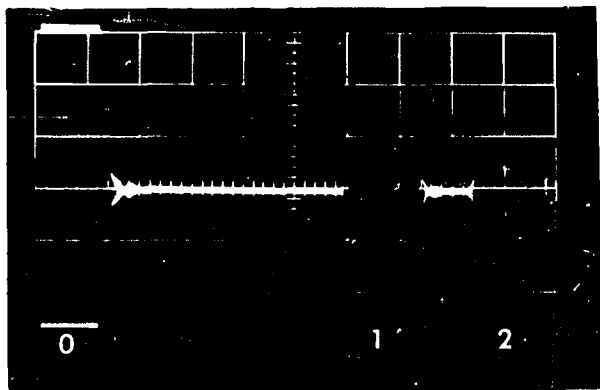
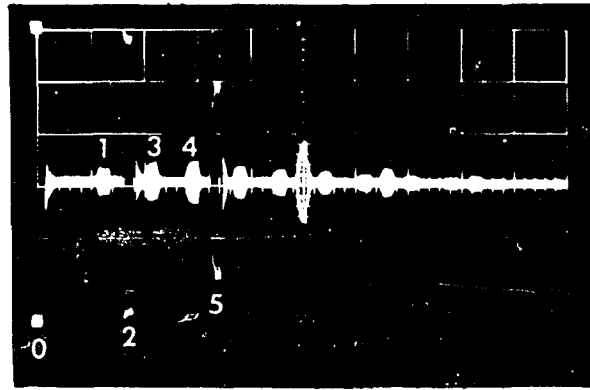
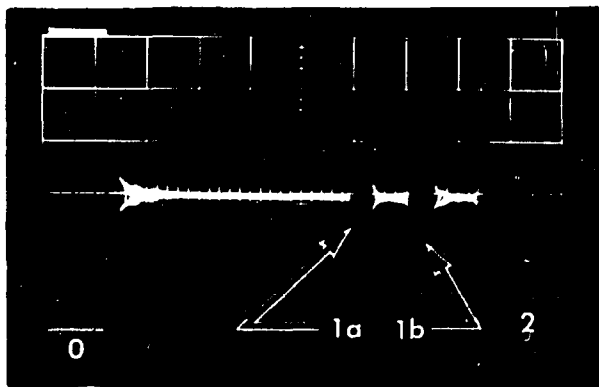
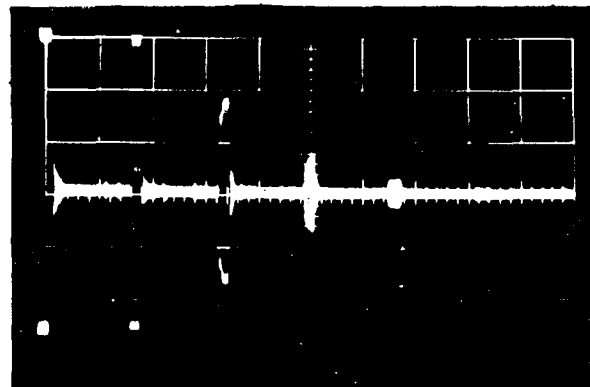
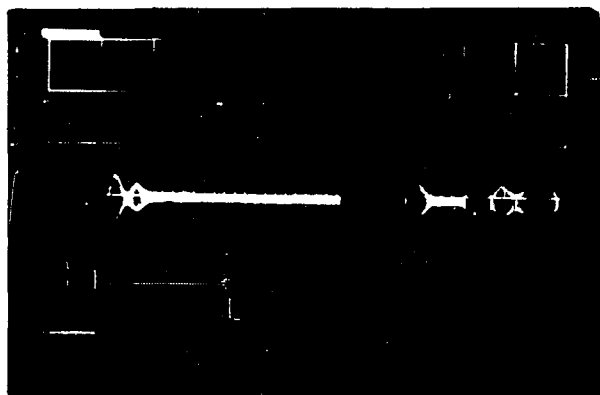
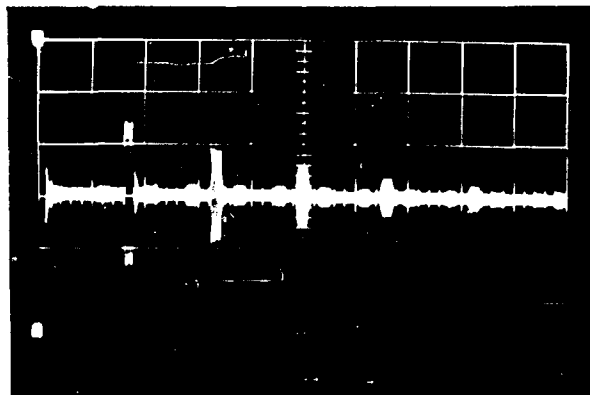
a, $f = 1.886$ MHza', $f = 1.855$ MHzb, $f = 1.980$ MHzb', $f = 1.985$ MHzc, $f = 2.056$ MHzc', $f = 2.131$ MHz

Figure II-2 Oscilloscope trace obtained as per Figure II-1 for steel (a, b and c) and polystyrene (a', b' and c') plates (see text)

figure, illustrations "a", "b" and "c" represent the sound pulses obtained for a steel plate (0.059" thick). Each picture shows the initial (0), reflected (1) and transmitted (2) sound pulses as discussed on page II-1. As can be seen, below resonance (part "a" - 1.886 MHz), most of the energy is reflected whereas, at resonance (part "b" - 1.980 MHz), virtually all of the sound energy is transmitted through the plate. Also visible in this image are the initial (1a) and final (1b) transients - each of approximately 10 microsecond duration. Hence, approximately 20 cycles are required to establish steady-state conditions in this plate. Finally, above resonance (part "c" - 2.056 MHz), most of the incident energy is again reflected.

Because the acoustic impedance of high-impact polystyrene and other plastics is comparable to that of water, the reflection coefficient is generally small and the bandwidth is relatively large. Hence, when using the pulsed sound immersion technique to evaluate plastic plates, it is expedient to observe a series of echoes rather than the first two. Parts a', b' and c' of Figure II-2 show the resulting oscillograms obtained with this technique for a 0.0215" thick, high-impact polystyrene plate. The echoes in image a' (1.855 MHz) may be readily identified with the aid of Figure II-1.

Hence,

Echo	Total distance travelled
0	initial pulse
1	$2x_1$
2	$2(x_1 + d + x_2)$
3	$2(x_1 + d + 2x_2)$
4	$2(2x_1 + d + x_2)$
5	$4(x_1 + d + x_2)$

Half-wave resonance is indicated in part b' ($f_0 = 1.985$ MHz). It will be noted that for this condition, a simultaneous null occurs in all those echoes which have reflected at least once from either surface of the plate. Above resonance (part c' - 2.131 MHz), the reflection coefficient increases again.

Evidently, once the half-wave resonant frequency f'_0 has been determined, the speed of sound c may be computed

$$c = 2 f'_0 d / n \quad n = 1, 2, 3, \dots \quad (\text{II-1})$$

where d is the thickness of the plate and "n" is an integer. For the steel and polystyrene plates discussed above, the sound velocity is 5.94×10^3 m/sec and 2.17×10^3 m/sec, respectively.

In addition to computing the speed of sound in thin plates, the pulsed sound, immersion technique may also be

used to determine the mechanical Q and the attenuation coefficient α of the material. The Q is readily obtained from the relative frequency dependence of $|t_p|^2$ or from the transients of the reflected wave at resonance.

In reference to the former, it should be noted that, for the geometry shown in Figure II-1, and under the condition that the tank wall reflects all of the incident sound energy.

1. Amplitude of the first echo is proportional to $|r_p|$
2. Amplitude of the second echo is proportional to $|t_p|^2$

A second method for determining Q is to use the relation $Q = \pi N$, where N is the number of cycles required for either transient of the reflected pulse at resonance (1a or 1b in Figure II-2b) to decay to $\exp(-1)$ of its maximum value.

For the purpose of calculating the attenuation coefficient α , refer to Figure I-1 and consider the amplitude of the second echo observed on the CRT when the plate is in half-wave resonance. Remembering that this pulse has traversed the plate twice, the observed signal amplitude V is

$$V = C |t_p|^2 P_0 \exp [-\alpha_w 2(x_1 + x_2)] \quad (\text{II-2})$$

where

C = proportionality constant

t_p = pressure transmission coefficient of the plate

P_0 = pressure amplitude of the initial sound wave at the transducer surface

x_1 = geometrical distance between the transducer and the front face of the plate (see Figure II-1)

x_2 = geometrical distance between the rear face of the plate and the tank wall (see Figure II-1)

α_w = attenuation coefficient of the water medium

d = thickness of the plate

If the plate is now removed, the signal amplitude V' of the corresponding echo is

$$V' = C P_0 \exp(-\alpha_w 2D) \quad (\text{II-3})$$

where $D = x_1 + d + x_2$. The ratio of these signals yields

$$V'/V = \exp(-\alpha_w 2d) / |t_p|^2 \quad (\text{II-4})$$

From the discussion of Appendix I, the transmission coefficient of a single, lossy half-wave plate may be determined in a straightforward manner. Hence, using relations (I-8) through (I-10) with $Z_a = Z_w$ and $\gamma = \pi - i\alpha d$, t_p becomes

$$t_p = \frac{1}{1 + [(Z^2 + Z_w^2)/2ZZ_w]\alpha d} \quad (\text{II-5})$$

Substituting (II-5) into (II-4) and solving for α yields

$$\alpha = \frac{2ZZ_w}{d(Z^2 + Z_w^2)} [\exp(\alpha_w d) (V'/V)^{\frac{1}{2}} - 1] \quad (\text{II-6})$$

Obviously, this method is useful for computing α at only selected frequencies, namely, at the half-wave resonant frequencies of the plate. In order to obtain the complete frequency dependence of α , it is possible, of course, to control the thickness of the plate, i.e. to vary its resonant frequencies.

The tacitly assumed condition that the sound wave be plane, is increasingly more difficult to maintain at low frequencies (below 500 KHz). For this reason, the pulsed sound method, as described in this appendix, may lead to some error in the measurements of c , Q and α (see Chapter VI). Nevertheless, its simplicity and versatility make this method an invaluable tool, particularly for the analysis described in Chapter VI.

REFERENCES

1. Adler, R.; Korpel, A. and Desmares, P., "An Instrument for Making Surface Waves Visible," IEEE, Trans. of Sonics and Ultrasonics, vol. SU-15, no. 3, July 1968, pp. 157-161.
2. Arkhangel'skii, M. E. and Afanas'ev, V. Ia., "Investigation of the Photodiffusion Method of Visualizing Ultrasonic Fields," Soviet Physics-Acoustics, vol. 3, no. 3, 1957, pp. 230-235.
3. Augustine, C. F., "Microwave Holograms Using Liquid Crystal Displays," Proc. IEEE, vol. 57, no. 3, March 1969, pp. 354-355.
4. Bennet, G. S., "A New Method for the Visualization and Measurement of Ultrasonic Fields," JASA, vol. 24, no. 5, Sept. 1952, pp. 470-474.
5. Bennet, G. S., "A Note on the Activation of Photographic Emulsions by Ultrasonic Waves," JASA, vol. 23, no. 4, July 1951, pp. 478-480.
6. Bennet, G. S., "On the Mechanism of the Photographic Effect of Ultrasonic Waves," JASA, vol. 25, no. 6, Nov. 1953, pp. 1149-1151.
7. Berger, H., "A Survey of Ultrasonic Image Detection Methods," Acoustical Holography, vol. 1, New York: Plenum Press, 1969, pp. 27-48.
8. Berger, H. and Kruska, I. R., "Photographic Film Detection Methods for Ultrasonic Field Visualization," JASA, vol. 34, no. 4, April 1962, pp. 518-519.
9. Bergmann, L., Der Ultraschall, Berlin, 1942, pp. 76-80.
10. Borgnis, F. E., "Acoustic Radiation Pressure of Plane Compressional Waves," Modern Physics, vol. 25, no. 3, July 1953, pp. 653-664.
11. Brenden, B. B., "A Comparison of Acoustical Holography Methods," Acoustical Holography, vol. 1, New York: Plenum Press, 1969, pp. 57-71.

12. Brenden, B. B., "Acoustical Holography as a Tool for Nondestructive Testing," Pacific Northwest Lab., Richland, Wash., Aug. 1, 1968.
13. Charlotte, H. F., "A Direct Recording Cathode Ray Tube," Electronic Engineering, vol. 29, no. 354, 1957, p. 373.
14. Chomse, H.; Hoffmann, W. and Seidel, P., "Die Sichtbarmachung von Wärme und Ultraschall durch Organo-Phosphore," Naturwissenschaften, vol. 40, 1953, pp. 288-289.
15. Clunie, D. M. and Roch, N. H., "The Laser Feedback Interferometer," Journal of Scientific Instruments, vol. 41, 1964, pp. 489-492.
16. Cuttler, C. Chaplin, "Coherent Light," International Science and Technology, no. 21, Sept. 1963, pp. 54-63.
17. Davidson, J. B. and Hull, J. F., "Recent Developments in Acoustic Imaging Systems," Davidson - Florida Atlantic University; Hull - Litton Industries, Electron Tube Division.
18. Deferrari, H. A.; Darby, R. A. and Andrews, F. A., "Vibrational Displacement and Mode-Shape Measurement by a Laser Interferometer," JASA, vol. 42, no. 5, 1967, pp. 982-990.
19. Deschamps, G. A., "Some Remarks on Radio-Frequency Holography," Proc. IEEE, vol. 55, no. 4, April 1967, pp. 570-571.
20. Dooley, R. P., "X-Band Holography," Proc. of IEEE, vol. 53, no. 11, Nov. 1965, pp. 1733-1735.
21. Dunn, F. and Fry, W. T., "Ultrasonic Absorption Microscope," JASA, vol. 31, no. 5, May 1959, pp. 632-633.
22. Eisner, E., "Design of Sonic Amplitude Transformers of High Magnification," JASA, vol. 35, no. 9, 1963, pp. 1367-1377.
23. Ernst, P. J., "Ultrasonography," JASA, vol. 23, no. 1, Jan. 1951, pp. 80-83.

24. Ernst, P. and Hoffman, C., "New Methods of Ultrasonoscopy and Ultrasonography," JASA, vol. 24, no. 2, March 1952, pp. 207-211.
25. Fergason, J. L., "Liquid Crystals," Scientific American, vol. 211, no. 2, Aug. 1964, pp. 76-85.
26. Fischer, W. K. and Zambuto, M., "Optical Holographic Detection of Ultrasonic Waves," Acoustical Holography, vol. 3, New York: Plenum Press, 1971, pp. 349-362.
27. Fritzler, D.; Marom, E. and Mueller, R. K., "Ultrasonic Holography via the Ultrasonic Camera," Acoustical Holography, vol. 1, New York: Plenum Press, 1969, ppg. 249-255.
28. Gabor, D., "A New Microscopic Principle," Nature, vol. 161, 1948, p. 777.
29. Gericke, G. R. and Grubinskas, R. C., "Utilization of the Liquid Surface Levitation Effect as a Means of Ultrasonic Image Conversion for Materials Inspection," Army Materials and Mechanics Research Center, Watertown, Mass., 1967.
30. Green, P. S., "A New Liquid-Surface-Relief Method of Acoustic Image Conversion," Acoustical Holography, vol. 3, New York: Plenum Press, 1971, pp. 173-187.
31. Green, P. S., "Acoustic Holography with the Liquid Surface Relief Conversion Method," Lockheed Missiles and Space Co., no. 6-77-67-42, Sept. 1967.
32. Green, P. S., "Final Report on Underwater Acoustic Imaging," (LMSC), report No. 4-17-65-5, 1967.
33. Green, P. S.; Bellin, J. L. S. and Knollman, G. C., "High Resolution Underwater Acoustic Imaging," (LMSC), report no. 6-77-67-42, Dec. 1967.
34. Greguss, P., "Ultraschall Hologramme," Research Film, vol. 5, no. 4, 1965, p. 530.
35. Halstead, J., "Ultrasound Holography," Ultrasonics, April 1968, pp. 79-87.
36. Hargrove, L. E., "Effects of Ultrasonic Waves on Gaussian Light Beams with Diameter Comparable to Ultrasonic Wavelength," JASA, vol. 43, no. 4, pp. 847-851.

37. Haul, R.; Studt, H. J. and Rust, H., "Verwendung chemischer Reaktionen zur akustisch-optischen Bildwandlung," Angewandte Chemie, vol. 62, no. 8, 1950, pp. 186-188.
38. Henry, G. E., "Ultrasonic Output Power Measurements in Liquids," IRE Trans. on Ultrasonic Engineering, Dec. 1957, pp. 17-31.
39. Hueter, T. F. and Bolt, R. H., Sonics, New York: John Wiley & Sons, Inc., 1955, pp. 86-163.
40. Jacobs, J. E., "Performance of the Ultrasound Microscope," Materials Evaluation, vol. 25, March 1967, pp. 41-45.
41. Jacobs, J. E., "Present Status of Ultrasound Image Converter Systems," Transactions of the N.Y. Academy of Science, Series II, vol. 30, Jan. 1968, pp. 444-456.
42. Jacobs, J. E.; Berger, H. and Collis, W. J., "An Investigation of the Limitations to the Maximum Attainable Sensitivity in Acoustical Image Converters," IEEE, Trans. on Ultrasonics Engineering, vol. UE-10, no. 2, Sept. 1963, pp. 83-88.
43. Jacobs, J. E.; Collis, W. J. and Berger, H., "An Evaluation of an Ultrasonic Inspection System Employing Television Techniques," Materials Evaluation, vol. 22, no. 5, May 1964, pp. 209-212.
44. Jarman, P., "Sonoluminescence: A Discussion," JASA, vol. 32, no. 11, 1960, pp. 1459-1462.
45. Kennedy, J. A. and Muenow, R., "Practical Improvements and Applications for the Ultrasonic Image Converter," IEEE, Trans. on Sonics and Ultrasonics, vol. SU-14, no. 2, April 1967, pp. 47-52.
46. Khanno, S. M.; Tonndorf, J. and Walcott, W. W., "Laser Interferometer for the Measurement of Sub-microscopic Displacement Amplitudes and Their Phases in Small Biological Structures," JASA, vol. 44, no. 6, 1968, pp. 1555-1565.
47. King, G. R. and Steward, G. J., New Scientist, vol. 17, 1963, p. 180.

48. Kinsler, L. E. and Frey, A. R., *Fundamentals of Acoustics*, New York: John Willey & Sons, Inc., 1952, pp. 128-138.
49. Kleinman, D. A. and Kisliuk, P. P., "Discrimination Against Unwanted Orders in the Fabry-Perot Resonator," Bell System Technical Journal, vol. 41, 1962, pp. 453-462.
50. Kogelnik, H. and Patel, C. K. N., "Mode Suppression and Single Frequency Operation in Gaseous Optical Masers," Proc. IRE, vol. 50, no. 11, 1962, pp. 2365-2366.
51. Korpel, A., "Acoustic Imaging and Holography," IEEE Spectrum, vol. 5, no. 10, Oct. 1968, pp. 45-52.
52. Korpel, A. and Desmares, P., "Rapid Sampling of Acoustic Holograms by Laser Scanning Techniques," JASA, vol. 45, no. 4, 1969, pp. 881-884.
53. Leistner, M. and Herforth, L., "Veränderungen der Lumineszenz von kontinuierlich angeregten Zinksulfid-Leuchschirmen bei Ultraschalleinwirkung," Naturwissenschaften, vol. 44, no. 3, 1957, p. 59.
54. Leith, E. and Upatnieks, "Reconstructed Wavefronts and Communication Theory," JOSA, vol. 52, 1962, pp. 1123-
55. Lurie, M., "Effects of Partial Coherence on Holography," Ph.D. Dissertation, Newark College of Engineering, Newark, N. J., 1967, p. 93.
56. Marinesco, N. and Truillet, J. J., Compt. Rend., vol. 196, 1933, pp. 858-860.
57. Marom, E.; Fritzler, D. and Mueller, R. K., "Ultrasonic Holography by Electronic Scanning of a Piezoelectric Crystal," Applied Physics Letters, vol. 12, 1967, p. 26.
58. Massey, G. A., "An Optical Heterodyne Image Converter," Proc. of IEEE, vol. 56, no. 12, Dec. 1968, pp. 2157-2161.
59. Massey, G. A., "Acoustic Holography in Air with an Electronic Reference," Proc. of IEEE, vol. 55, no. 6, June 1967, pp. 115-117.

60. McNamara, F. L. and Rogers, T. F., "Direct Viewing of an Ultrasonic Beam in a Transparent Solid," JASA, vol. 25, no. 2, March 1953, pp. 338-339.
61. McSkimin, H. J., "Empirical Study of the Effect of Diffraction on Velocity of Propagation of High-Frequency Ultrasonic Waves," JASA, vol. 32, no. 11, 1960, pp. 1401-1404.
62. McSkimin, H. J. and Andreatch, P., "A Water Immersion Technique for Measuring Attenuation and Phase Velocity of Longitudinal Waves in Plastics," JASA, vol. 49, no. 3 (part 2), 1971, pp. 713-722.
63. Meier, W. Richard, "Magnification and Third-Order Aberrations in Holography," JOSA, vol. 55, no. 8, Aug. 1965, pp. 987-992.
64. Metherell, A. F. and El-Sum, H. M. A., "Simulated Reference in a Coarsely Sampled Acoustical Hologram," Applied Physics Letters, vol. 11, no. 1, July 1967, p. 20.
65. Metherell, A. F.; El-Sum, H. M. A. and Dreher, L., "Image Reconstruction from Sampled Acoustical Holograms," Applied Physics Letters, vol. 10, no. 10, May 1967, pp. 277-279.
66. Metherell, A. F.; El-Sum, H. M. A.; Dreher, J. J. and Lamore, L., "Optical Reconstruction from Sampled Holograms Made With Sound Waves," Physics Letters, vol. 24A, no. 10, May 1967, pp. 547-548.
67. Mueller, R. K. and Keating, P. N., "The Liquid-Gas Interface as a Recording Medium for Acoustic Holography," Acoustical Holography, vol. 1, New York: Plenum Press, 1969, pp. 49-55.
68. Mueller, R. K. and Sheridan, "Sound Holograms and Optical Reconstruction," Applied Physics Letters, vol. 3, 1966, p. 328.
69. Petermann, L., "A New Photographic Method of Detecting Ultrasonic Radiation," JASA, vol. 24, no. 4, 1952, pp. 416-417.

70. Pigulevskii, E. D., "The Sensitivity and Resolution of Acoustic-Optical Image Conversion at a Liquid Surface," Soviet Physics-Acoustics, vol. 4, 1953, pp. 359-365.
71. Pohlman, R., "Materialdurchleuchtung mittels schalloptischer Abbildungen," Zeitschrift fur angewandte Physik, vol. 1, no. 4, 1948, pp. 181-187.
72. Pohlman, R., "Uber die moglichkeit einer akustischen Abbildung in Analogie zur optischen," Zeitschrift fur angewandte Physik, vol. 113, 1939, pp. 697-707.
73. Preston, K. and Kruezer, J. L., "Ultrasonic Imaging Using a Synthetic Holographic Technique," Applied Physics Letters, vol. 10, no. 5, March 1967, pp. 150-152.
74. Raman, C. V. and Nath, N. S., "The Diffraction of Light by High Frequency Sound Waves: Part I," Proc. of the Indian Academy of Sciences, vol. II, sect. A, 1935, pp. 406-412.
75. Rozenberg, L. D., "Survey of Methods Used for the Visualization of Ultrasonic Fields," Soviet Physics - Acoustics, vol. 1, 1955, pp. 105-116.
76. Rudd, M. J., "A Laser Doppler Velocimeter Employing the Laser as a Mixer-Oscillator," Journal of Scientific Instruments, (Journal of Physics E), series 2, vol. 1, 1968, pp. 723-726.
77. Rust, H.; Haul, R. and Studt, H. J., "Verwendung chemischer Reaktionen zur akustisch-optischen Bildwandlung," Naturwissenschaften, vol. 36, no. 12, 1949, pp. 374-375.
78. Schreiber, H. and Degner, W., "Sichtbarmachung von Ultraschallwellen," Naturwissenschaften, vol. 37, 1950, pp. 358-359.
79. Schuster, K., "Ultraschall-optische Abbildung nach dem Reliefbild-Verfahren," Jenaer Jahrbuch, 1951, pp. 217-228.
80. Sette, D., "Ultrasonic Lenses of Plastic Materials," JASA, vol. 21, no. 4, July 1949, pp. 373-381.

81. Shaw, E. A. G., "On the Resonant Vibrations of Thick Barium Titanate Disks," JASA, vol. 28, no. 1, 1956, pp. 38-50.
82. Sittig, E., "An Acoustical Impedance Transformer Using an Inverted Solid Cone," IEEE Transactions on Ultrasonics Engineering, vol. UE-10, no. 2, Sept. 1963, pp. 104-106.
83. Smith, R. B., "Ultrasonic Imaging Using a Scanned Hologram Method," IEEE Ultrasonics Symposium, Vancouver, Canada, Oct. 1967.
84. Smith, R. B. and Brenden, B. B., "Refinements and Variations in Liquid Surface and Scanned Ultrasound Holography," presented at the IEEE Symposium on Sonics and Ultrasonics, New York City, Sept. 25-27, 1968.
85. Smyth, C. N., "The Ultrasound Camera - Recent Considerations," Ultrasonics, vol. 4, Jan. 1966, pp. 15-20.
86. Smyth, C. N. and Sayers, J. F., "The Ultrasound Image Camera," Proc. of IEEE, vol. 110, no. 1, Jan. 1963, pp. 16-28.
87. Sokolov, S., "The Ultrasonic Microscope," Doklady Akademii Nauk, S.S.S.R., vol. 64, 1949, p. 333.
88. Sokolov, S. Ia., "Ultrasonic Methods for Detecting Internal Defects in Metal Products," Zavodskaya Lab., vol. 1, 1935, pp. 1463-1473.
89. Stroke, G. W., An Introduction to Coherent Optics and Holography, New York: Academic Press, 19 , pp. 48-57.
90. Suckling, E. E., "A New Method of Transducing an Ultrasonic Shadowgraph or Image for Display on an Oscilloscope," JASA, vol. 27, no. 2, March 1955, pp. 297-301.
91. Thorpe, H. A., "Acoustic Transmission Augmentation Across an Air/Water Interface," JASA, vol. 42, no. 4, 1967, pp. 909-911.

92. Thurstone, F. L., "On Holographic Imaging with Long Wavelength Fields," Proc. IEEE, vol. 56, no. 4, April 1968, pp. 768-769.
93. Thurstone, F. L. and Sherwood, A. M., "Three-Dimensional Visualization Using Acoustical Fields", Acoustical Holography, vol. 3, New York: Plenum Press, 1971, pp. 317-331.
94. Torkikai, Y. and Negishi, K., "A Simple Method for the Visualization of Ultrasonic Fields," J. Phys. Soc. Japan, vol. 10, 1955, pp. 1110-1113.
95. Van Valkenburg, H. E., "Evaluation of the Pohlman Technique, a Historical Note," Sperry Products Division, Automation Industries, Inc., Danbury, Conn.
96. Von Ardenne, M., "Uber ein Schallsichtverfahren mit elekronoptischen Bildwandler," Nachrichten Technik, vol. 5, no. 2, Feb. 1955, pp. 49-51.
97. Woodmansee, W. E., "Cholesteric Liquid Crystals and Their Application to Thermal Nondestructive Testing," Materials Evaluation, vol. 24, no. 10, Oct. 1966, pp. 564-572.
98. Young, J. D. and Wolfe, J. E., "A New Record Technique for Acoustic Holography," Applied Physics Letters, vol. 11, no. 9, Nov. 1967, pp. 294-296.
99. Zambuto, M. and Lurie, M., "Holographic Measurement of General Forms of Motion," Applied Optics, vol. 9, no. 9, 1970, pp. 2066-2072.

VITA

The author was born on _____ in _____ . He emigrated to the United States in 1952 and completed his primary education at Mahwah, New Jersey.

In 1964, he received the degree of BSEE from Newark College of Engineering. One year later, he received the degree of MSEE from Stanford University, majoring in electromagnetic fields.

The author then joined the faculty of Newark College of Engineering and became a candidate for the degree of Doctor of Science in Electrical Engineering in 1967. He has been devoting his full time to the research on which this dissertation is based, since 1968.

The author is a member of Tau Beta Pi, Eta Kappa Nu, and the IEEE. In 1970, he presented a paper on "Optical Holographic Detection of Ultrasonic Waves" at the Third International Symposium held at Newport Beach, California.

He has been an employee at the New London Laboratory of the Naval Underwater Systems Center (formerly the U. S. Navy Underwater Sound Laboratory) for the past four years.